

**GCES OFFICE COPY
DO NOT REMOVE!**

GLEN CANYON ENVIRONMENTAL
STUDIES OFFICE

JAN 03 1996

FINAL REPORT

**RECEIVED
FLAGSTAFF, AZ**

**Extension Study: Daily Dynamics of Grand Canyon Sandbars;
Monitoring With Terrestrial Photogrammetry**

Leland R. Dexter - Co Principal Investigator
Brian L. Cluer - Co Principal Investigator

With assistance from:

Glenn Dunno - Research Assistant
Merrienne Etter - Research Assistant
Kyle Bohnensteil - Research Assistant
Mark F. Manone - Research Assistant

Department of Geography
Northern Arizona University
Box 15016
Flagstaff, Arizona 86011

December 30, 1995

Sponsored by the
U. S. Department of the Interior
National Park Service
Cooperative Agreement # CA 8000-8-0002

Jim Thompson, Technical Representative

500.03
PRT-10.00
G757
20541

1094149-5-82

P11

Table of Contents

Abstract	iii
Introduction	1
Background	1
Project Review	5
Hypothesis	6
Objectives	6
Methods	7
Site Description and Selection	7
Field Procedures	13
Image Processing	14
Results	24
Methodological Results	24
Environmental Results	29
Discussion and Conclusions	91
Accuracy of the Methodology	91
Magnitude of Erosional Events	91
Frequency Distribution of Sandbar Areas	92
Temporal Trends of Erosion	94
Spatial and Geomorphic Trends	98
Simulation Studies	99
Summary	102
Acknowledgments	102
Literature Cited	104
Appendices	107

Abstract

This report presents the extension study of a technique developed to monitor fluvial sandbars along the highly regulated Colorado River in Grand Canyon National Park. Oblique photographs were taken daily, automatically, from 20 fixed position programmable cameras. Digital image processing techniques resulted in planimetric analyses of 18 of the 20 sandbars for a period beginning in January 1994 through June, 1995. The image processing technique can achieve spatial accuracy to within 1%. River stage variations decreased application accuracy depending on local site and camera-view geometry. The strength of the technique lies in daily sandbar area evaluation capability.

Rapid erosional events were reduced in number from the initial study period. Sandbars remained dynamic but over longer time intervals. Rapid change to reduced flow conditions is correlated to most sandbar area reductions.

Sandbar area frequency was bimodal with negative kurtosis, indicating that measurements taken at long time steps are not likely to document mean area but rather minima or maxima. Seasonality was also observed in area-frequency distribution related to seasonal adjustments in dam discharge patterns.

Key words: sandbar, fluvial erosion, image analysis, Colorado River, Grand Canyon National Park, Glen Canyon Dam.

Introduction

Background

The construction and operation of Glen Canyon Dam has profoundly influenced the downstream riparian environment throughout Grand Canyon National Park (Dolan, Howard, and Gallenson 1974; Andrews 1991; Dawdy 1991; Johnson 1991). Until recently, water resource management policies in the west were not evaluated in terms of their impact on the downstream environment (Ingram et al. 1991). Since 1982, assessment of the types and magnitudes of changes downstream of Glen Canyon Dam has been coordinated by the U. S. Bureau of Reclamation's Glen Canyon Environmental Studies office (GCES).

Although the Colorado River flows in a bedrock gorge, the fluvial sediment resources of the system have been a major emphasis of the GCES investigations. The fluvial sediments serve as substrate for vegetation (Johnson, 1991), as water stilling structures and water warming structures for aquatic fauna (Valdez and Williams, 1993), and as camping sites for river runners (Dolan, Howard, and Gallenson, 1974). Not only is the morphology of sediment deposits important, but the amount of sediment in storage, delivery from tributaries, the dynamics of sediment transport and the sediment balance are all important components of the overall river ecosystem and its management. Indeed the Colorado River fluvial sediment resource is the first management priority of Grand Canyon National Park (River Management Plan, Grand Canyon National Park, 1994).

The fluvial sediment resources can be described by a simple categorization of three basic particle classes, made by Howard and Dolan (1981), that clarifies the importance of fluvial sediments in this bedrock gorge. Classification is based on probable time-scales of mobility.

In this scheme, the largest category includes bedrock and large boulders which are considered mobile only during extreme floods or over geologic time-scales of tens or hundreds of thousands of years.

The intermediate category includes gravel and cobbles that are mobilized during floods that recurred frequently prior to dam construction but occur only rarely since then (i.e. the 1983 emergency releases that exceeded 90,000 cfs). The finest particle size category is sand. This particle size has been the focus of three decades of one-time studies as well as continuous and semi-continuous monitoring programs.

Sand receives the most attention because it is mobile, or potentially mobile, under all flow conditions. Sand responds to, and records, cause and effect relationships resulting from dam operations. Although the sand transport capacity of the Colorado River has been reduced mostly because of flood water storage behind Glen Canyon Dam, the supply of sand is also stored behind the dam. The post-dam supply of sand is limited to that in storage (which is poorly known) and by introduction from ephemeral tributaries. It has been calculated that the balance between sand supply and transport can be positive or negative depending on operation of the dam (Smillie, Jackson, and Tucker, 1993).

Many terms have been used to describe the sand deposits along the banks of the Colorado River. In this report, the fluvial sand deposits, regardless of geomorphic position or genesis, are referred to simply as sandbars in order to reduce confusion induced by terminology. Sand is deposited in zones of low velocity that are created by perturbations to the velocity profile. In the Grand Canyon, low velocity zones generally occur where the channel is constricted by rock outcrops or debris deposits. Constrictions of the channel cause local acceleration of flow velocity resulting in supercritical or shooting flow (of the rapids).

The accelerated flow separates from the bank at the apex of the channel constriction and leaves a low velocity, re-circulating eddy zone downstream and a bounding shear zone between the shooting flow and the eddy zone called the eddy fence (Kieffer, 1985). As the shooting flow of the rapid decelerates, flow reattaches to the bank at some point downstream (Kieffer, 1985).

Sandbars are persistent features over long time-scales (Webb, in press). They occur in predictable locations based on the interaction between river hydraulics and the less mobile controlling features such as bedrock or boulders (Schmidt, 1990). The usual resulting sandbars are shown under low-stage conditions in Figure 1. Sandbars typically are found along the upstream face of channel constrictions (upper pool bars), along the downstream face of channel constrictions (separation bars), in the quiet water of the eddy center (eddy bars), and at the stagnation zone of the flow attachment (reattachment bars). Zones of low velocity are most commonly associated with debris deposits that form where tributaries and minor side channels introduce large quantities of particles of sizes not readily mobilized by the normal range of discharges. Uncommon depositional environments include point bars on the inside of meanders and thin channel margin sandbars between outcrops of bedrock or large boulders.

The Colorado River in Grand Canyon is entirely regulated by Glen Canyon Dam. The most notable difference in flow regime resulting from regulation is the change from an annual flow cycle (100,000 cfs - 2,000 cfs) dominated by a snowmelt flood occurring usually between late May and early June to a diurnal flow cycle (30,000 cfs - 8,000 cfs) optimized for electrical power generation based on peak electricity demand in the region. Discharges in excess of powerplant capacity (approximately 31,000 cfs) occur only during rare facilities tests or emergency conditions.

The mechanisms by which sandbars can change form and size are of interest to scientists as well as resource managers and planners. Three major mechanisms are active in the reworking of sandbars (Budhu, 1992):

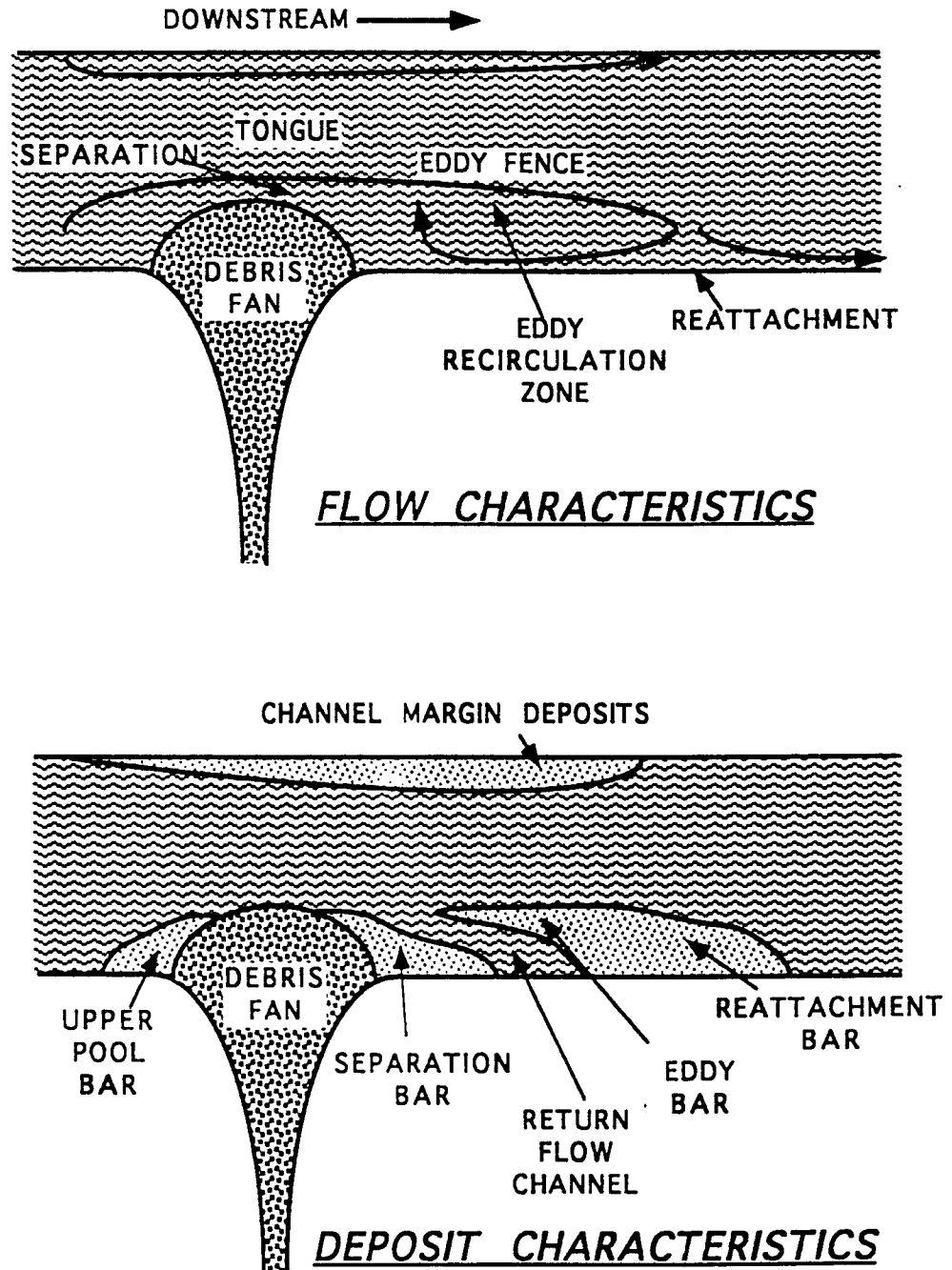


Fig. 1. The top panel illustrates the major hydraulic components of a Grand Canyon rapid and the bottom panel illustrates the resulting alluvial deposits shown at low water.

1. seepage induced failure during low flow,
2. wave induced erosion from surface turbulence, wind, and boats, and
3. drag forces from bottom turbulence and downstream flow.

Project Review

The initial effort of GCES Phase II research was directed at obtaining baseline volumetric estimates and short term volumetric changes of sandbars within Grand Canyon in response to a series of very specific controlled flow regimes (test flow program). One early method involved inserting thin wire cables of known length vertically into sandbars at node points of precisely surveyed grids. In theory, the wires could be re-measured quickly on subsequent trips and supply data necessary for volumetric change estimates. Quite often, however, subsequent survey trips would find that sandbars had changed so much in just two weeks that large portions of the wire grids could not be found. This technique was replaced out of necessity by a much more labor intensive approach using total station plane surveying at biweekly intervals.

From these field observations, we felt that some form of short time interval sampling method of sandbar morphology was needed. Two traditional techniques that were technically possible and available were land surveying and aerial photography. Both techniques were considered to be excessively expensive and intrusive for the desired time step, thus were ruled out. An alternative method was developed to meet the technical criteria within the fiscal limitations.

In the initial phase of this study, oblique photographs were taken daily, automatically, from 43 fixed position programmable cameras. Digital image processing techniques resulted in planimetric analyses of 20 sandbars for a period beginning in February 1991 through December 1993 (Cluer and Dexter, 1994). The methodology developed for this phase of the project was carried into the extension phase and is described below.

Hypothesis

Volumetric survey data indicated that major changes in sandbar morphology occurred between surveys. General field observations of sandbars made while floating the Colorado River included occasionally seeing sandbar face calving, and the aftermath-vertical sandbar faces. These factors prompted the development of the hypothesis that some types of sandbar changes are neither uniform, nor consistent from sandbar to sandbar. The time between significant changes in sandbar morphology and volume was speculative. To test the hypothesis and determine timing, the following project objectives were set.

Objectives

The objectives of this extension project were to:

1. extend the daily photographic record of 20 sandbars along the Colorado River between Lee's Ferry and Diamond Creek (December, 1994),
2. digitize selected photographs for analytical purposes on about a monthly interval,
3. rectify these images from oblique to planimetric views and further assess the accuracy involved,
4. and use the results of these objectives to analyze the temporal and spatial characteristics of short term change in sandbar size and morphology, thus addressing the contract requirements to:
 - a. determine if fluvial deposits have been stabilized by the interim flow prescription, and
 - b. compare fluvial deposit physical stability characteristics during the interim flow period to deposit dynamics observed during the test flow and pre-test flow periods,
 - c. compare the results from the initial study with those of this extension study.

Methods

Site Description and Selection

Twenty of the original forty-three sandbars (Figure 2) were selected for daily monitoring. Descriptions of each site follow.

2.6L, Cathedral Wash Camp. This sandbar is formed downstream of several large blocky rocks and a mass of talus material. Hydraulic control is provided by a debris fan constriction approximately 0.1 mile downstream at Cathedral Wash. The sandbar studied is a reattachment bar with a bare sand eddy bar at the upstream end. The site was first measured in 1985 by Schmidt and Graf (1990) and subsequently monitored during the test flow period by Beus and Avery (1992). Daily photography began in March 1992. This site was selected for its proximity to the critical sediment delivery tributary, the Paria River, approximately 2.5 miles upstream.

16.4L, Hot Na Na. This sandbar consists of an eddy bar with high elevation separation deposits from prior high discharges. The river is characterized in this reach by a narrow width constricted by the vertical walls of Marble Canyon. USGS benchmarks predate the first published measurements made on this sandbar by Beus and others in 1992. Daily photography began in March 1992. Hydraulic controls exist at the constriction which forms the deposit, and 0.5 mile downstream at the Rider Canyon debris fan and House Rock Rapid. The site was selected to represent the narrow Marble Canyon reach and because of its proximity to the Paria River sediment supply.

Location of Sandbar Stability Monitoring Sites

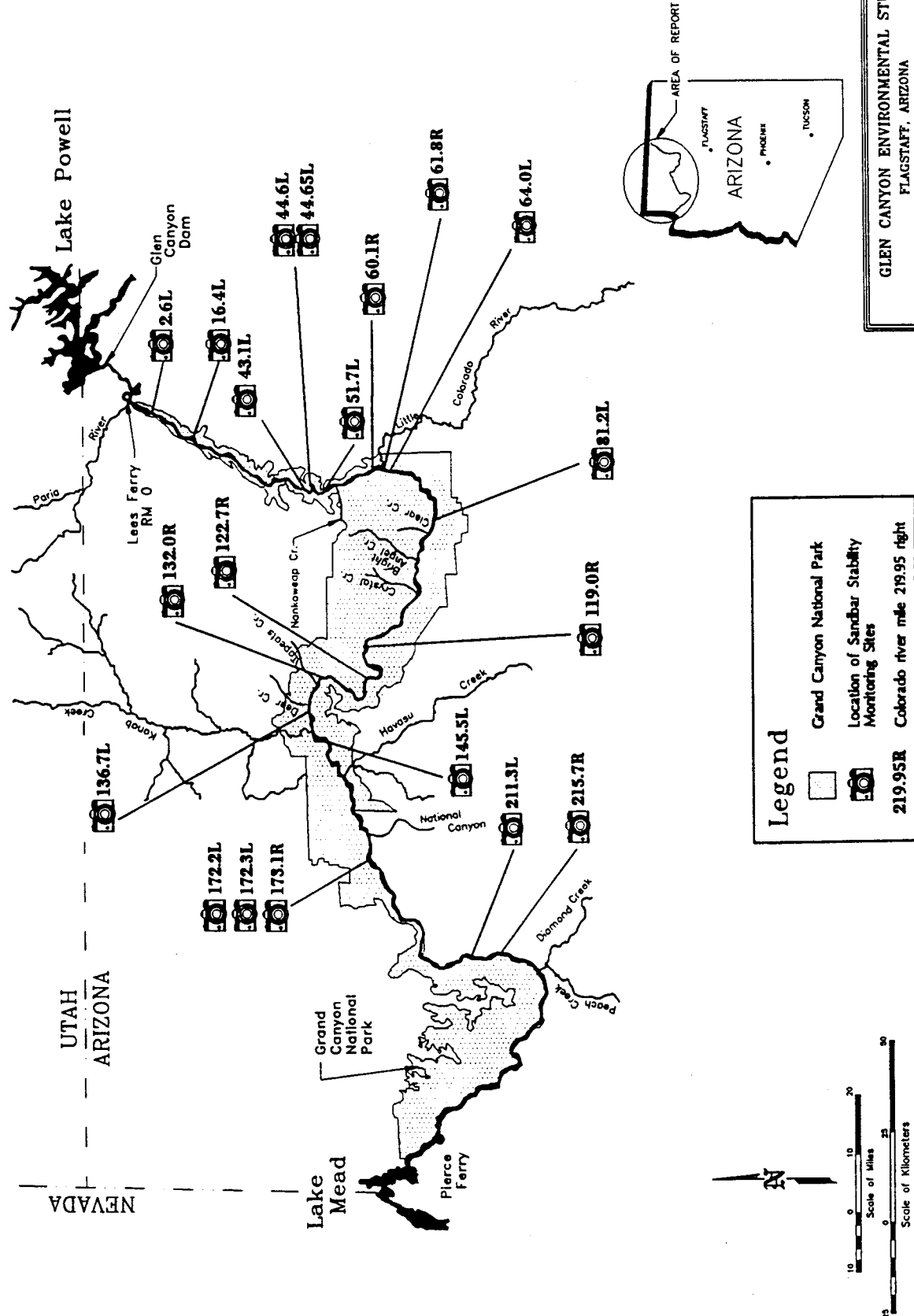


Fig. 2. Sandbar photography site index map.

43.1L, Anasazi Bridge. This is a large sandbar in an upper pool environment upstream of a debris fan channel constriction that provides hydraulic control. Its name is derived from the remains of a log structure that crosses a chimney along a South Rim/North Rim route presumed to be a foot bridge used by the Anasazi. The first published measurements are from Beus and Avery (1992) although USGS benchmarks predate this work. Photography began in November 1990 as one of seven original daily photography sites.

44.6L and 44.65L, Eminence Break. This separation sandbar is at the foot of the Eminence Break trail, just downstream of President Harding rapid. It was first surveyed in 1985 by Schmidt and Graf (1990). Daily photography began in March 1992 at this sandbar and, simultaneously, at the reattachment sandbar immediately downstream within the riffle-pool unit. Surface waves continually rework the upstream half of the separation bar at all flow levels. The reattachment and eddy bars are the largest sampled due to its position on the outside of the meander bend called Point Hansbrough. The site was selected for its size and for coverage of the dual deposits within the riffle-pool unit.

51.7L. This enormous reattachment bar lies between two small debris fans in the low gradient Marble Canyon rock. This site has been under geomorphic study since 1989. It has developed extensive fluvial wash and bar platform vegetation. It has supported endangered Southwest Willow Flycatchers during the past decade.

60.1R. This sandbar is unlike most other monitoring sites in this or other studies and had not been measured prior to initiation of daily photography in March 1992. It is a low elevation eddy bar downstream of 60 Mile Rapid that is rarely visible at most discharges and, consequently, is not used for recreation. It is included in this project to monitor changes in sediment storage where the effects of higher elevation sand storage are not a factor. Typically, high elevation sand deposits result from prior high discharges and may supply sediment from above the zone of interim flow fluctuations.

At this site, nearly vertical bedrock outcrops prevented deposition of sand at elevations exceeding the current maximum river stage. Hydraulic control is provided by the debris fan constriction of 60 Mile Rapid immediately upstream, and downstream by gravel deposits of the L.C.R. (Little Colorado River) confluence.

61.8R. This is the first sandbar down stream of the L.C.R. confluence and was first surveyed by Howard (1975). Daily photographic records began in March 1992. The field of view includes the separation and eddy bars formed by a debris cone on river right. The debris channel constriction forms a recirculation zone that is vertically confined by bedrock. The site was selected for its proximity to the L.C.R. which provides ephemeral sediment laden discharges. At high discharge rates, the eddy covers about half of the downstream end of the sandbar. Surface waves continually rework the upstream part of the separation sandbar at all flow levels.

64.0L, Hopi Salt Mines. This reattachment bar is adjacent to the sacred Hopi Salt Mines. Since this site is closed for camping, it could be useful in the future as a control for camping impact assessment and monitoring. Hydraulic controls are provided by an elongated debris constriction along the upstream left bank, and downstream by a debris fan constriction that forms a riffle. This site is included for its proximity to the L.C.R. and, because of the desire to monitor a series of sites in spatial proximity. Daily photography began on March 1992.

81.2L, Grapevine. The Grapevine Camp is important because of its location in the Inner Gorge where few sandbars exist and campsites are widely spaced. It is a bare sandbar that is the result of flow deflection from the left bank by large rocks. The large rocks occurring at both the upstream and downstream ends of the sandbar create a low velocity zone along the left bank where the sandbar is formed. A long history of studies have included 81.2L beginning with Howard (1975). Daily photography began in June 1991. This site was selected to represent sandbars in the Inner Gorge reach and the somewhat unique hydraulic controls of channel margin deposits.

119.0R. This reattachment sandbar exists in a large eddy downstream from the 119 Mile Canyon debris fan complex. The bar is presently occupied by dense arrowweed and a patch of salt cedar. It has been under study as part of the N.A.U. Beus and Kaplinski sandbar erosion project since 1990.

122.7L, Forester. This site is in an upper pool bar. This bar has been under study since the mid 1970's and has undergone extensive reworking by high mainstream flows and tributary floods from Forester Canyon. The site has been used for monitoring vegetation and avifauna change from the mid 1980's to the present.

132.0R. The Stone Creek study site lies at the foot of Deubendorff Rapid in a reattachment setting. It was formed by debris fans from both Galloway and Stone Creeks. This is a wave dominated setting in the moderate-width Middle Granite Gorge reach. Although it is heavily used by river runners, data on this deposit were scanty prior to this study.

136.7L. This deposit type is reattachment with a large eddy bar visible at low stages. The study photography began in March 1992. Hydraulic controls are the upstream riffle and downstream pool. This sandbar has extensive deposits at elevations several meters higher than stages from normal dam operations.

145.5L, above Olo Canyon. This sandbar is a narrow reattachment bar in a narrow reach downstream from Kanab Creek and upstream from Olo Canyon. It has the highest vertical relief of any sandbar in this study, probably due to a combination of flood discharges and aeolian processes. The first measurements were made in 1990 by Beus and Avery (1992) and photography began in March 1992. The site was selected to represent the narrow Tapeats Sandstone reach and also because of its location downstream of a major ephemeral tributary, Kanab Creek.

172.2L, below Mohawk Canyon. A locally derived talus cone forms a channel constriction at this site. This sandbar is the separation bar that accompanies the large reattachment sandbar 172.3L. The separation sandbar was first studied beginning in March 1992 with daily photography. 172.3L is a reattachment and eddy bar that completes the riffle-pool unit formed by a channel constriction upstream at 172.2L. Hydraulic controls are provided by the upstream channel constriction and riffle, and downstream by a broad shallow riffle and a minor channel constricting debris fan. The first study of this site was in 1990 by Beus and Avery (1992). It is one of the seven original time-lapse study sites, with daily photographic records beginning in February 1991. The 172.2L camera was installed to provide coverage of the separation bar not visible by the 172.3L camera.

173.1L. This small sandbar was selected to provide information about the possible effects of erosional events known to occur upstream at 172.3L. It consists of a low elevation eddy deposit and remnant high elevation reattachment and eddy deposits. Hydraulic controls are provided upstream by the riffle that provides downstream control for 172.3L, and downstream by a channel constriction and riffle. Daily photography began in March 1992. The site was not measured previously.

211.3L. This is one of the seven original daily photography sites with the installation of the camera in December 1990. It consists of a large flat eddy bar and high elevation reattachment bar formed downstream of a debris fan. Hydraulic controls are provided upstream by the debris fan channel constriction and downstream by a wide riffle. The sandbar was selected for its high elevation steep reattachment deposit that appeared to be actively slumping into the river and because recreational use was rare.

215.7 This sandbar lies in a reattachment setting formed by the debris fan constriction of a small unnamed tributary. This elevated sand deposit underwent extensive deposition in 1983 and is the largest remaining sandbar in the lower Granite Gorge reach.

Field Procedures

A land-based time-lapse camera system was built from relatively inexpensive off-the-shelf products. The core of the system was the Pentax IQZ 105 programmable camera. The microprocessor controlled camera allowed the built-in timer to be set for repeat exposures once every 24 h at a pre-set time of day. Each camera was secured to an alignment base which was fastened snugly inside of a military ammunition can. A large, round hole was cut into the side of the box congruent with the position of the camera lens and fitted with Plexiglass. A small metal gable was fashioned to protect the Plexiglass from the elements. The boxes were painted in earth tones to make them inconspicuous.

At each sandbar site, a camera was located a sufficient distance away to photograph the entire subject and avoid interference by or with park visitors. Usually cameras were located across, and elevated above the river to provide an oblique view. Camera boxes were attached with silicon sealant to large boulders or to bedrock outcrops. Timers were set to expose the film daily at pre-determined times selected to take advantage of local low river stage and to avoid local shading. Each camera was loaded with 36 exposure, color slide film (Jan. 1995 to present color negative film has been used), attached to the base, and sealed in the box along with a packet of desiccant. Twenty sandbars were included in the photographic sample with each of the five major geomorphic reaches (Schmidt and Graf, 1988) well represented (Figure 2).

While the cameras were being sited, aerial photography control panels were temporarily fixed at points around the field of view. A surveying crew then located the position coordinates of the panels and the camera lens/film plane using total station plane surveying techniques. Once the camera had photographed the area with the control panels in place, the panels were removed. Subsequently, the film was recovered approximately monthly.

Image Processing

In the initial study, and for part of the work in the extension study, film was processed conventionally and left in strips to facilitate scanning. A high resolution Nikon LS-3510AF film scanner was used to convert the analog images to digital form. The digital Tagged Image Format File (TIFF) created by the scanner was controlled using Picture Publisher software. Beginning in January 1995, film processing was contracted to API Inc. in Fort Collins, Colorado. This company developed the film and transferred the images to CD ROM. The digital images were then imported into ERDAS V.7.5 for image rectification and analysis (Figure 3; ERDAS 1992).

The images were subsequently rectified from an oblique view to a planimetric model (Figure 4). The pixel location of the control panels in the images were matched with the precisely surveyed coordinates of the same panels on the ground through a transformation equation. A variety of transformation equation orders or exponential powers may be applied. The benefit of higher order equations is a reduced RMS error between image and ground (Figure 5). Each higher order equation requires an increase in the number of ground control points. Control panels were no longer necessary once the desired transformation equation had been established. Fixed natural features in the images were used to control subsequent transformations. Typically, these natural features were chosen from bedrock or debris fans surrounding the area of interest. Occasionally images were difficult to rectify due to poor exposure quality. We learned that the use of images reduced to only one or two of the primary color bands often eased the difficulty of pinpointing control features.

There are certain environmental factors (e.g. sun angle, steep cliffs) that sometimes result in film exposure problems. Several sandbars are prone to severe lighting contrasts and images may be over or under exposed, or both. We have developed a technique to enhance these difficult images.

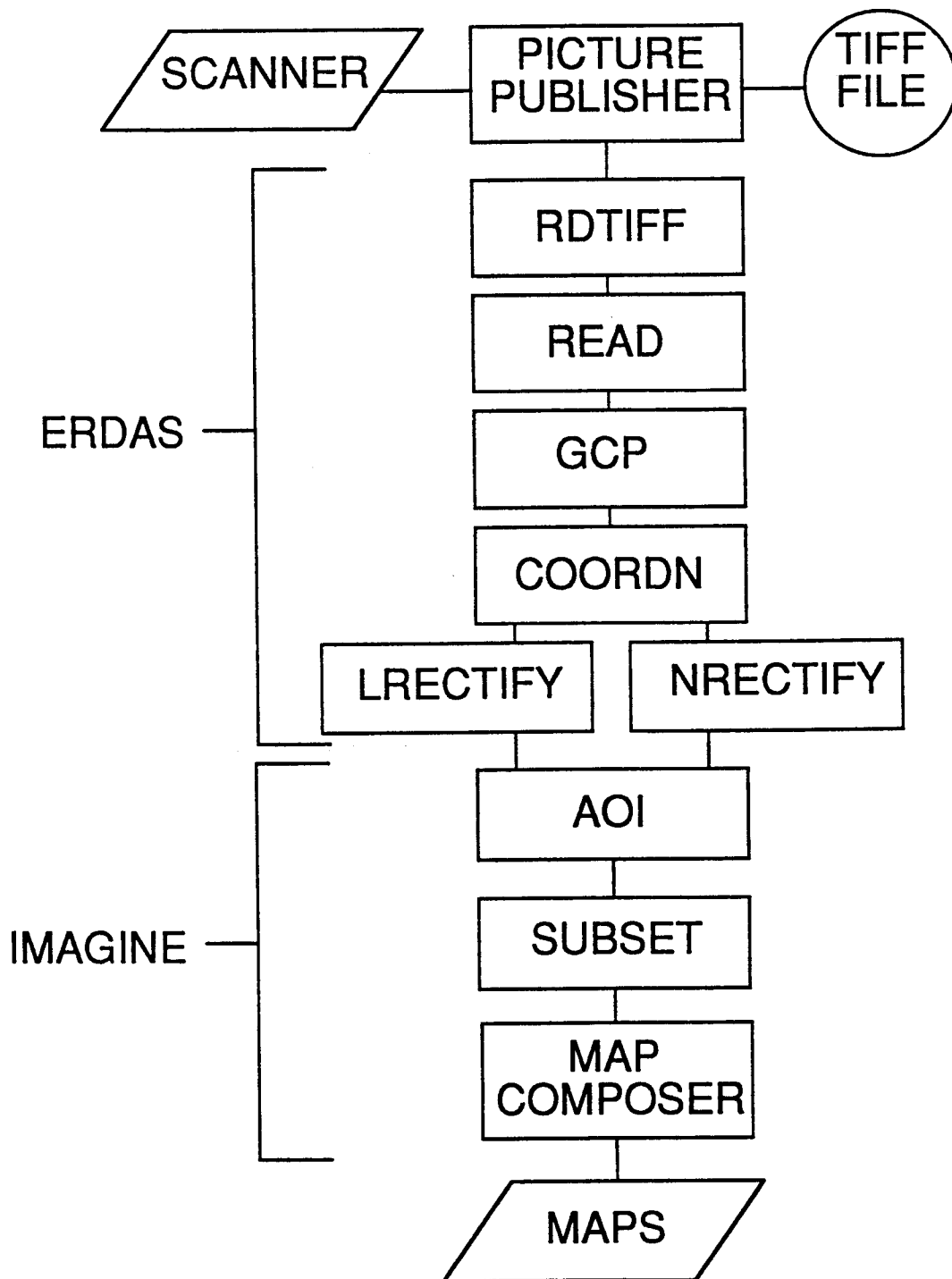


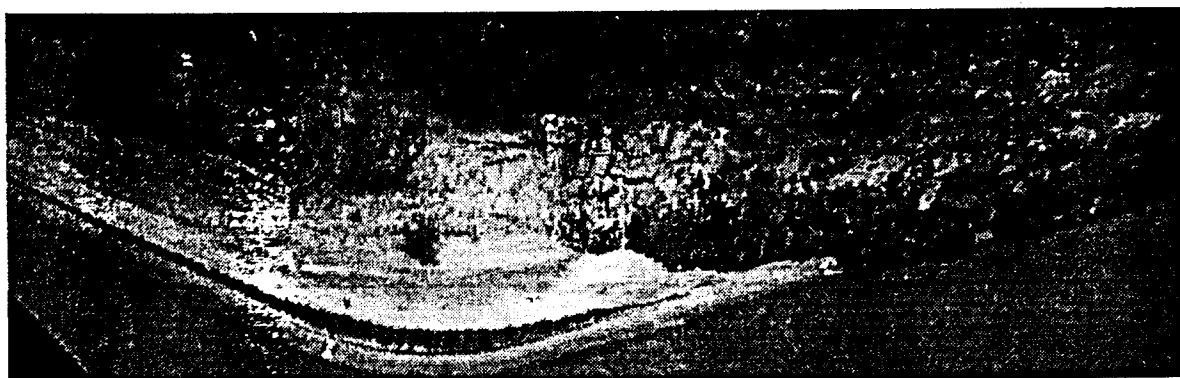
Fig. 3. Major image processing procedures and modules used in this study.

Sandbar 173.1R

11/16/92



Unrectified Surveyed Control Image



Rectified Control Image Employing a Second Order Transformation
Root Mean Square Error (pixels) = 1.86



Fig. 4. Pre-transformation (top) and post-transformation (bottom) images in ERDAS of 173.1R showing control panels in place.

Table 1. Point position error analysis for images of three Grand Canyon sandbars using second order transformations.

16.4L Hot Na Na (approximately 100 meters long)

Point #	Error in X (m)	Error in Y (m)	Z value (m)
5 (Front)	0.17	1.10	95.98
7 (Front)	0.72	0.11	96.00
F1 (Middle)	0.31	0.44	97.31
F2 (Middle)	0.74	2.28	97.62
RMS = 0.928	$\bar{X} = 0.49$	$\bar{Y} = 0.98$	DZ = 1.74 DZ All = 1.94

61.8R first beach below the Little Colorado River (approximately 100 meters)

Point #	Error in X (m)	Error in Y (m)	Z value (m)
4 (Front)	0.21	0.16	101.29
7 (Back)	0.40	2.26	127.09
RMS = 4.78	$\bar{X} = 0.61$	$\bar{Y} = 1.21$	DZ = 25.8
5 (Front)	0.23	0.31	110.17
9 (Middle)	0.00	1.95	128.89
10 (Back)	2.17	6.65	166.06
RMS = 4.68	$\bar{X} = 0.80$	$\bar{Y} = 2.97$	DZ = 55.89 DZ All = 77.14

81.21 Grapevine Camp (approximately 100 meters long)

Point #	Error in X (m)	Error in Y (m)	Z value (m)
3 (Front)	0.95	0.68	95.00
9 (Back)	2.44	1.38	96.97
RMS = 3.9	$\bar{X} = 1.70$	$\bar{Y} = 1.03$	DZ = 1.97
2 (Front)	1.61	0.61	95.07
7 (Back)	3.52	0.85	96.40
RMS = 1.83	$\bar{X} = 2.57$	$\bar{Y} = 0.73$	DZ = 1.33 DZ All = 3.40

Table 2. Summary of point position error analysis for oblique single point photogrammetry as used in this study.

A summary of the RMS curves presented earlier is given as:

First order	20.39 meters
Second order	4.44 meters
Third order	0.41 meters

Results of point position tests on the second order transforms from three beaches yield the following values:

	Mean (m)	Standard Deviation (m)
DZ < 60.0 m	1.99	1.81
DZ < 5.0 m	1.76	1.08

Compared to the equivalent RMS values for the associated transformation:

	Mean (m)	Standard Deviation (m)
DZ < 60.0 m	4.37	1.73
DZ < 5.0 m	2.21	1.52

Applying confidence intervals to the reported RMS Values:

Confidence	Order 2 RMS (m)	Order 3 RMS (m)
80 % ($\alpha=0.2$)	6.15	0.75
90 % ($\alpha=0.1$)	7.04	0.92
95 % ($\alpha=0.05$)	7.78	1.07

Table 3. Rectification area measurement experiment.

<i>offset angle</i>	<i>35.6 degrees</i>	<i>44.8 degrees</i>	<i>11.4 degrees</i>	<i>20.5 degrees</i>	<i>28.5 degrees</i>
<i>reference area</i>	<i>area=160.569</i>	<i>area=183.450</i>	<i>area=191.331</i>	<i>area=120.776</i>	<i>area=120.776</i>
	Bounded by GCP's			Not bounded by GCP's	
Area for 1.9 degrees	167.798	188.423	216.254	138.314	128.132
Area for 5.18 degrees	158.824	186.565	191.604	128.189	128.181
Area for 7.9 degrees	157.862	184.037	190.704	169.252	125.695
Area for 10.3 degrees	158.921	186.052	189.917	141.346	124.748
Area for 12.8 degrees	161.579	186.392	191.369	172.369	120.208
Area for 15.4 degrees	158.152	182.485	190.739	115.211	125.926
Area for 17.7 degrees	160.144	183.223	191.927	140.479	125.776
Area for 19.85 degrees	160.421	186.632	190.888	122.941	134.931
Area for 22.34 degrees	161.411	182.347	191.899	123.809	122.761

Table 4. Operator error comparison.

	<i>Operator</i>		<i>Operator</i>	<i>Operator</i>
		<i>ME</i>	<i>KRB</i>	<i>GAD</i>
<i>Sandbar</i>	<i>Date</i>	<i>Area sq. meters</i>	<i>Area sq. meters</i>	<i>Area sq. meters</i>
61.8R	941217	4171	4151	4148
	940219	4293	4307	4317
	950226	3930	3966	3899
132.0R	941004	3166	3282	3023
	941107	3328	3327	3310
	950302	2808	2582	2382
145.5L	940118	991	993	984
	940506	997	992	966
	950311	798	800	816

Table 5. Hypsometric (elevation-area) index for determining susceptibility of sandbars to stage induced area error. Class 1 sandbars exhibit large changes in area with respect to changes in river stage. Class 2 sandbars exhibit moderate changes in area with respect to changes in river stage. Class 3 sandbars exhibit small changes in area with respect to changes in river stage.

<i>Sandbar</i>	<i>Elevation-Area Class</i>
2.6L	1
16.4L	2
43.1L	3
44.6L	2
44.65L	1
60.1R	1
61.8R	2
64.0L	2
81.2L	3
119.0R	3
122.7L	2
132.0R	1
136.7L	2
145.5L	3
172.2L	2
172.3L	1
173.1R	2
211.3L	2

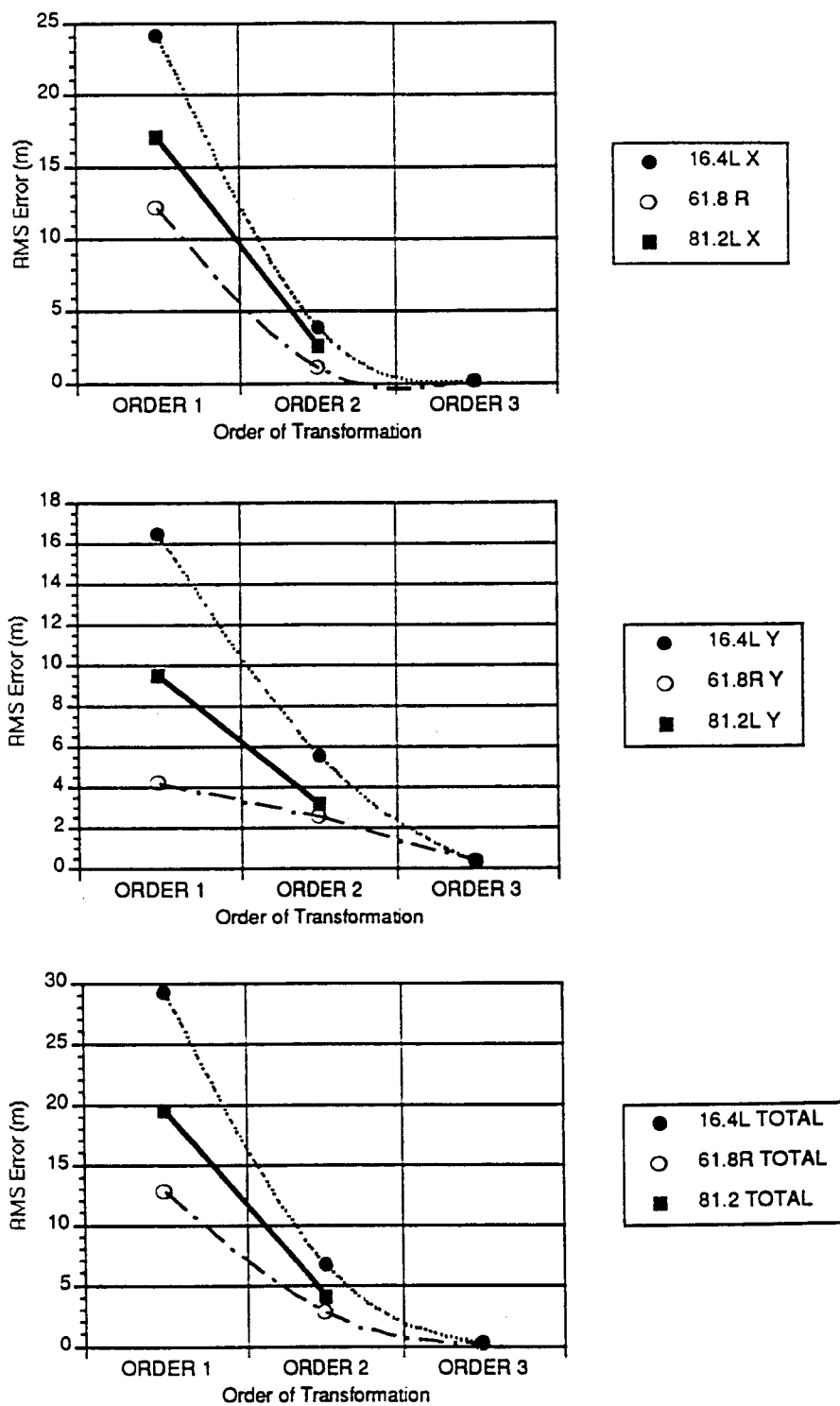


Fig. 5. Transformation order versus RMS error as reported by ERDAS.

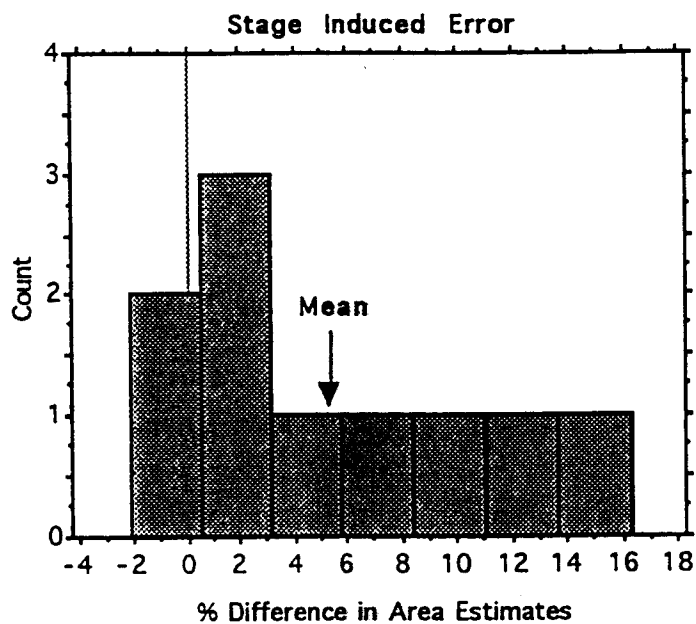


Fig. 6. Frequency distribution of stage induced error estimates.

Table 6. Summary statistics for stage induced error estimates.

Mean:	Std. Dev.:	Std. Error:	Variance:	Coef. Var.:	Count:
5.296	5.956	1.883	35.473	112.46	10
Minimum:	Maximum:	Range:	Sum:	Sum of Sqr.:	# Missing:
-2.18	15.29	17.47	52.96	599.731	0
t 95%:	95% Lower:	95% Upper:	# < 10th %:	10th %:	25th %:
4.261	1.035	9.557	1	-.88	.88
50th %:	75th %:	90th %:	# > 90th %:	Mode:	Geo. Mean:
3.285	10.05	14.325	1	•	•
Har. Mean:	Kurtosis:	Skewness:			
•	-1.114	.501			

The Nikon scanner allowed us to scan a number of different formats. These range from black and white positive to color negative. In addition, the scanner can separate color film into its three primary colors: red, green, and blue. This is extremely useful since ERDAS can view these spectral bandwidths individually. By manipulating the exposure time of each color we can bring out detail. For example, information within dark shadows is enhanced by increasing the amount of blue scanned. On the other hand, features washed out by over exposure is improved by decreasing the red. This procedure allowed us to customize each image bringing out useful detail that would otherwise be unseen.

After image rectification, the resulting planimetric photo models were screen digitized using the AOI module in Imagine v. 8.2. Screen digitizing the sandbars allowed approximate area and perimeter measurements to be determined from each photo (see the master data set in Appendix A). These data were tabulated to hard copy. Lateral erosional or depositional rates were computed by comparing image pairs. Quantitative estimates of height change and sand volume cannot be made with single camera photogrammetry.

The AOI module also produced digital polygon files which enabled the rectified image of each sandbar to be extracted and placed into a map composition using Imagine SUBSET and MAP COMPOSER modules respectively.

Since rectifiable images must meet certain quality standards as described above, not all of the sandbars photographed were suitable for image analysis. Of the twenty sandbars that were photographed, two could not be used for rectified image analysis due to site specific problems. 51.7 could not be used due to low camera angle and 215.7 could not be used due to blurry control images.

Results

Methodological

Analysis of Rectification Induced Error

Point Position Accuracy Assessment. One objective was analysis of the spatial accuracy of the techniques developed. The simplicity of the technique, and the ability to vary the repeat interval of the photography makes these methods usable in a wide variety of environmental assessments. Such information could be input into image analysis or GIS applications.

Possible sources of error accrued through the image capture and processing steps included: non-planar sandbar surfaces and abrupt changes in elevation, slight shifts in camera position during maintenance, diurnal environmental heat flux, scanning error (film curl etc.), manual identification of control points, and limitations in masking target image in batch processing.

In the initial study, we developed procedures to assess the cumulative spatial error involved in the procedures. This analysis is presented in this extension report also, as it bears on the quality of the analysis. Three sandbars of about the same linear extent (approximately 100 m long) with different amounts of vertical relief were selected. The sandbars selected were 16.4L (Hot Na Na), 61.8R (first site below the Little Colorado River confluence), and 81.2L (Grapevine Camp). The sandbar at 61.8R was included because of its high relief while 16.4L and 81.2L represented more typical relief.

Several of the control panels were withheld from the test transformation. The transformation operation was run using the remaining control points. Finally, the transformed test image was queried for the location of the withheld panels.

The resulting queried coordinates reflected accumulation of all errors propagated through the system when used in a likely manner for spatial analyses. These queried coordinates were obtained using the CURSES module of ERDAS (Figure 3). When the queried coordinates were compared to the surveyed coordinates for the panels, a Euclidean distance error could be computed for each panel withheld.

ERDAS internally computes a Root Mean Square (RMS) error for the transformed image compared to the control points used (Figure 4). It would be convenient if the transformation RMS value could be used as an estimate of error for any point on the transformed image. We set out to evaluate the validity of that possibility by comparing the RMS error to the Euclidean distance errors for the control points that were withheld. The salient statistics for the individual sandbar error analyses are illustrated in Table 1. While performing the error analysis, so many points must be withheld that third order transforms were not possible. Therefore, the results are derived using second order transforms and subsequently extrapolated to third order transforms (Table 2).

Results of the error analysis suggest that the RMS value is typically (but not always) a conservative estimation of the Euclidean distance error (Table 1), hence confidence intervals should be applied. Order three transforms are the optimal choice considering a balance between accuracy and surveying effort. Order three transform RMS suggest better than 1 in 100 spatial accuracy at an alpha level of 0.05 or 95% confidence (Table 2). Therefore, the techniques used here allow computation within +/- 1 meter of planimetric position for 95% of the point positions sampled.

Full Polygon Area Accuracy Assessment. We have developed additional error analysis techniques new to the extension study. A test to determine the accuracy of full polygon area calculations was carried out in the summer of 1995. The eight story Sechrist dormitory on the Northern Arizona University campus was used to simulate nine levels of camera placements above and opposite a sandbar. Three polygons were surveyed on the parking lot below using total station methods.

Aerial photography control panels were placed at the polygon vertices and at ground control points. The areas of the polygons were 60.569 m², 183.450 m², and 191.331m².

A photograph was taken on each floor through a Plexiglass window using the same type of camera that is utilized in the Grand Canyon. Photographs were taken on nine levels of the building to approximate nine different camera angles above a sandbar. A horizontal offset angle was calculated for each series of photographs. This is the angle from the bottom of the building directly below the camera locations to the center of the photo and ranges from 11.4 to 44.8 degrees. A photograph taken with the camera perpendicular to the Plexiglass window (looking straight out of the building) would have an offset angle of 0 degrees. The vertical angle from the center of the photo to the camera location was also calculated and is the elevation angle of the camera. This ranges from 1.9 degrees to 22.34 degrees above horizontal. The negatives were scanned and rectified using Erdas 7.5 or Imagine 8.2. Second order, non-linear transformations were used with a minimum of eight ground control points (GCP) for each image to duplicate the methodology used in the sandbar rectifications.

All images were imported to Imagine 8.2 and the polygon area calculated with the AOI module. The GCPs either completely enclosed the polygon or formed the vertices of the polygon to be tested. This duplicates the GCP layout used in most of the sandbar rectifications. Another test was performed that calculated the area of a polygon that was completely outside of all GCPs but was not further than 30 meters from the most distant GCP. Summary results are presented in Table 3.

Polygon areas 160.569 m², 183.450 m², and 191.331 m² are bounded by GCPs. Therefore the measured areas are very close to ground truth. The polygon with 120.776 m² was not bounded by GCPs and was measured from two sets of photos. The photos with an offset angle of 20.5 degrees are not centered on the polygon and hence the area is closer to ground truth. The photos with an offset of 28.5 degrees have the test polygon nearly centered in the photograph.

Based on the results of this test, oblique images can be rectified and polygon area calculation can be performed precisely and accurately. Horizontal offset angle is only a limiting factor when camera elevation angles are low. Camera elevation is not as important if GCPs are clearly visible in the imagery. One factor to consider is “pixel smear” or the distortion of objects with vertical displacement. In the case of sandbars this is not important because the beaches are relatively flat. Trees, bushes and rocks do become severely distorted in the sandbar rectification process. Higher camera angles reduce pixel smear and allow consistently more accurate rectifications. However, accurate data can be obtained with camera angles as low as 5 degrees if the polygon area of interest is bounded by GCPs.

Analysis of Operator Error

To ensure that each operator obtains consistent and accurate area measurements, an independent test was devised for comparison. The objective was to determine how closely each operator determined area measurements relative to others performing the same analyses of the same sandbar. Sandbar selection was based on relative difficulty of rectification (low, medium, and high). One sandbar from each difficulty class was chosen and three dates were chosen for each sandbar. Each operator followed outlined procedures to image match, rectify, and determine sandbar areas. Table 4 summarizes the results of the test.

For 61.8R mile, the maximum difference in area calculations was 67 square meters. For 145.5L, the maximum difference was 31 square meters. This represents less than one percent of the total area for both of the sandbars.

132.0R mile was problematic. One comparison shows all operators were within 1% of the total area. However, the another comparison showed a maximum difference of 426 square meters, roughly 20% of the total area. Due to difficulty in the rectification process, this was not unexpected.

We believe the reasons for the difficulty in rectifying this sandbar include: 1) a relatively low camera height above the sandbar making for an extremely high-oblique view, 2) poor visibility of the control points due to shadows in several of the images that were not in the control image and, 3) sensitivity of the sandbar to stage elevation differences.

The sandbars that were less difficult to rectify had more consistent area measurements between operators. The test revealed that most areas were relatively consistent between operators.

Analysis of Discharge Induced Error

One of the most persistent problems with interpretation of sandbar areas from any kind of imagery is the problem of water level. Different discharges translate to different stage levels. Different stage levels expose different areas of alluvial deposits without any true aerial modification of the deposit. The problem becomes even more difficult when the sub-aqueous channel configurations change along with the exposed portion of the deposit. Discharge-stage relations established on transient deposit material will not hold; thus discharge-stage-area relationships continually alter through time. One of our future objectives is to establish stage-discharge relations at each of the monitored sandbars using "hard" or bedrock derived control points which will free us from the transient channel shape problems.

For the work presented here, poorly defined discharge-to-stage-to-area relations were constantly problematic. Problems arose over long-term (seasonal) changes in stage, and in analysis of images taken before and after short term erosional events. Whenever possible, comparable discharge days were used as a selection criterion for images although the number of constant 8000 cfs flows was less than with the initial study. Cameras were set to trigger for local low flows at each sandbar whenever possible. We further classed each deposit in terms of its general hypsometry (area-elevation relationship) in effort to isolate less reliable results (see Table 5).

A three level classification was used where class one represents sandbars with large stage related changes in area while class three represents small stage related changes in area.

To assess the effects of misinterpreted stage levels in the short term comparison area calculations, we preserved varying area estimates made on the same deposit at the same time. Results are presented in Figure 6 and Table 6. In general, stage errors averaged five percent total area but were skewed by occasional high values as much as 17 percent total area.

Attempts were made to statistically remove the effects of the pronounced long term seasonal variations in discharge on all area measurements made during the extension study. This was done by regression techniques using minimum discharge as the independent variable and sandbar area as the dependent variable. Minimum discharge was selected because most photos were taken close to low water. Minimum discharge values used in this study were obtained at time of release from Glen Canyon Dam. A three day moving average of minimum discharge was computed under the assumption that three days represents the residence time of an individual daily discharge event as it travels through the Grand Canyon. The minimum discharge value used for the independent variable in this analysis therefore represents a mean value for three days.

Environmental

Hydrologic Inputs

Glen Canyon Dam Discharges. Since August 1991, and during the course of this project, Glen Canyon Dam has been operating under interim flow operating criteria. The specific criteria for interim flow releases are as follows:

Maximum flow:	20,000 cfs
Minimum flow:	5,000 cfs (up to 6 hours at night) 8,000 cfs (7 a.m. to 7 p.m.)
Change per day:	5,000 cfs for low volume months 6,000 cfs for medium volume months 8,000 cfs for high volume months
Ramping rates:	upramp, no greater than 8,000 over 4 hours with a maximum of 2,500 cfs/h downramp, no greater than -2,500 cfs/h

Figure 7 shows maximum, mean and minimum daily discharge frequency along with estimated daily upramp and downramp frequencies derived from the daily maximum and minimum discharge values. Figure 8 is a time-series presentation of discharge for the extension study period. Modified Julian day continues the sequence established in the initial study. Results presented in this extension study begin on modified Julian day 672 (January 1, 1994) (summary statistics provided in Appendix B). We have included daily maximum, mean, and minimum discharge values in graphical form as part of each sandbar time series plot (Figures 18 through 35). Figure 9 is a series of correlograms (autocorrelation plots) for daily maximum, mean and minimum flows. Note the pronounced seven day lag positive peak (and successive seven day harmonics positive peaks) in the maximum and mean discharge. These peaks are a product of periodic weekend low flows.

Analysis of Site Responses Using Oblique and Rectified Image Photogrammetry

Rectified Image Photogrammetry. Results of the ERDAS derived area measurements for eighteen of the twenty study sandbars are presented in time-series plots (Figures 18 through 35) and sample rectified images (Figures 10 through 17). Data for these time-series plots and images were acquired between January 1, 1994 and June 1, 1995. Detailed analyses of these eighteen sandbars are presented in the following section. In this report we provide a routine rectified area measurement approximately every 30 days with the exception of a four month gap between the end of the initial study and the beginning of this extension study (approximate modified Julian days 800-1000).

Also included are several area measurements for randomly selected dates for each sandbar. Finally, rectified area measurements were also taken before and after notable erosional events. Additional evaluations of sandbar areas were qualitatively determined by inspecting daily oblique photographs, noting area increase, decrease, or no change, and noting the location on the sandbar where changes were occurring. Consequently, the time scale of evaluation is daily. Some of the details of geomorphic activities not apparent in the rectified images but obvious in the original color slides are also discussed.

Magnitude and Frequency Results. Table 7 presents overall summary statistics for the sandbars included in the extension study. Full summary statistical tables are included in Appendix A and C. Tukey box and whisker plots (Tukey, 1988) are provided (Figure 37) to give a quick visual overview of area-distribution relations by sandbar. This plot is organized on a downstream basis but no relation to true downstream scale exists on this plot. Other time series graphs (Figures 38 through 42) are provided to show true downstream scale.

Individual frequency histograms for each sandbar are presented in the composite Figure 36. Each histogram is divided into fifteen class intervals with the number of occurrences of measured areas (see the master rectified image data set in Appendix A) plotted against the area class. Summary tables (Tables 8 and 11) have been derived from these frequency analyses.

Table 8 is a listing of important distribution characteristics which are often used in assessing the normality of any frequency distribution. Kurtosis, skewness and visual assessment of distribution mode type are listed in the right three columns, while frequency class membership is summarized in the left three columns. The frequency class membership is based on 3 categories: 1) number of deposit areas falling in the 3 middle classes of the fifteen class distribution, 2) number of sandbar areas falling in the upper tail, and, 3) the number of sandbar areas falling in the lower tail.

A normally distributed "synthetic" sandbar was numerically generated to have the same approximate area values and the same sample size as a typical Grand Canyon sandbar (see Figure 43 for a frequency histogram and Table 9 for statistical characteristics). In summary, the synthetic sandbar has 43 percent of its population in the middle three classes, and 29 percent of its population in each of the tail classes. This synthetic normal sandbar can be used to compare distribution characteristics of the 18 real sandbars. In addition, the histograms for each sandbar have a normal distribution curve superimposed on the plot.

Two further analyses were conducted to investigate seasonal and sub-seasonal distribution characteristics. Table 10 brings out seasonal trends in sandbar areas. Areas for each deposit are averaged by season over the six study seasons. The resulting time-series plot of the seasonally averaged areas for each sandbar is categorized relative to the mean area for the deposit. Each mean area is given a rank with one being smaller than average, two being about average and three being larger than average. Each class covers about one third the total range between maximum and minimum mean areas. These ranks are arranged by season with summary statistics presented. Seasons with relatively small sandbars compared to their individual means will sum up to lower values, while seasons with relatively large sandbars compared to their individual means will sum up to higher values. Results of this analysis are quite consistent and are easily related to dam discharge.

Table 11 is similar to Table 8 in that it summarizes frequency distributions for normality. The difference is that the time step is divided seasonally so that resulting distribution characteristics are made free of the seasonal cycling which was emphasized in Table 10. It is important to note that the bimodal and tail heavy distribution of sandbar areas obviously persists into sub-seasonal time steps.

Regression Analysis of Area-Discharge Relationships. As previously described, additional attempts were made to statistically reduce the effects of longer term seasonal variations in discharge on all area measurements made during the extension study. This was done by regressing sandbar area as the dependent variable against a three day moving mean of minimum discharge as the independent variable. Results of the regression analysis are presented in composite Figure 44.

Based on the residual area values obtained from the regression analysis, frequency histograms were constructed to verify the presence of distribution characteristics found in the raw data. Composite Figure 45 shows the residual histograms.

Time-Series Results. Figures 18 through 35 contain the time sequenced results of sandbar area measurements both for routine sampling intervals and for significant failure events. Significant erosional events are highlighted and eroded areas are listed alongside each event.

Time series plots are also presented in composite Figure 47 which show areas corrected for discharge effects. Here the areas are presented as a plus or minus residual value measured from the mean expected area for the discharge occurring at the time. Zero values indicate area measurements that should be typical for the discharge. Large excursions of the time line away from or toward the zero line represent significant erosion-deposition periods. Large positive or negative values indicate area values different from that which is typical for the prevailing discharge.

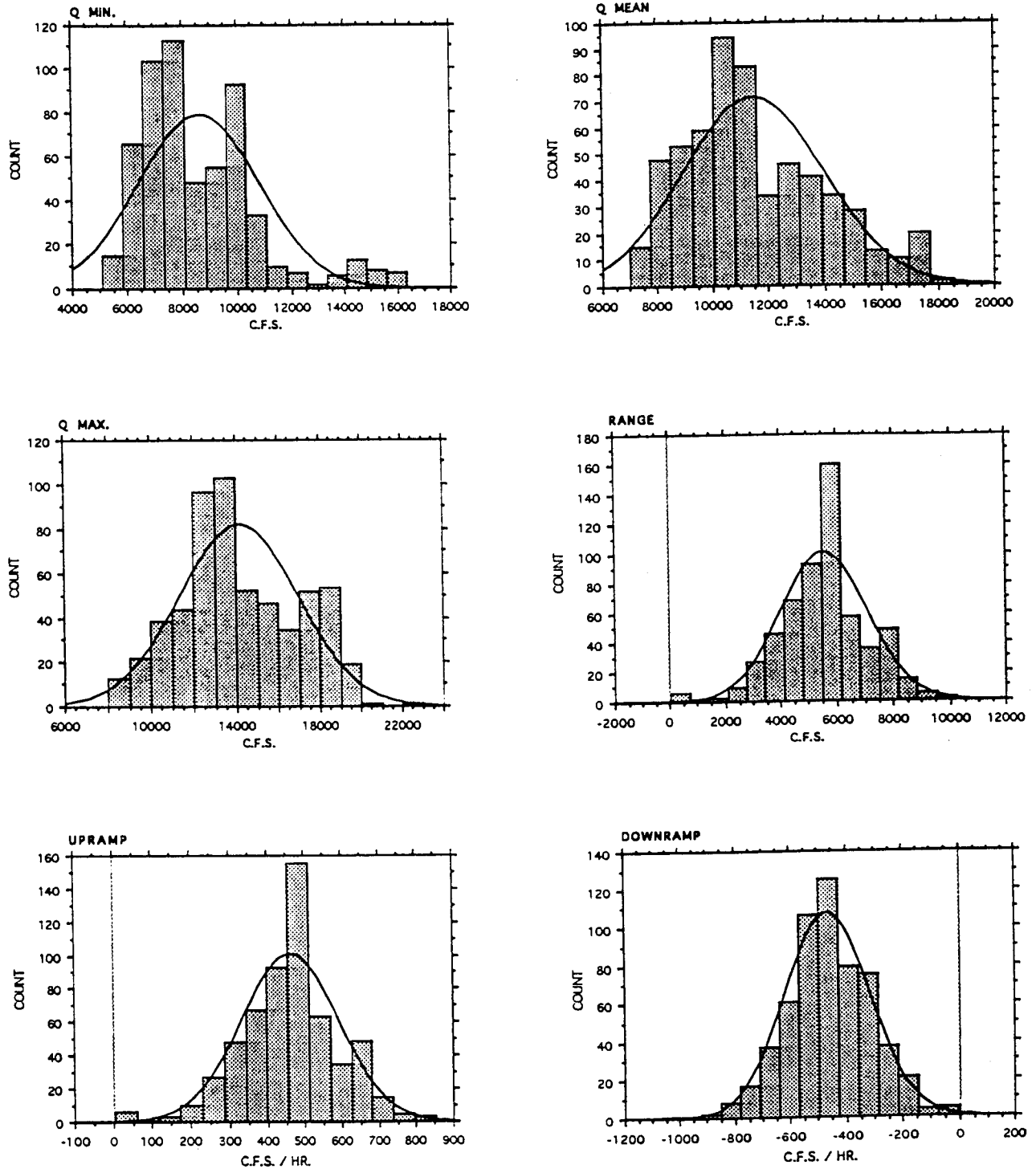


Fig. 7. Frequency distributions of discharge parameters from Glen Canyon Dam, December 10, 1993 (mjd 650) through July 12, 1995 (mjd1229).

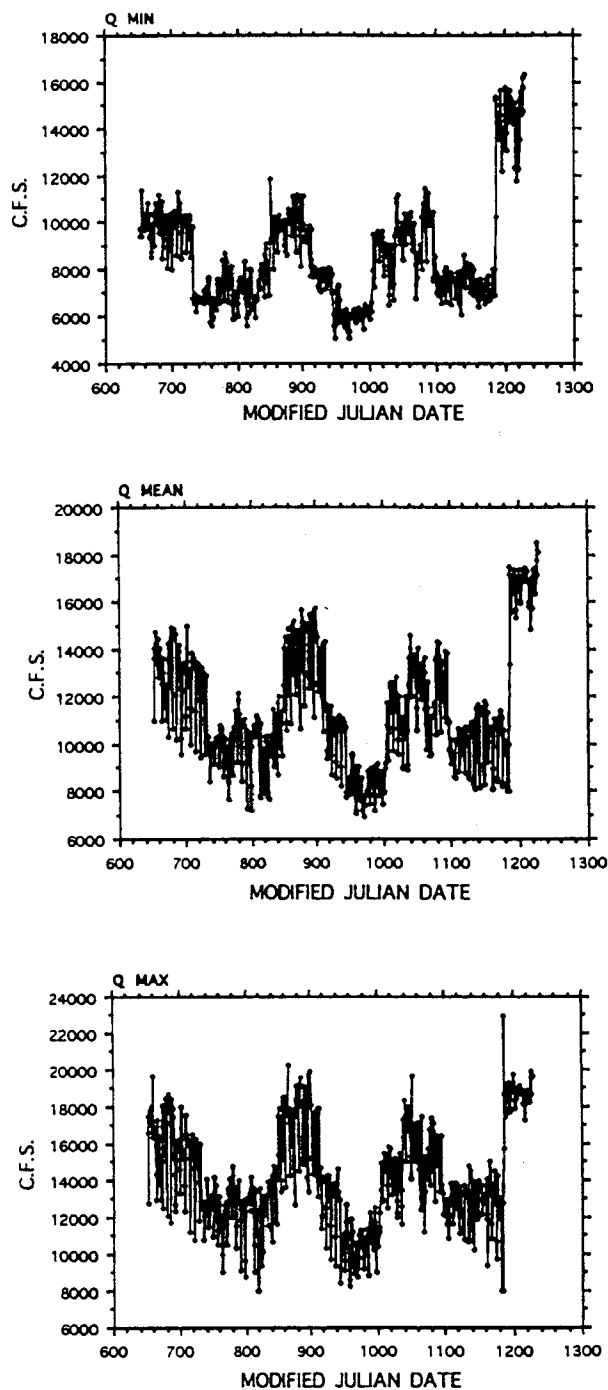


Fig. 8. Time series plots of discharge parameters from Glen Canyon Dam, December 10, 1993 (mjd 650) through July 12, 1995 (mjd 1229).

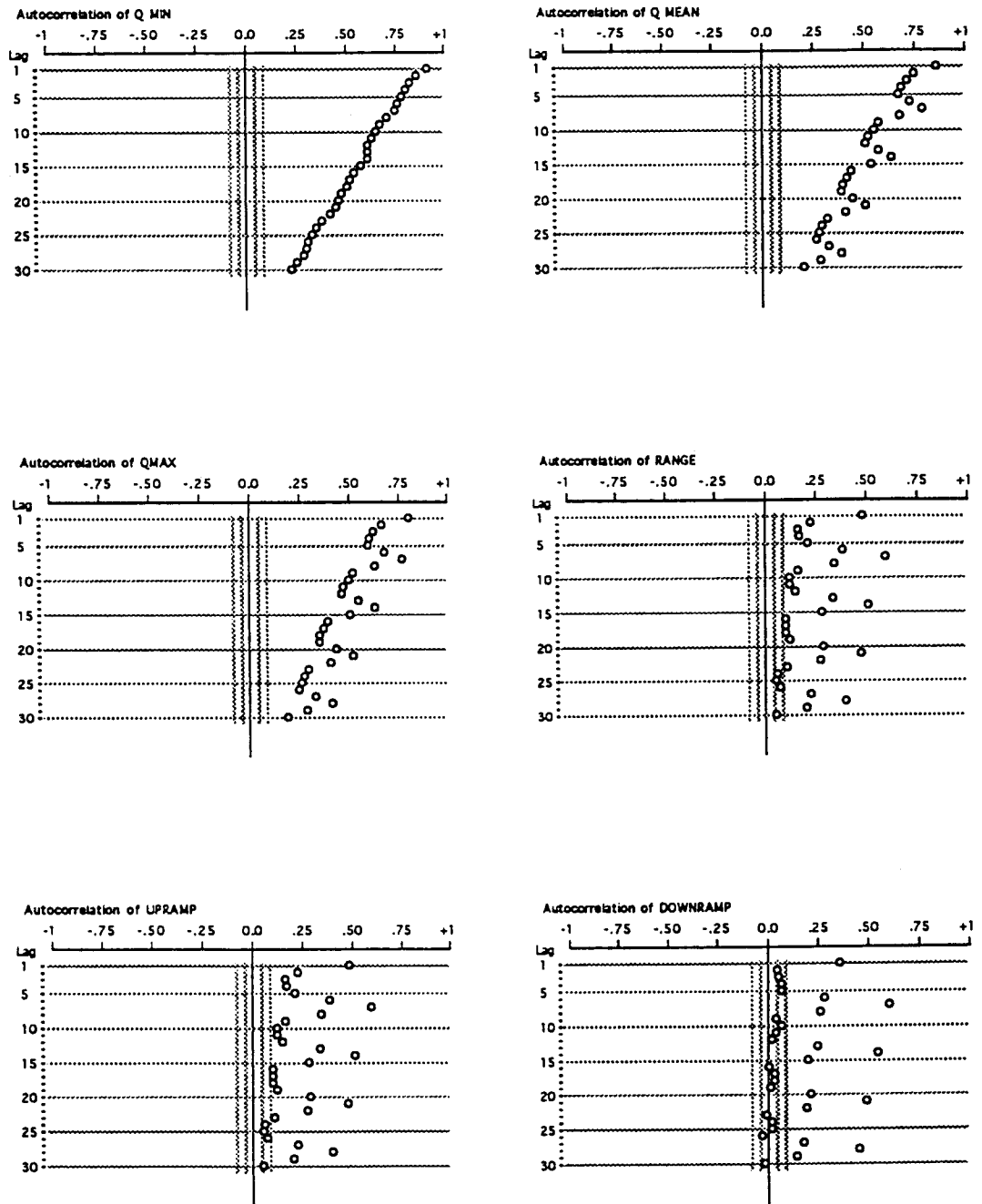
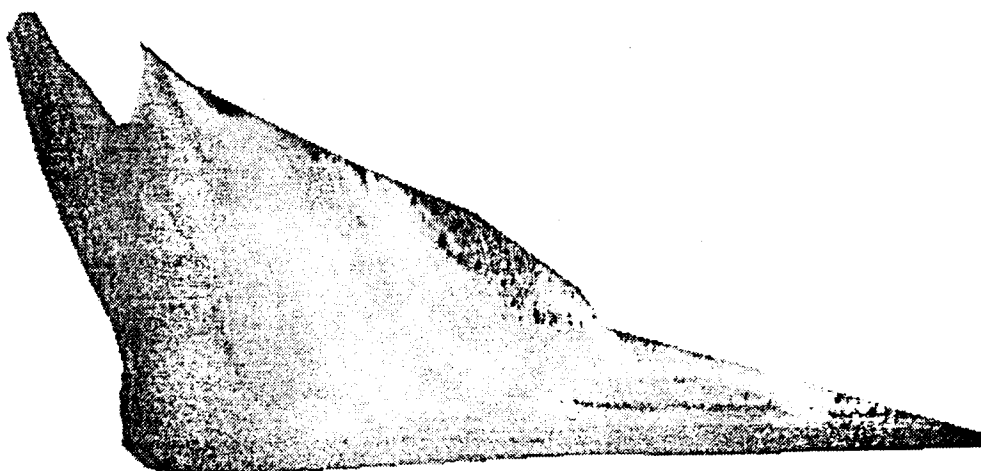
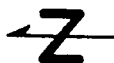
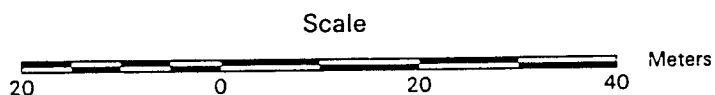


Fig. 9. Correlograms (autocorrelation plots) of hydrological parameters from Glen Canyon Dam, December 10, 1993 (mjd 650) through July 12, 1995 (mjd 1229). The positive peak at the seven day lag (and subsequent seven day harmonics) shows the periodicity introduced by weekend low flows.

Sandbar 2.6L
Grand Canyon, Arizona
05/27/95



River Flow →



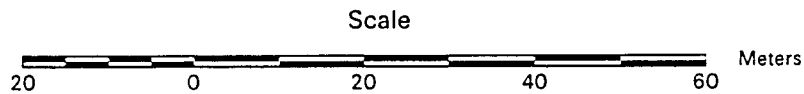
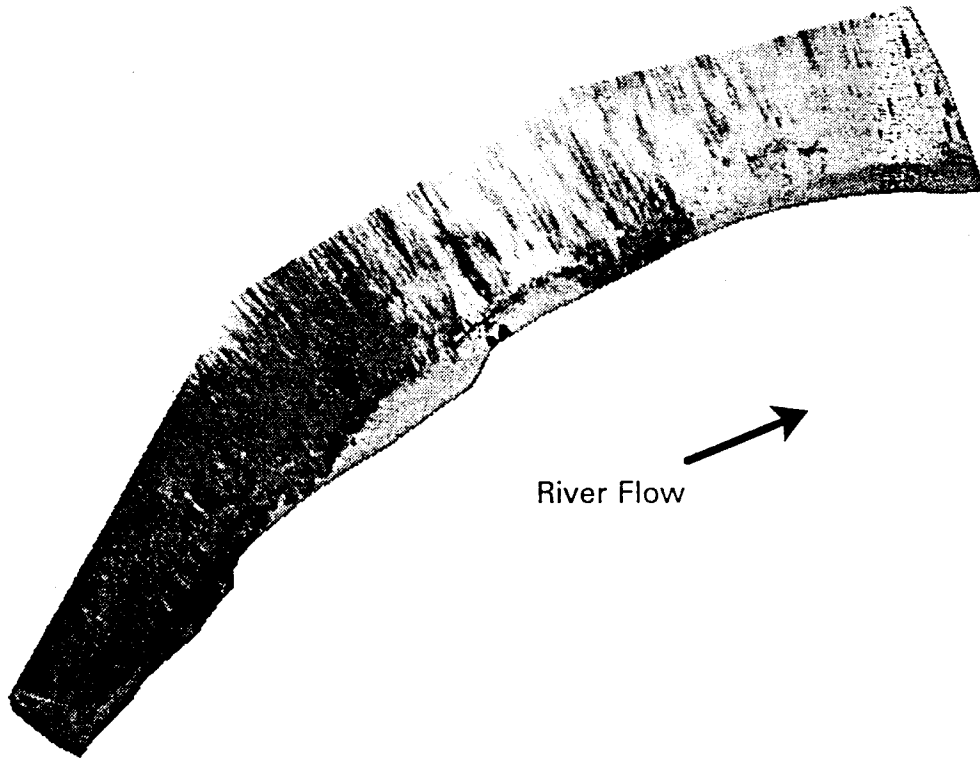
Area (sq. m) = 1893
Perimeter (m) = 256
Ave. Input Pixel Size (sq. m) = 0.23
Total RMS Error (pix) = 3.83
River Flow (cfs) = 8000

Fig. 10. Rectified image map of sandbar 2.6L, 05/27/95, 8000 cfs flow.

Sandbar 43.1L

Grand Canyon, Arizona

05/27/95



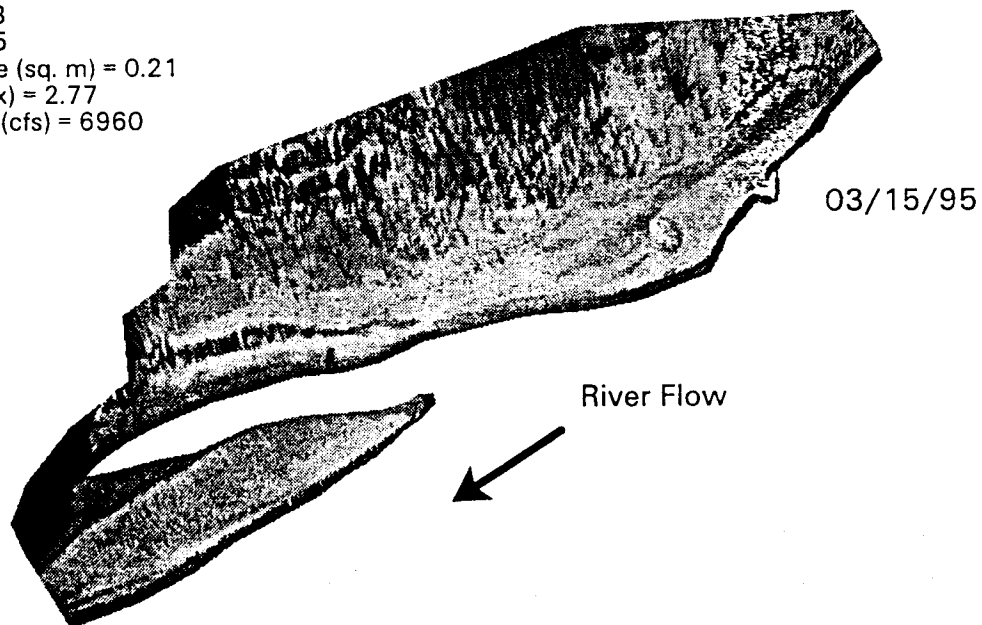
Area (sq. m) = 2678
Perimeter (m) = 308
Ave. Input Pixel Size (sq. m) = 0.18
Total RMS Error (pix) = 3.81
River Flow (cfs) = 8000

Fig. 11. Rectified image map of sandbar 43.1L 05/27/95, 8000 cfs flow..

Sandbar 61.8R

Grand Canyon, Arizona

Area (sq. m) = 4958
Perimeter (m) = 465
Ave. Input Pixel Size (sq. m) = 0.21
Total RMS Error (pix) = 2.77
Approx. River Flow (cfs) = 6960



Area (sq. m) = 4349
Perimeter (m) = 418
Ave. Input Pixel Size (sq. m) = 0.21
Total RMS Error (pix) = 2.77
Approx. River Flow (cfs) = 7650

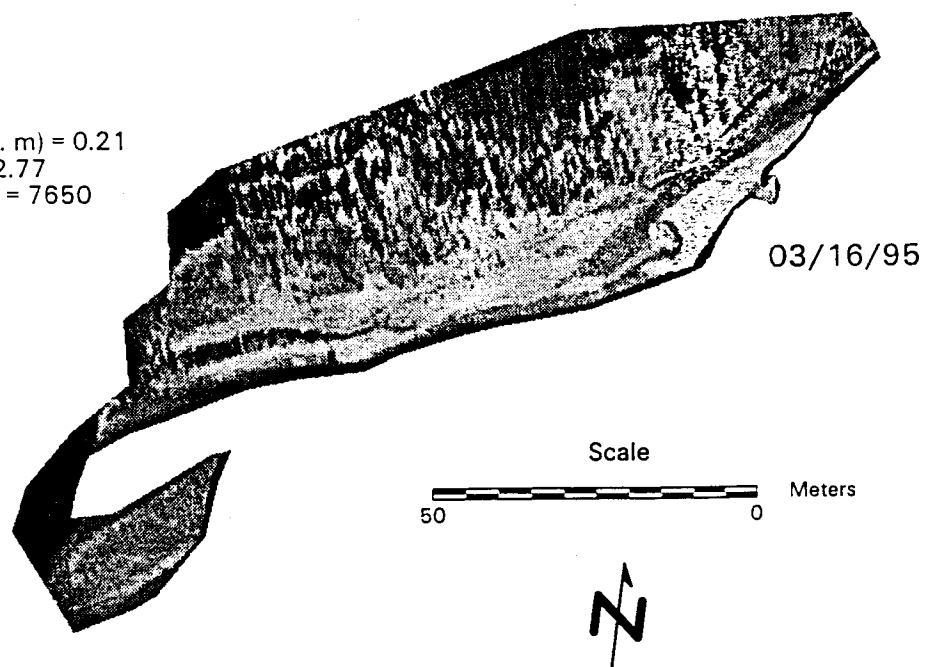
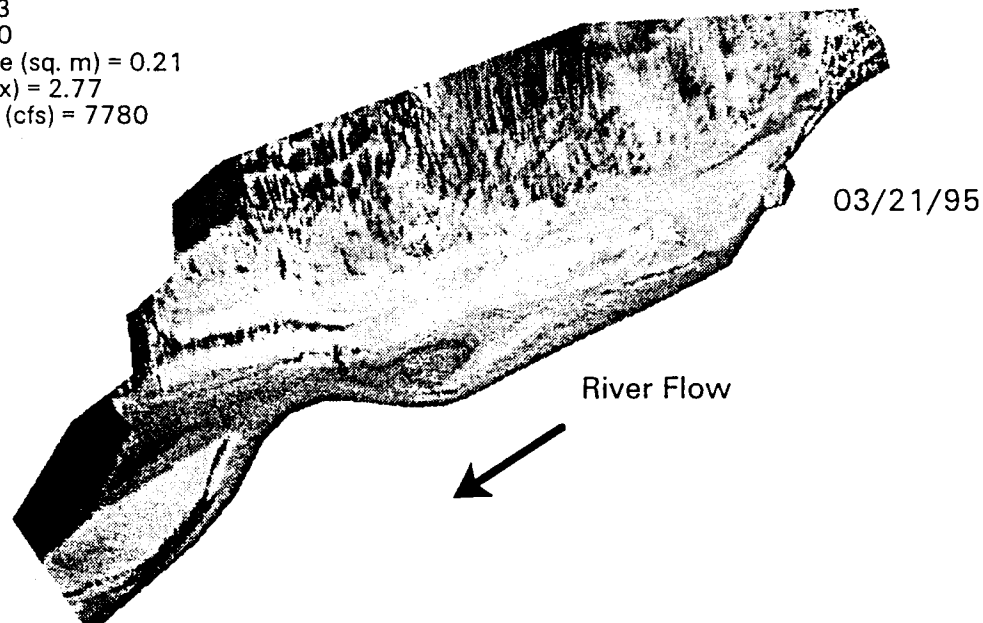


Fig. 12. Rectified image map of sandbar 61.8R, 03/15/95 top, 03/16/95 bottom.

Sandbar 61.8R

Grand Canyon, Arizona

Area (sq. m) = 5163
Perimeter (m) = 360
Ave. Input Pixel Size (sq. m) = 0.21
Total RMS Error (pix) = 2.77
Approx. River Flow (cfs) = 7780



Area (sq. m) = 4443
Perimeter (m) = 318
Ave. Input Pixel Size (sq. m) = 0.21
Total RMS Error (pix) = 2.77
Approx. River Flow (cfs) = 7620



Scale

50 0 Meters

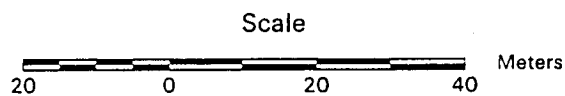
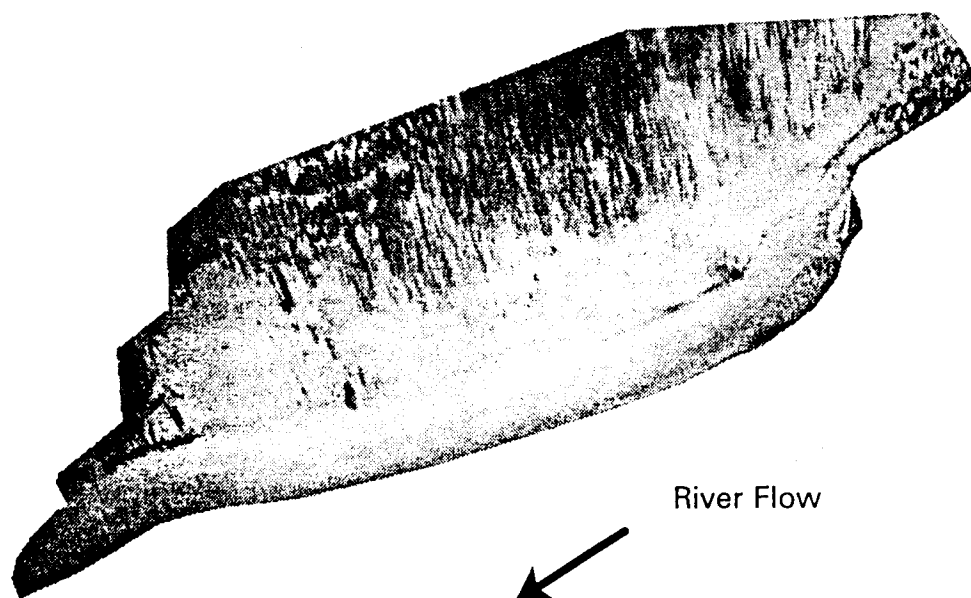


Fig. 13. Rectified image map of sandbar 61.8R, 03/21/95 top, 03/22/95 bottom.

Sandbar 61.8R

Grand Canyon, Arizona

05/28/95



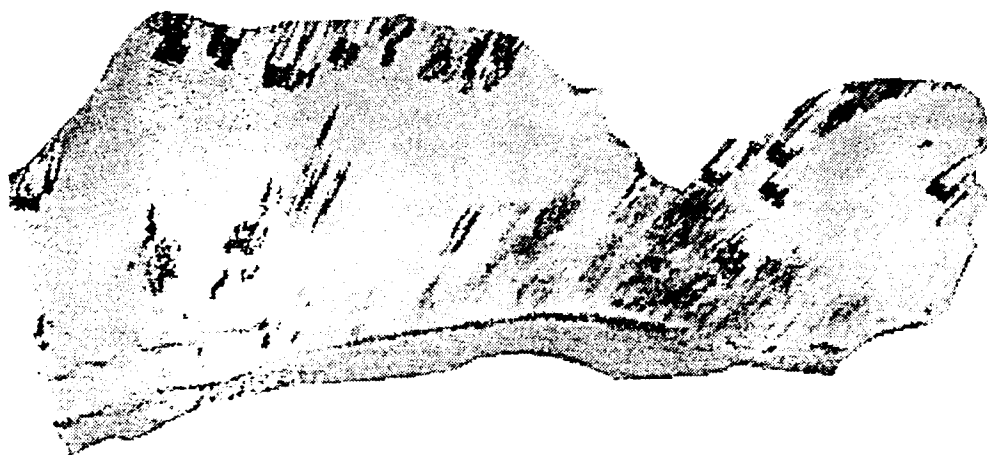
Area (sq. m) = 4967
Perimeter (m) = 342
Ave. Input Pixel Size (sq. m) = 0.21
Total RMS Error (pix) = 2.77
River Flow (cfs) = 8000

Fig. 14. Rectified image map of sandbar 61.8R, 05/28/95, 8000 cfs flow.

Sandbar 81.2L

Grand Canyon, Arizona

05/28/95



River Flow



Scale



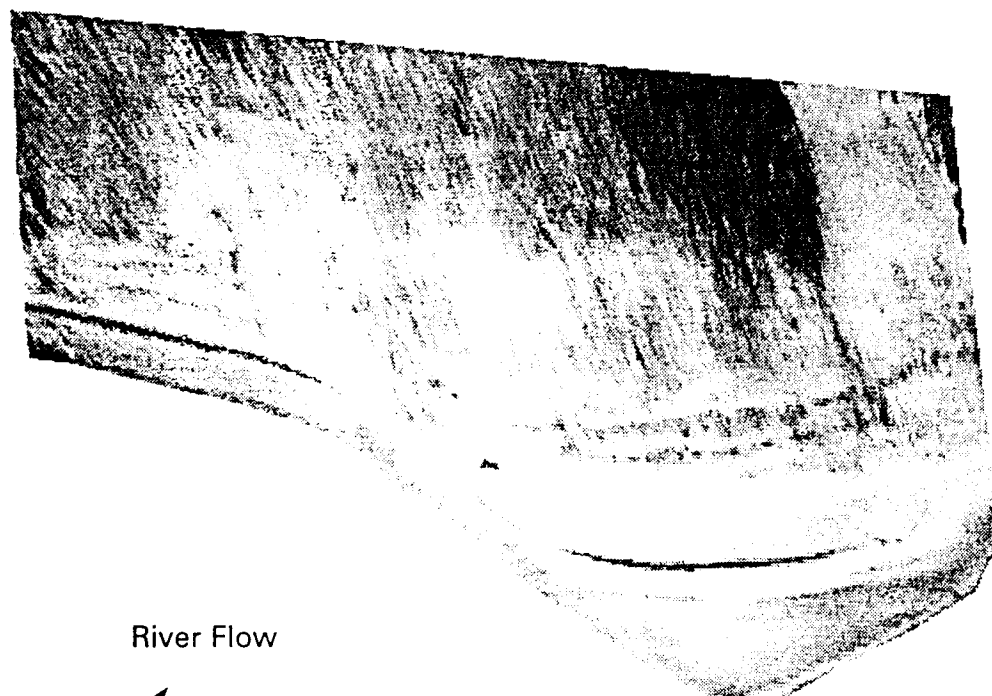
Area (sq. m) = 2006
Perimeter (m) = 221
Ave. Input Pixel Size (sq. m) = 0.19
Total RMS Error (pix) = 3.88
River Flow (cfs) = 8000

Fig. 15. Rectified image map of sandbar 81.2L, 05/28/95, 8000 cfs flow..

Sandbar 119.0R

Grand Canyon, Arizona

05/29/95



River Flow



Scale



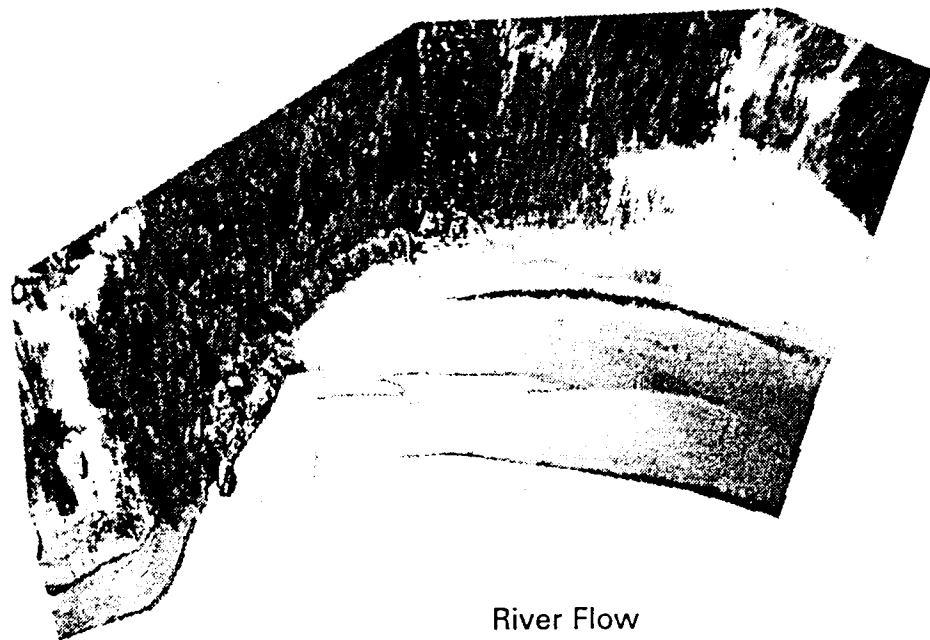
Area (sq. m) = 4257
Perimeter (m) = 276
Ave. Input Pixel Size (sq. m) = 0.22
Total RMS Error (pix) = 8.78
River Flow (cfs) = 8000

Fig. 16. Rectified image map of sandbar 119.0 R 05/29/95, 8000 cfs flow.

Sandbar 136.7L

Grand Canyon, Arizona

05/29/95



River Flow



Scale



Area (sq. m) = 4190
Perimeter (m) = 378
Ave. Input Pixel Size (sq. m) = 0.17
Total RMS Error (pix) = 6.62
River Flow (cfs) = 8000

Fig. 17. Rectified image map of sandbar 136.7L 05/29/95, 8000 cfs flow.

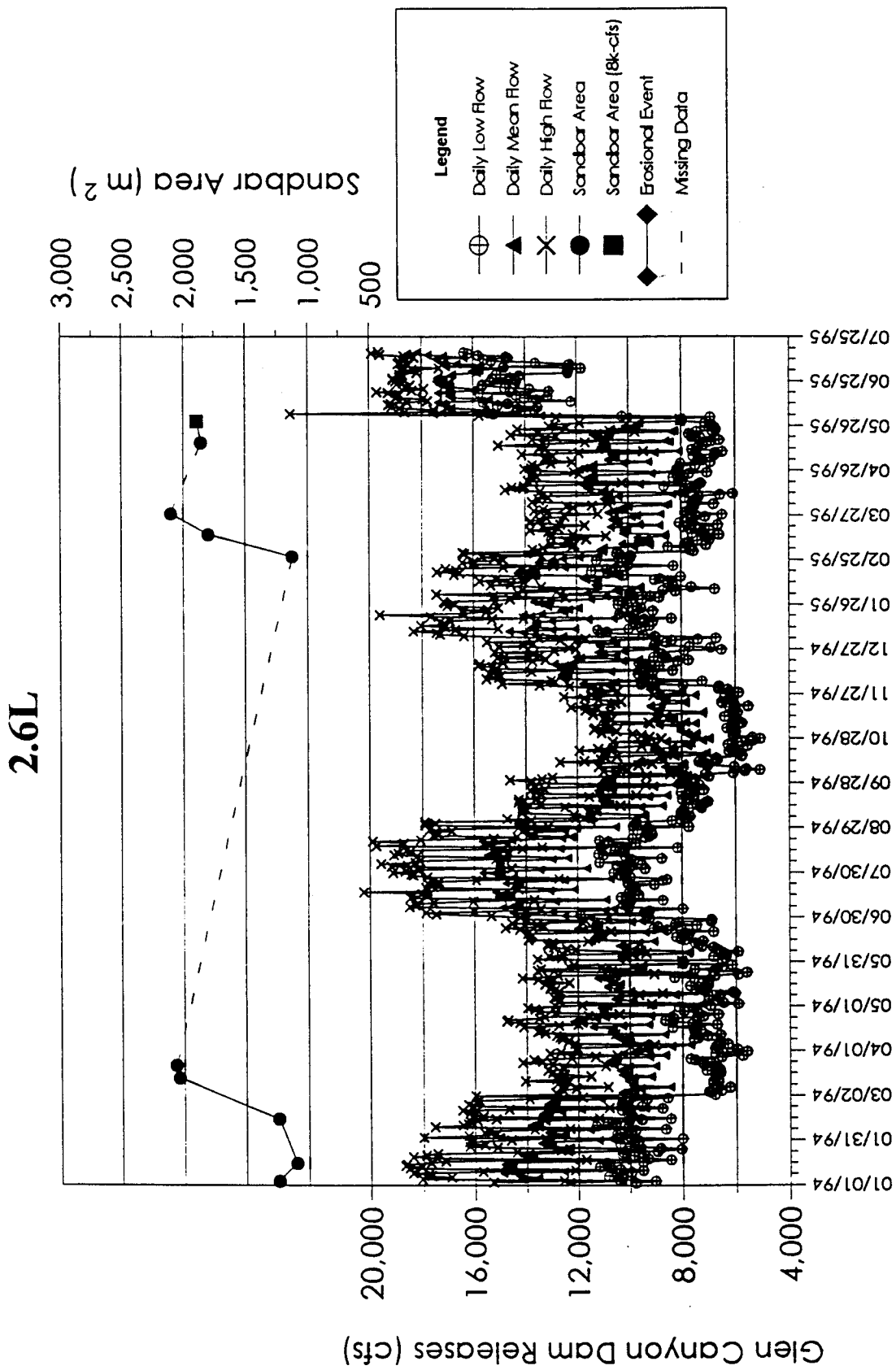


Fig. 18. Time-series plot showing area and discharge for sandbar 2.6L.

16.4L

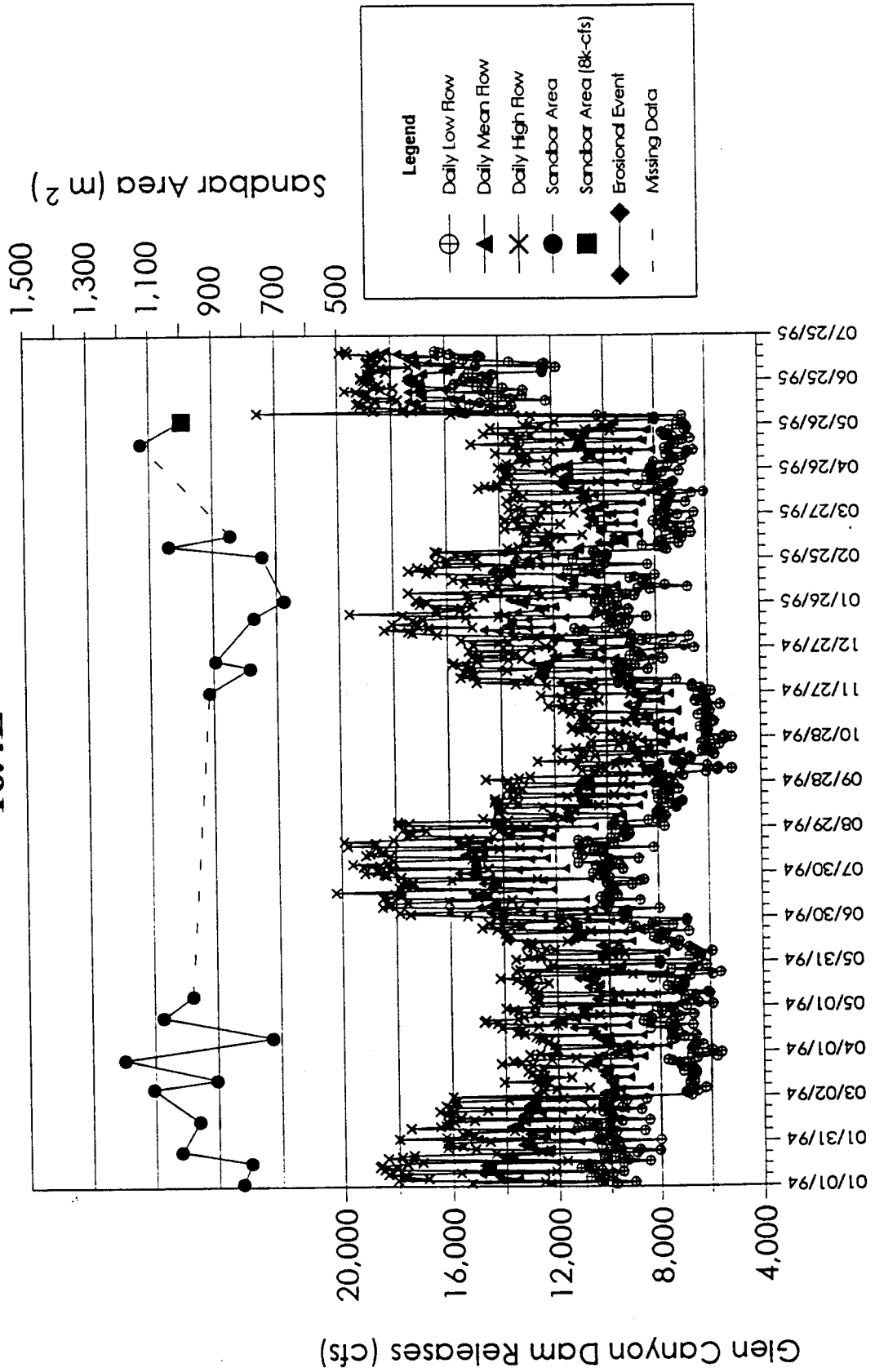


Fig. 19. Time-series plot showing area and discharge for sandbar 16.4L.

43.1L

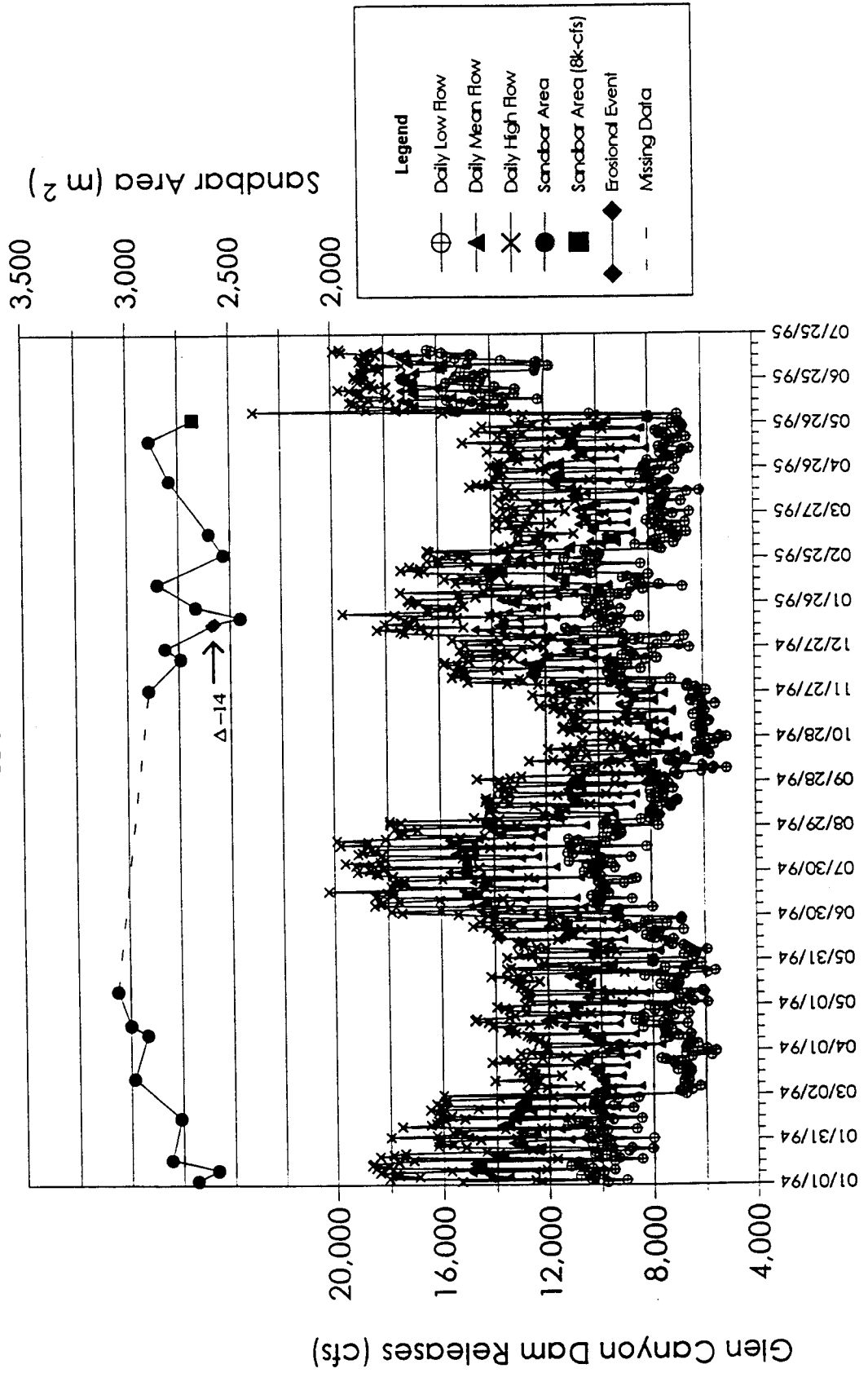


Fig. 20. Time-series plot showing area and discharge for sandbar 43.1L.

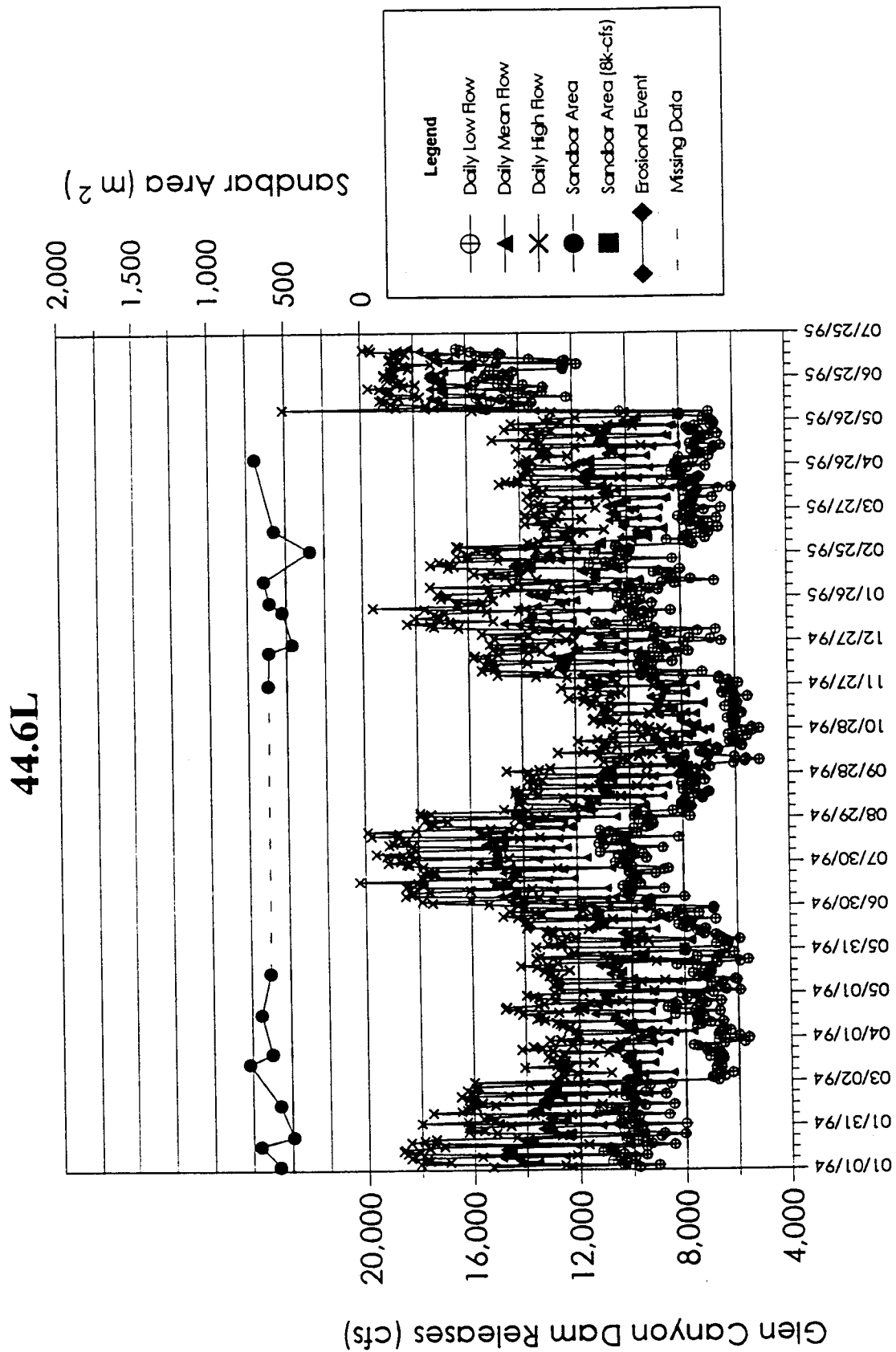


Fig. 21. Time-series plot showing area and discharge for sandbar 44.6L.

44.65L

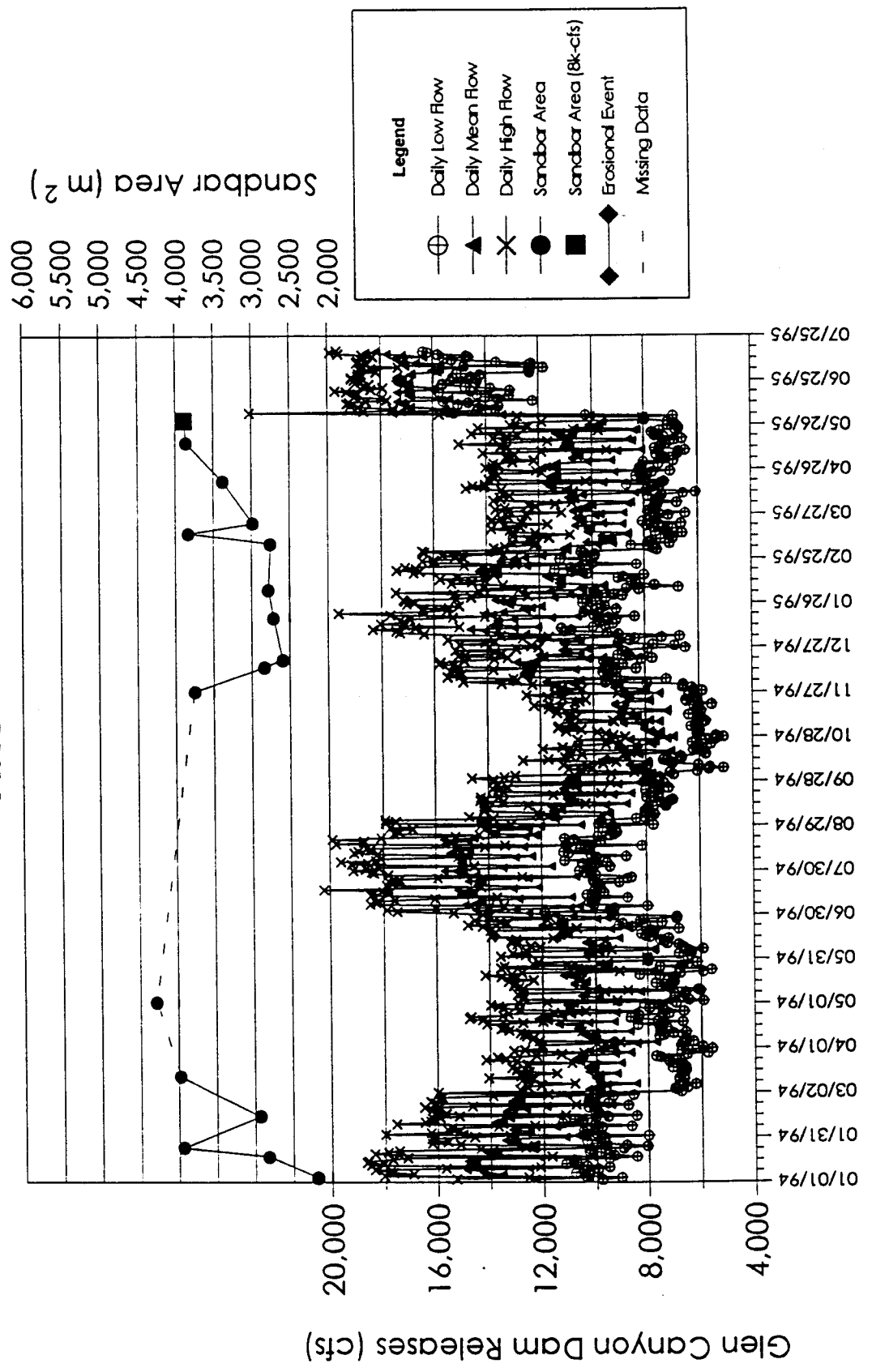


Fig. 22. Time-series plot showing area and discharge for sandbar 44.65L.

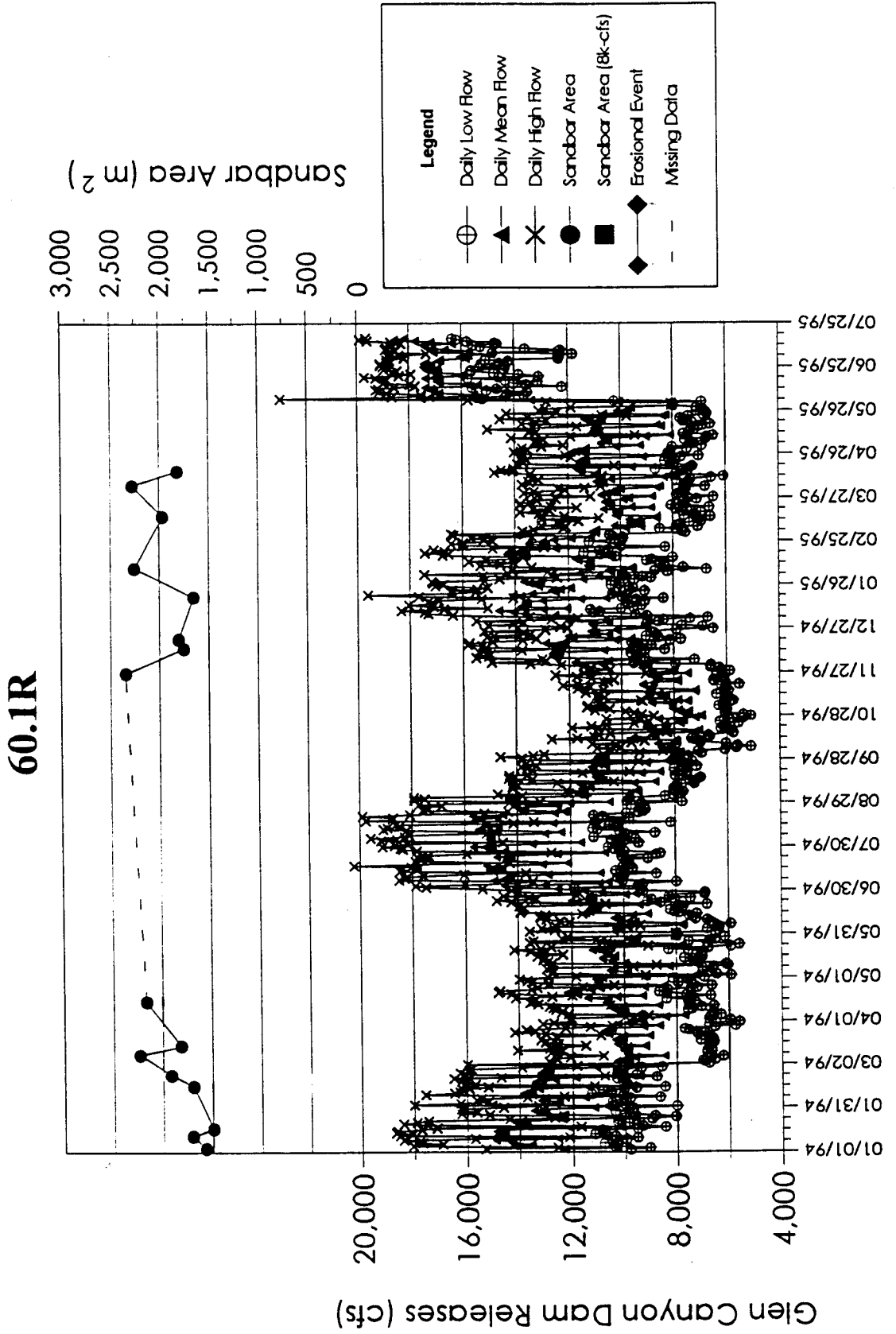


Fig. 23. Time-series plot showing area and discharge for sandbar 60.1R.

61.8R

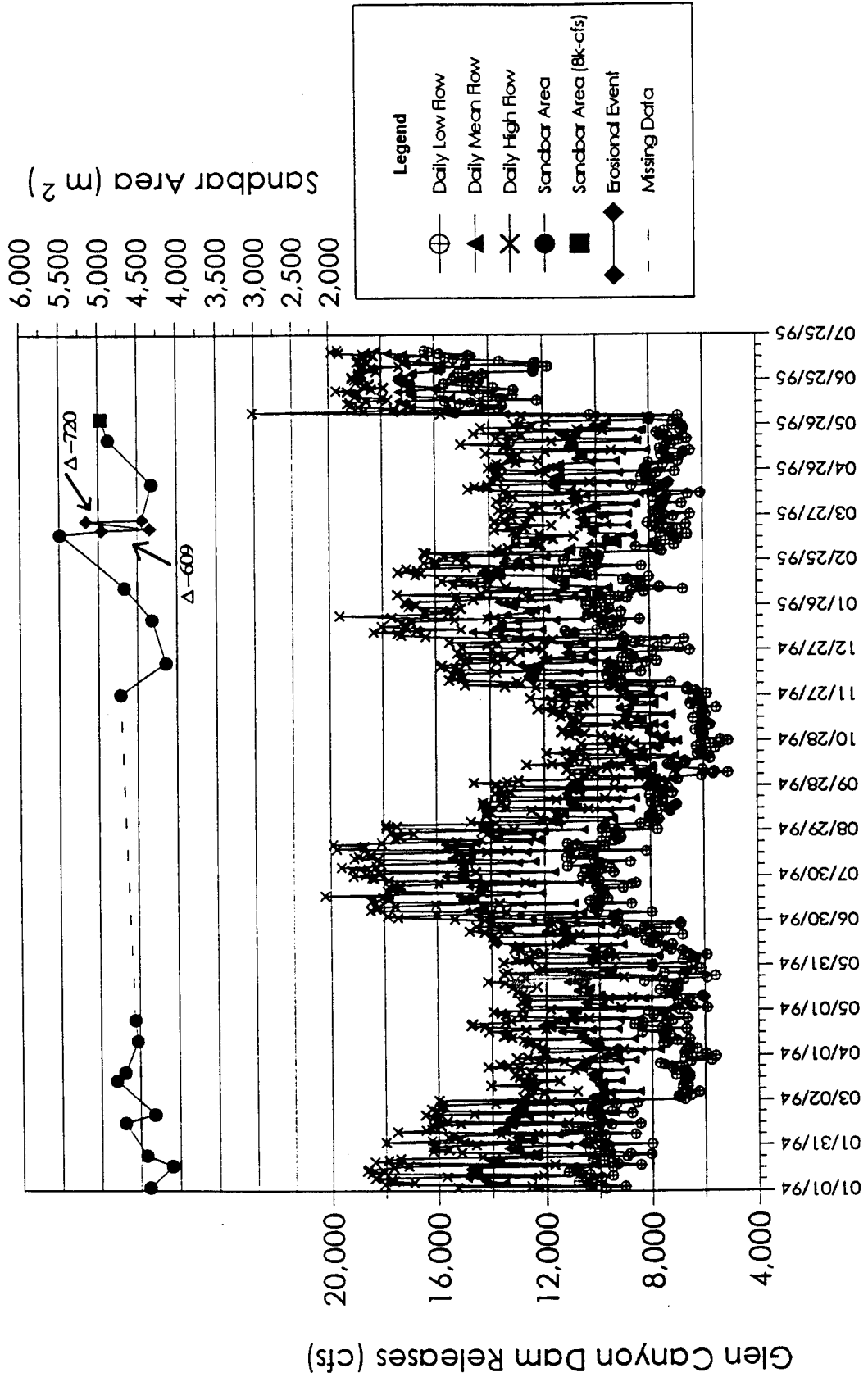


Fig. 24. Time-series plot showing area and discharge for sandbar 61.8R.

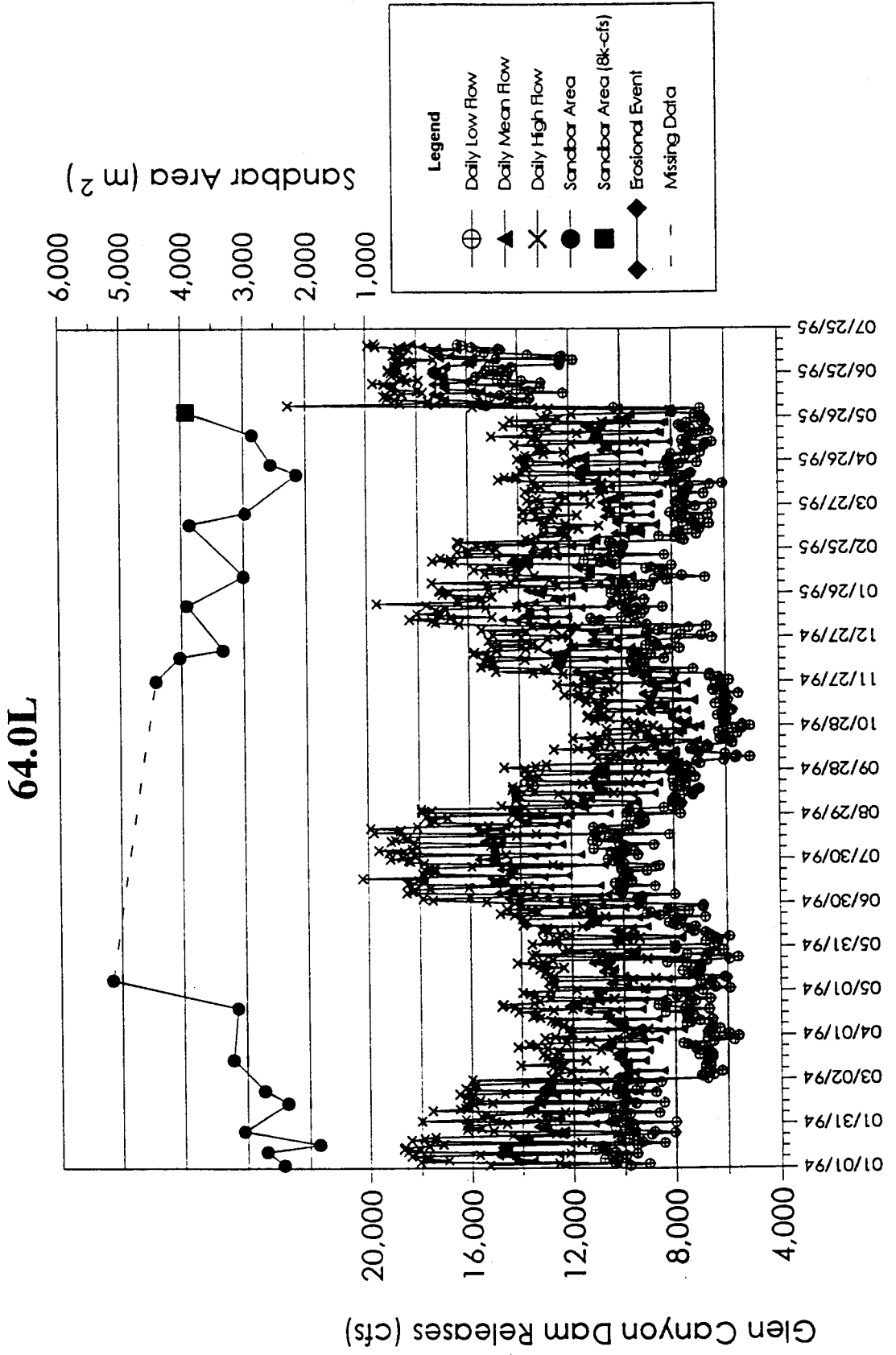


Fig. 25. Time-series plot showing area and discharge for sandbar 64.0L.

81.2L

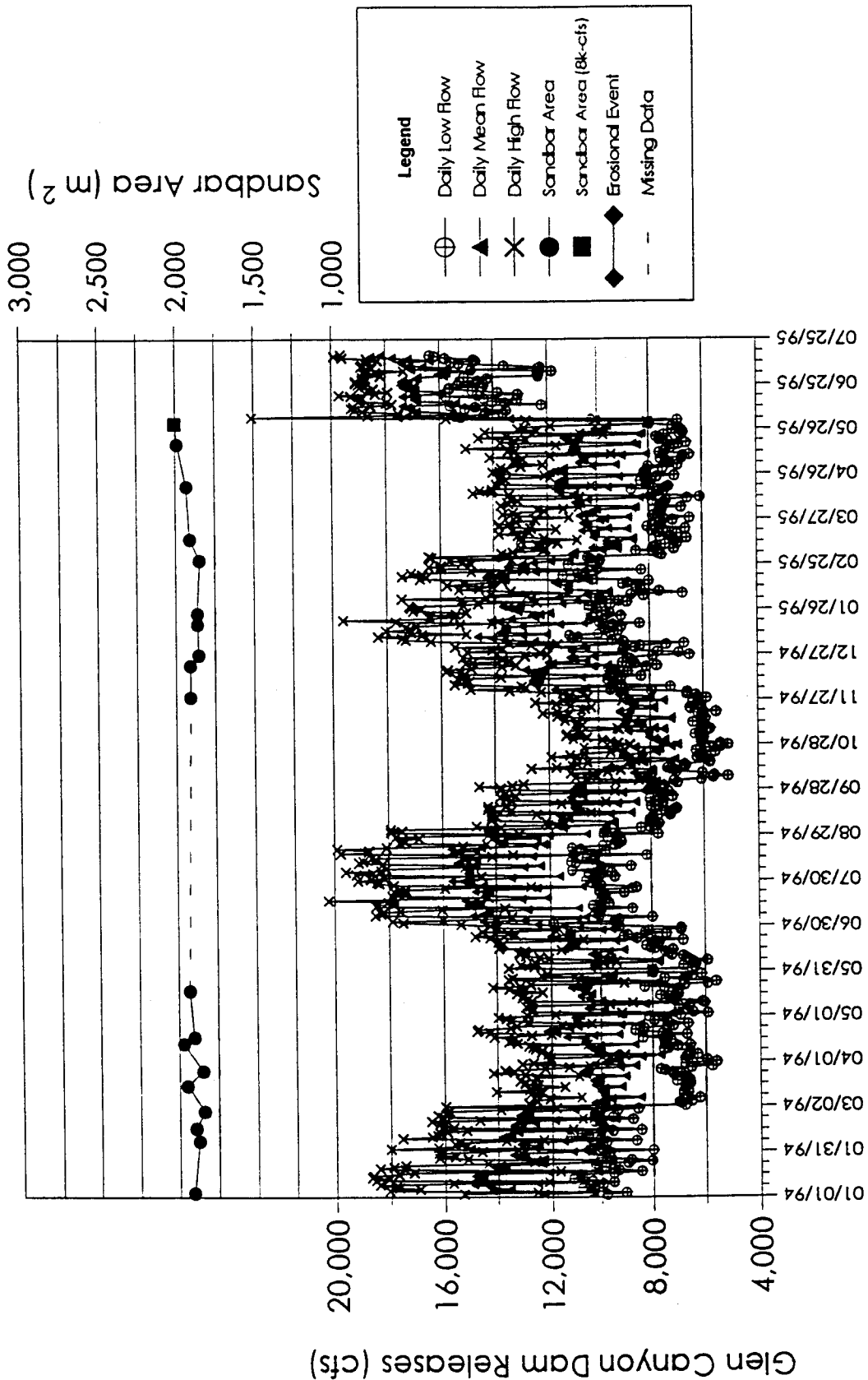


Fig. 26. Time-series plot showing area and discharge for sandbar 81.2L.

119.0R

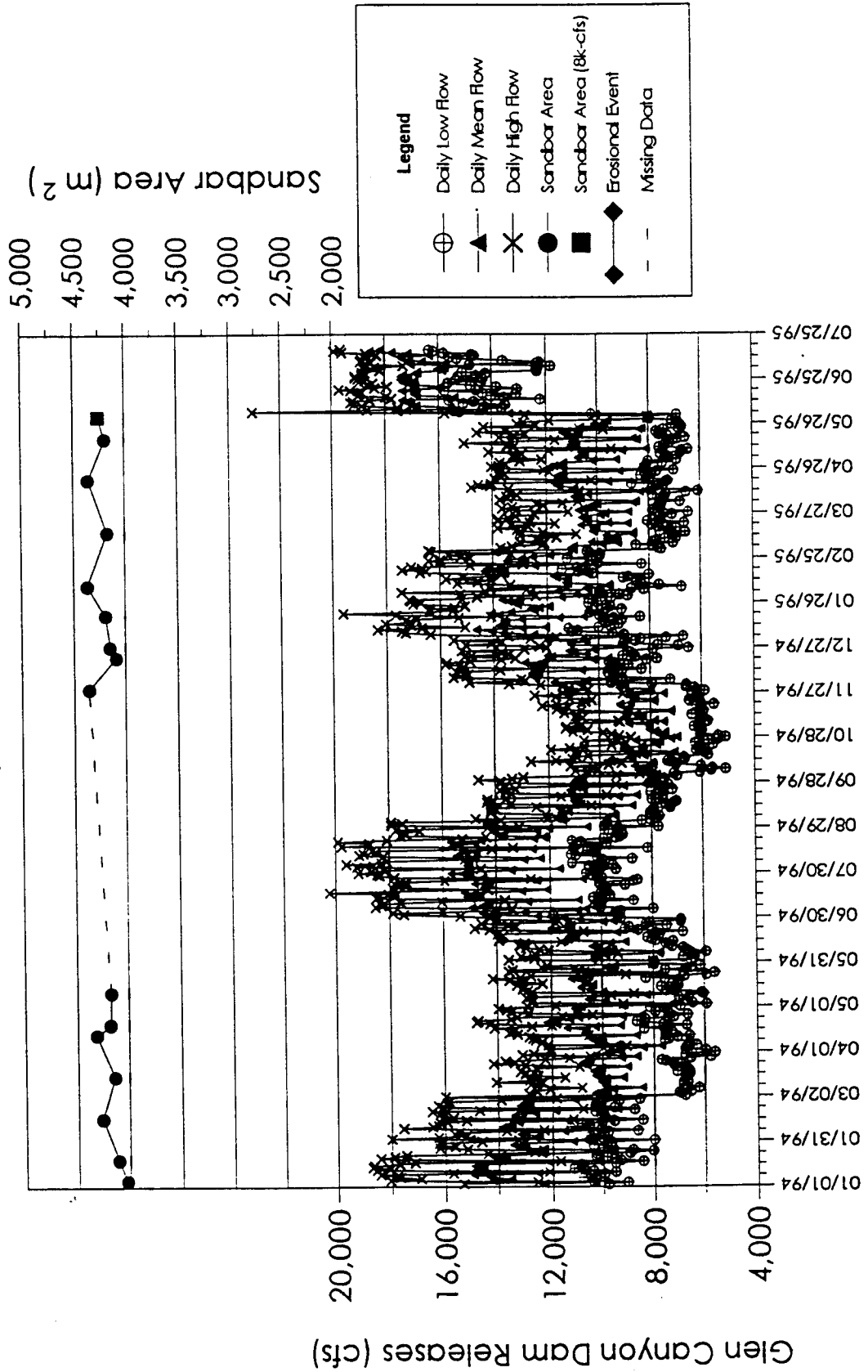


Fig. 27. Time-series plot showing area and discharge for sandbar 119.0R.

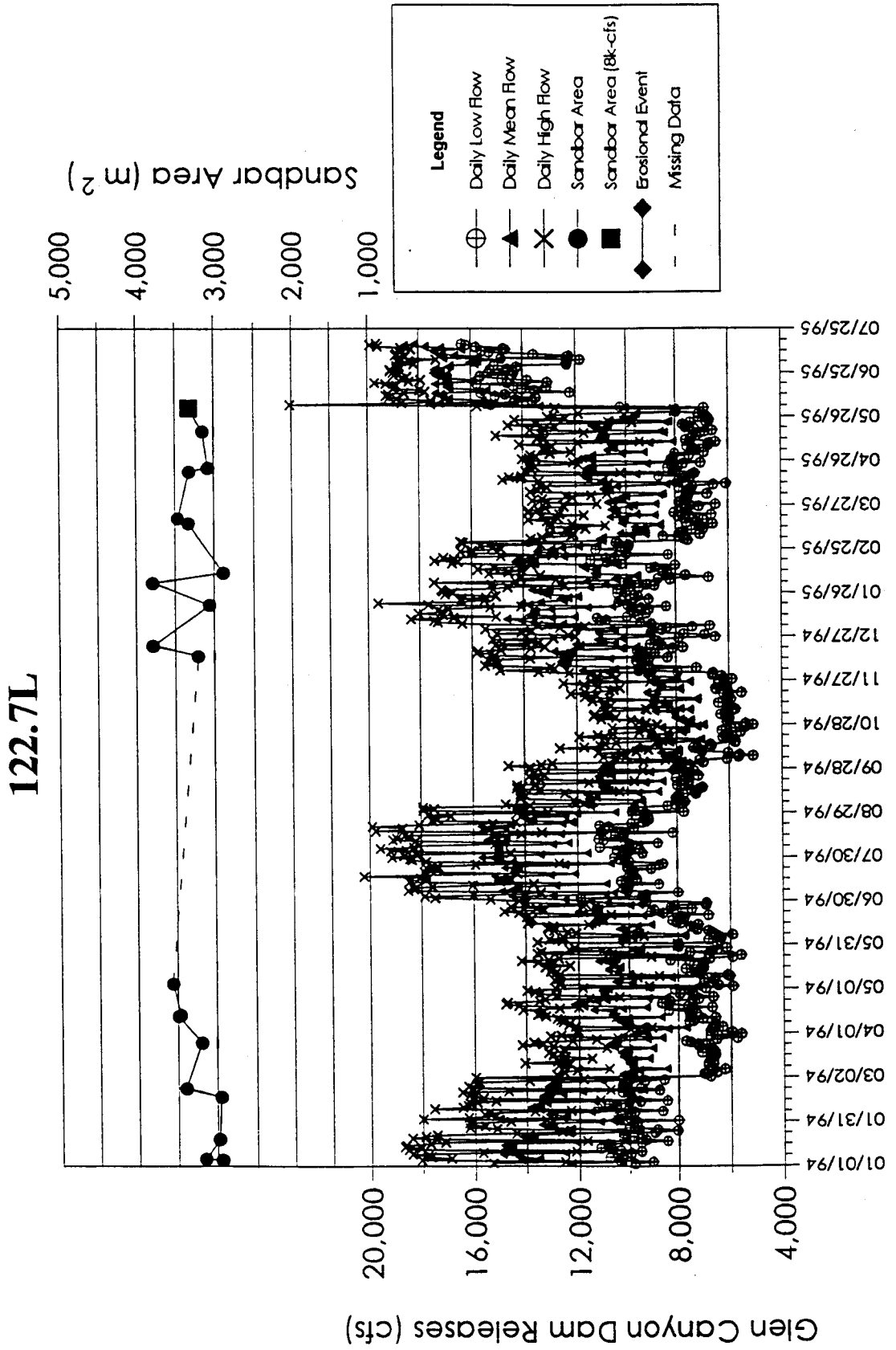


Fig. 28. Time-series plot showing area and discharge for sandbar 122.7L.

132.0R

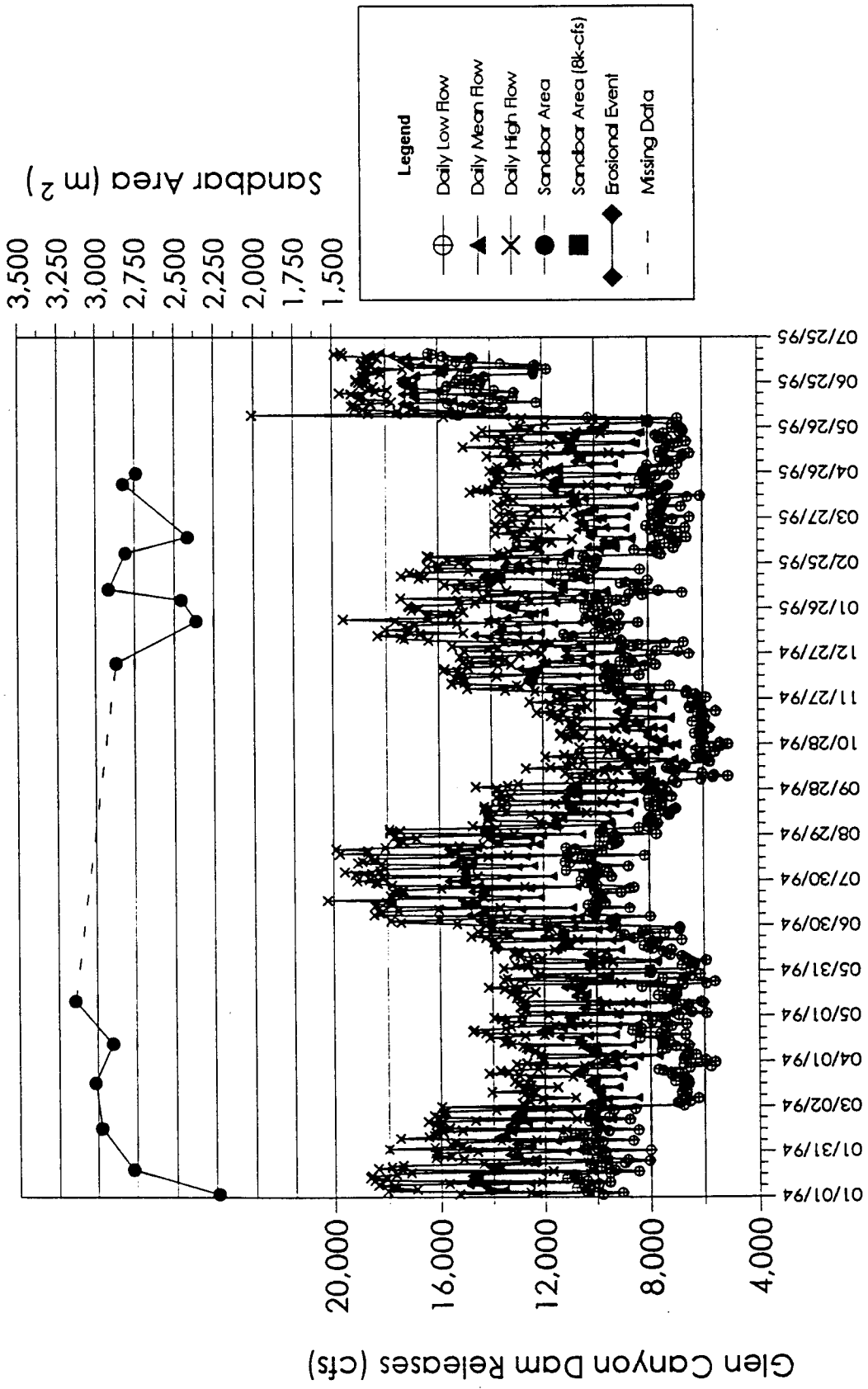


Fig. 29. Time-series plot showing area and discharge for sandbar 132.0R.

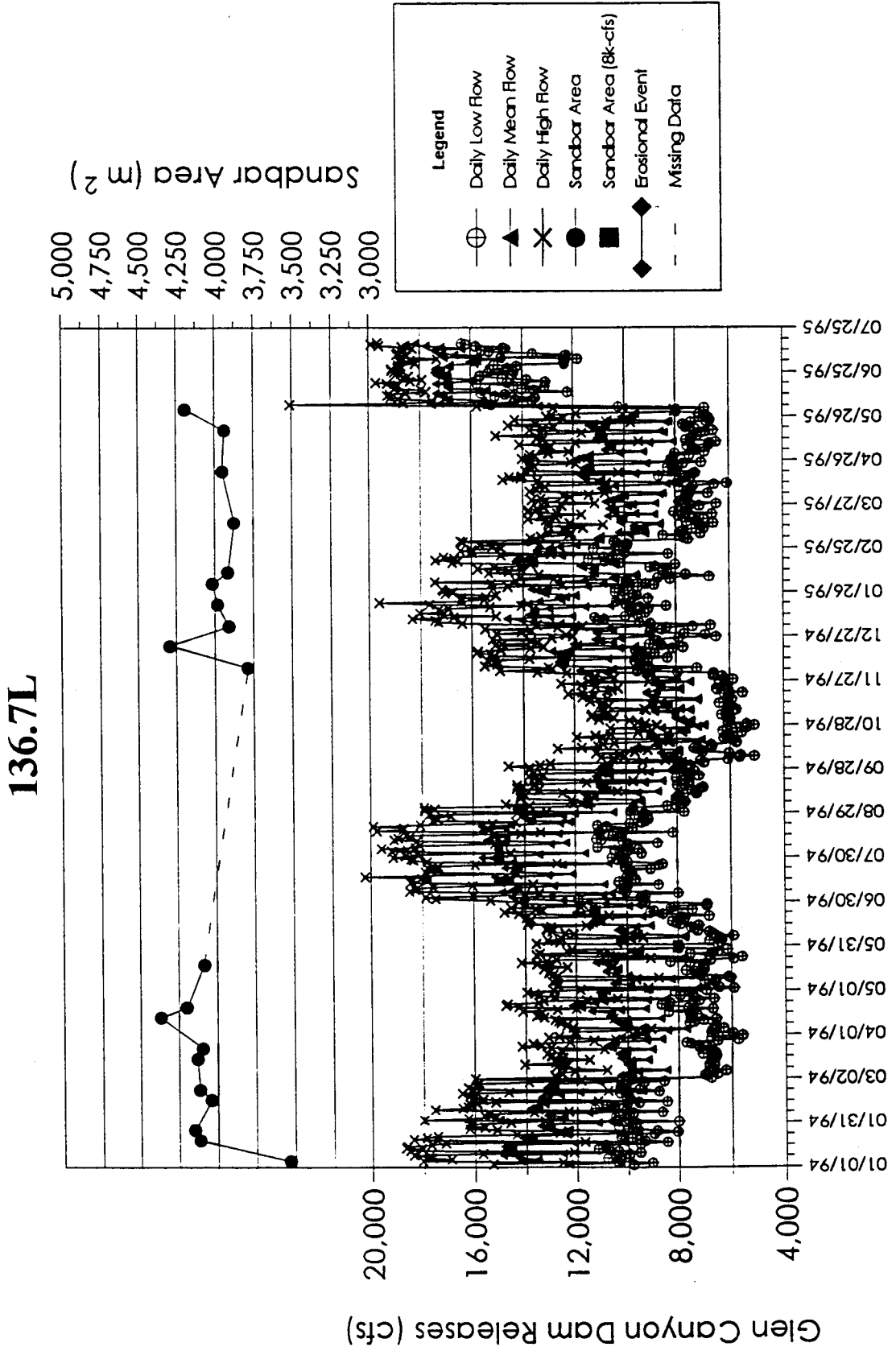


Fig. 30. Time-series plot showing area and discharge for sandbar 136.7L.

145.5L

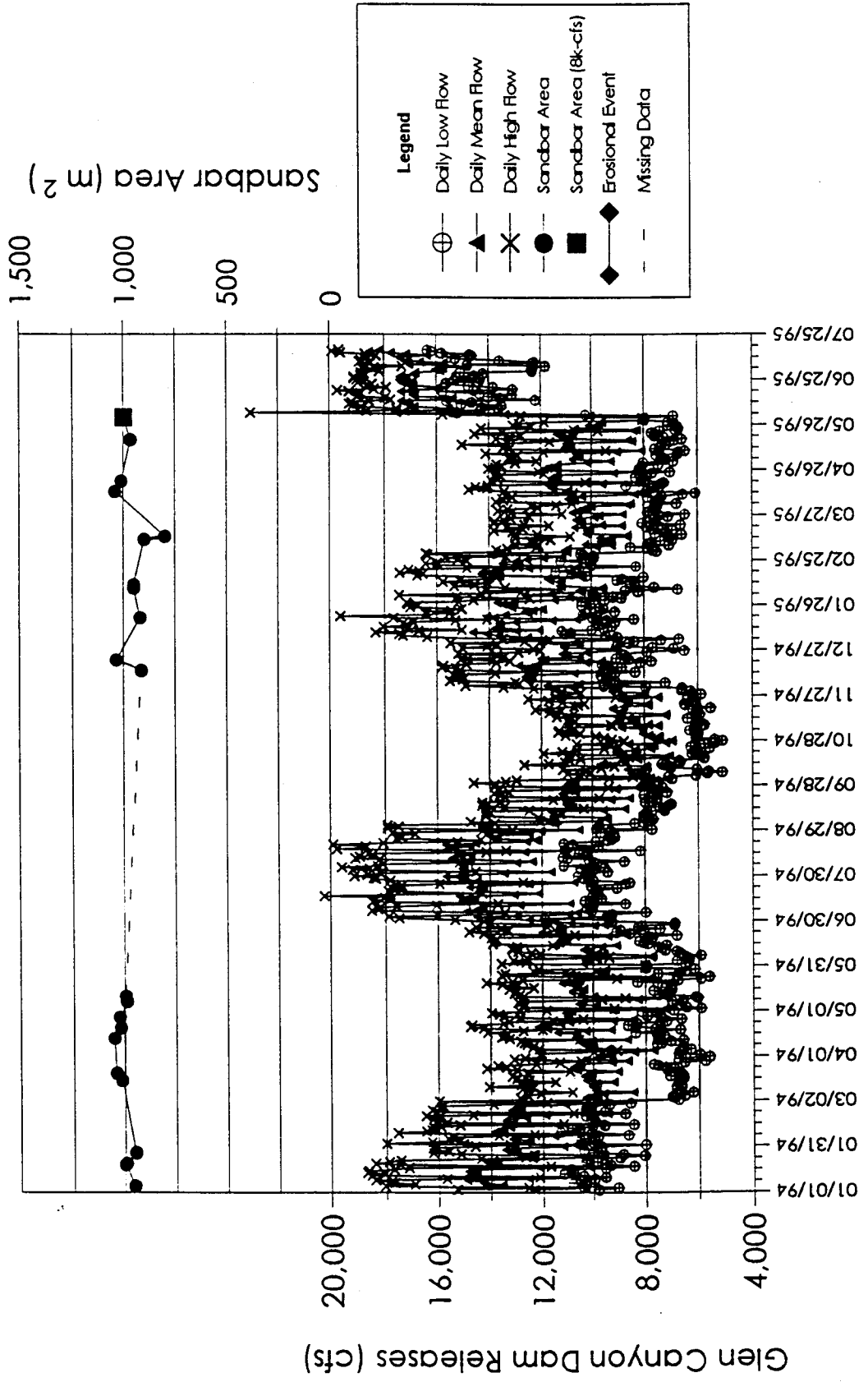


Fig. 31. Time-series plot showing area and discharge for sandbar 145.5L.

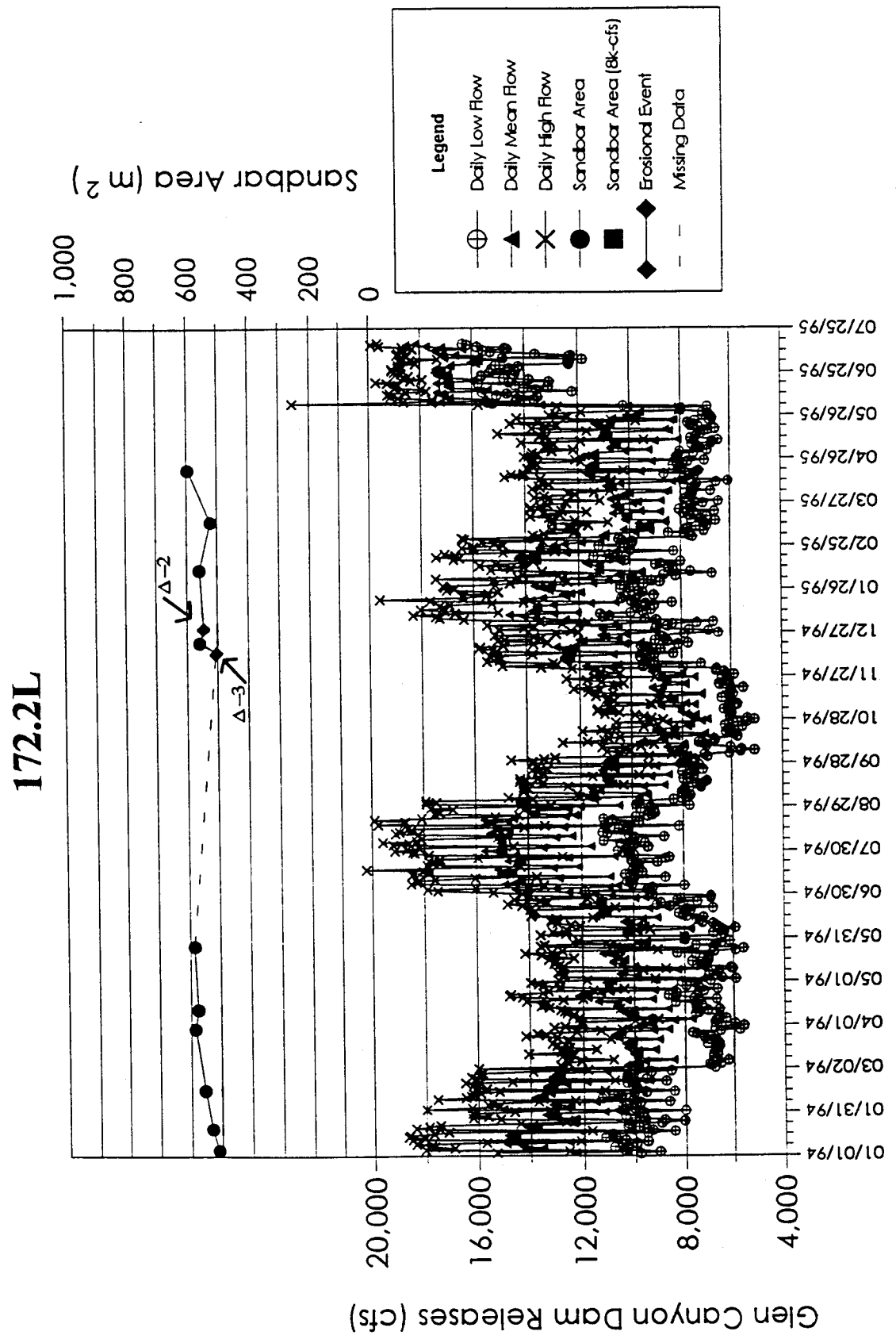


Fig. 32. Time-series plot showing area and discharge for sandbar 172.2L.

172.3L

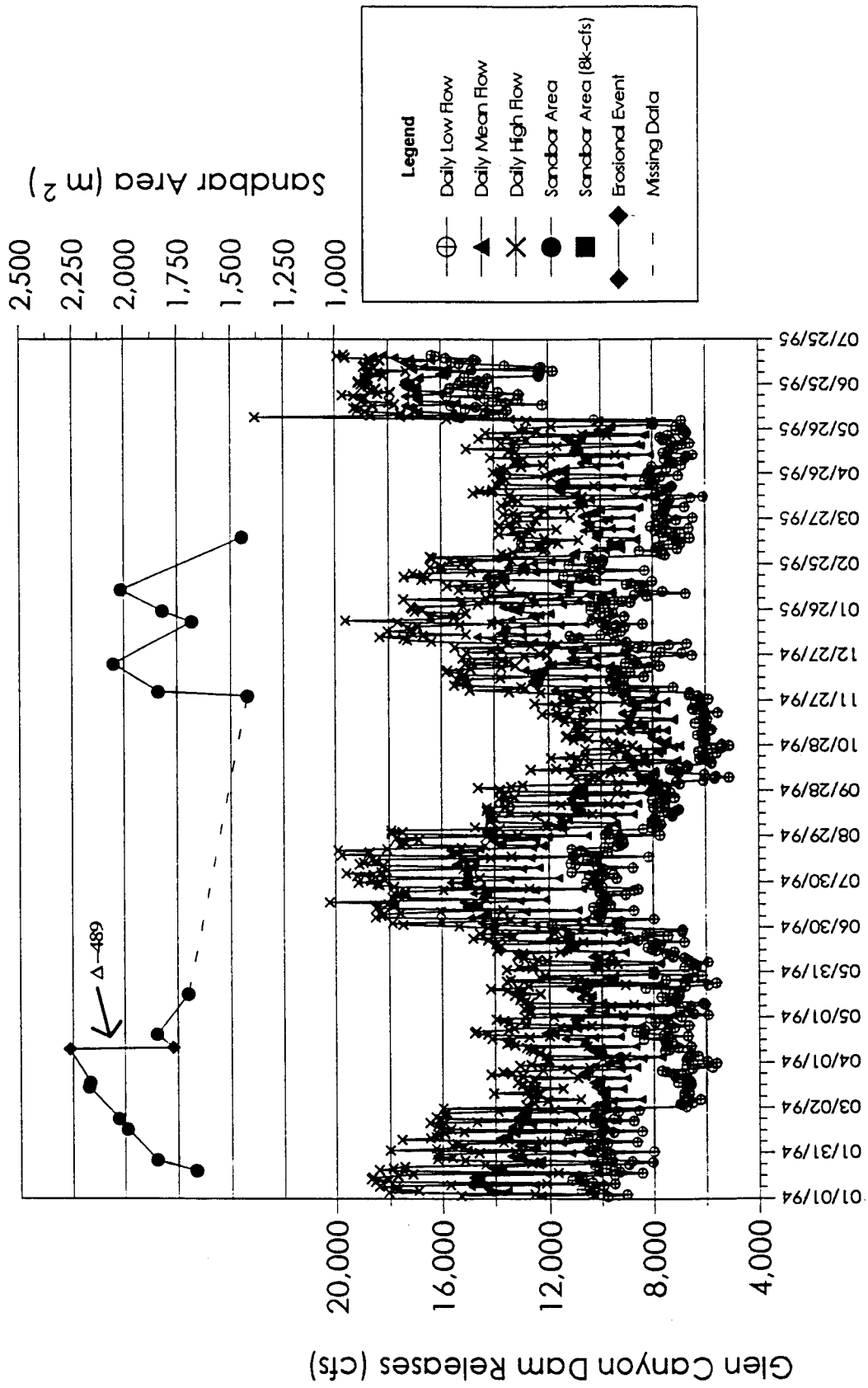


Fig. 33. Time-series plot showing area and discharge for sandbar 172.3L.

173.1L

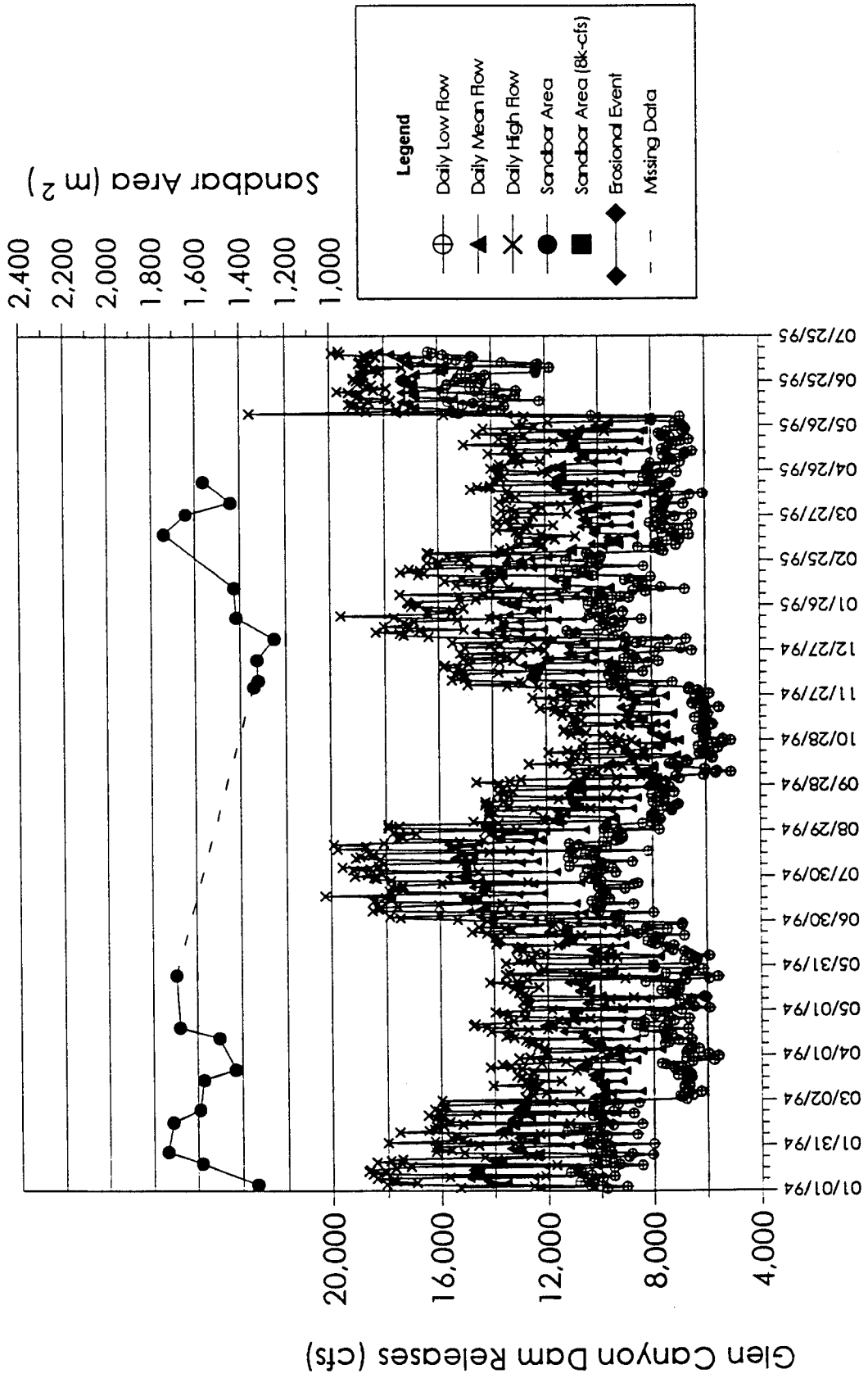


Fig. 34. Time-series plot showing area and discharge for sandbar 173.1L..

211.3L

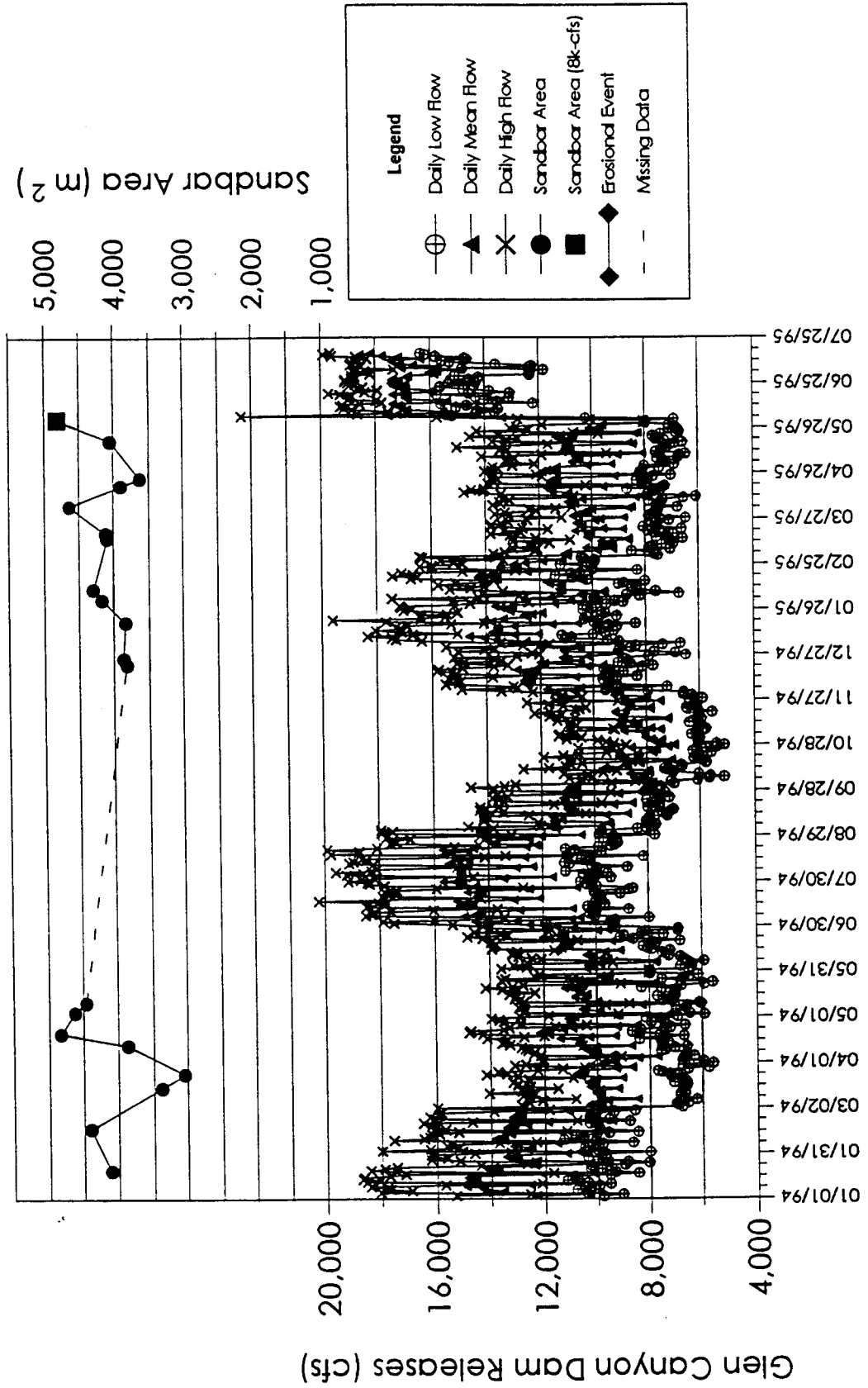


Fig. 35. Time-series plot showing area and discharge for sandbar 211.3L.

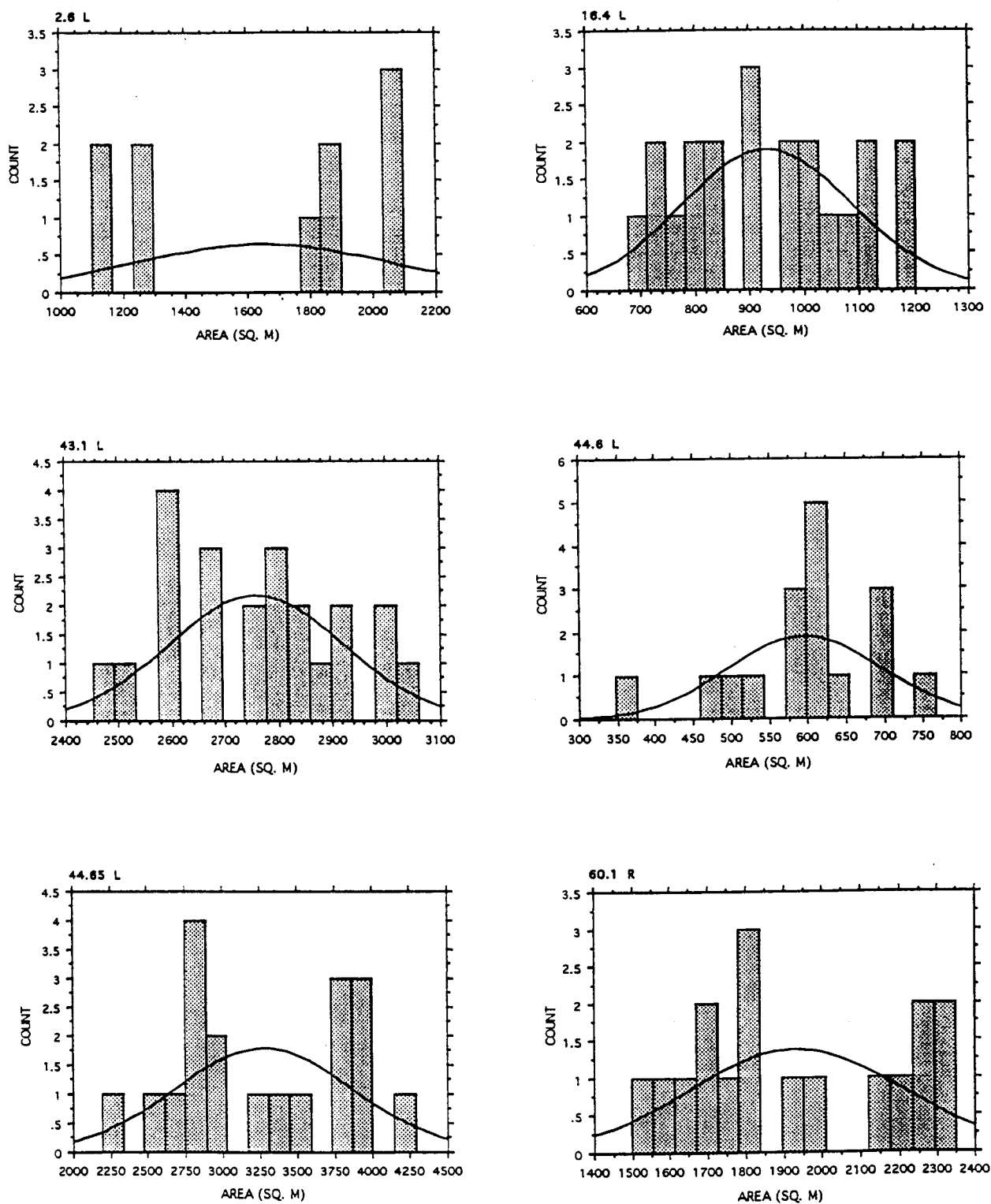


Fig. 36. Composite figure of frequency distributions for the eighteen rectified sandbars, January 1, 1994 (mjd 672) through June 1, 1995 (mjd 1188).

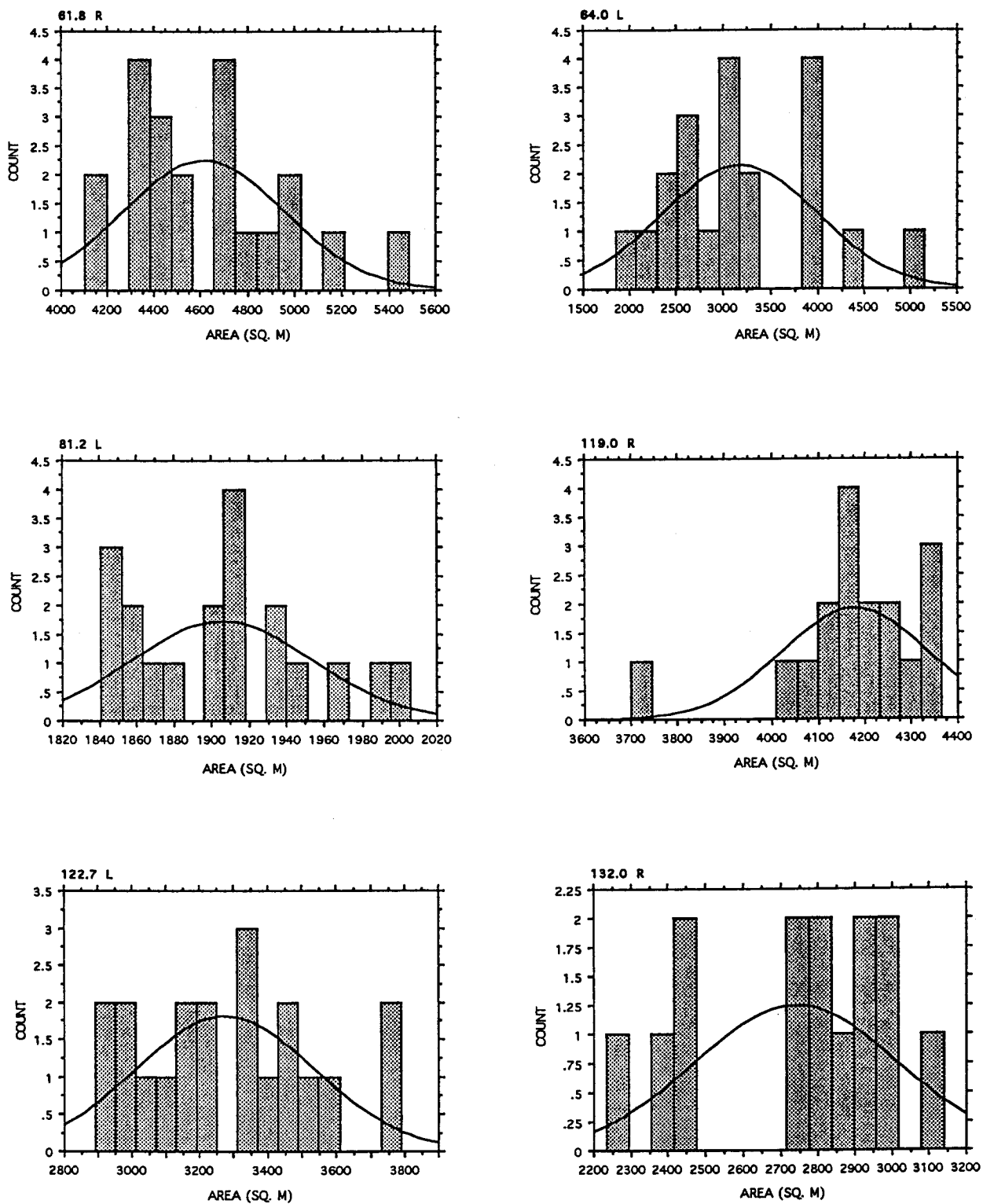


Fig. 36 (Continued). Composite figure of frequency distributions for the eighteen rectified sandbars, January 1, 1994 (mjd 672) through June 1, 1995 (mjd 1188).

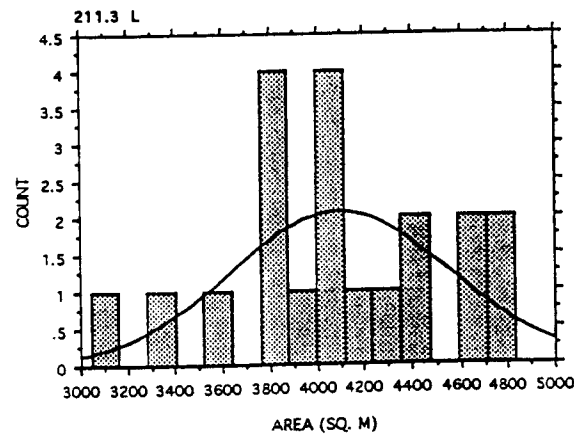
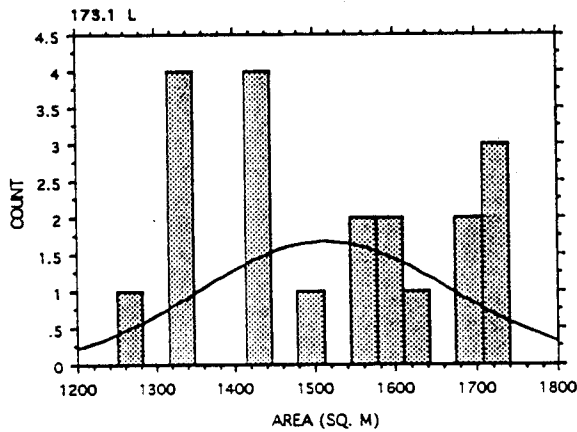
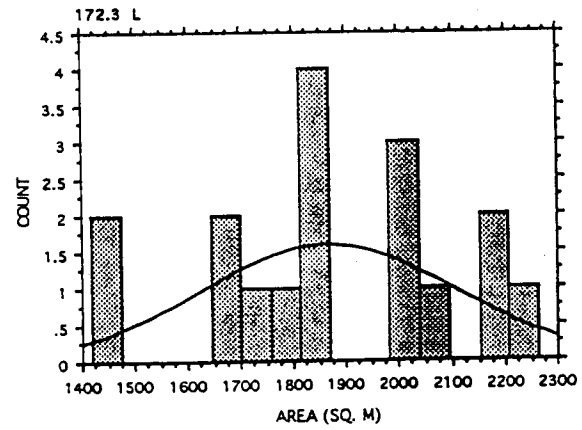
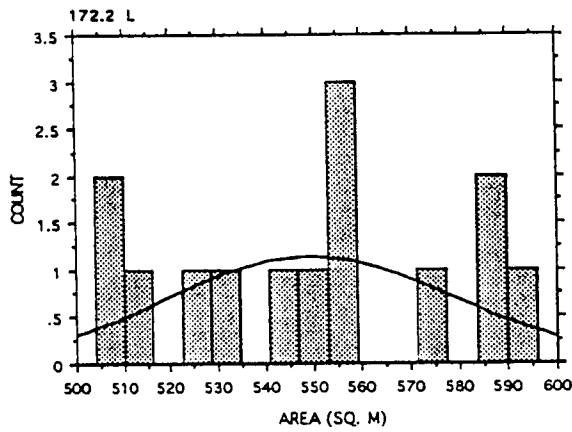
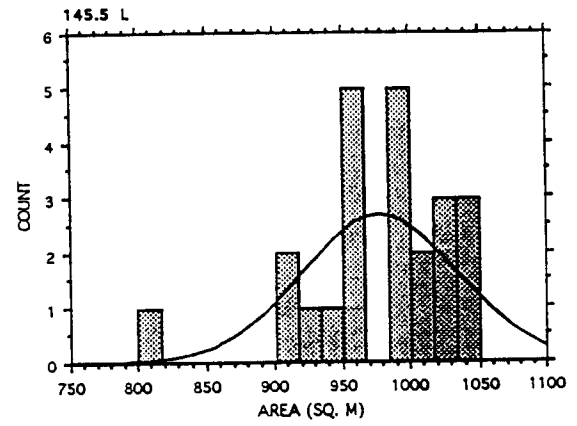
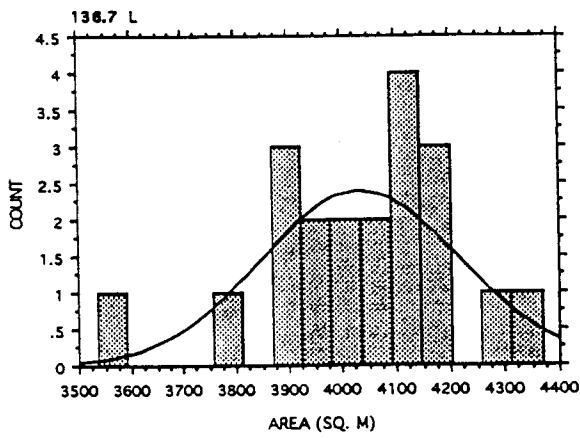


Fig. 36 (Continued). Composite figure of frequency distributions for the eighteen rectified sandbars, January 1, 1994 (mjd 672) through June 1, 1995 (mjd 1188).

Table 7. Summary Statistics for the eighteen rectified sandbars included in the extension study. Time span covers January 1, 1994 to June 1, 1995.

PARAMETER	S.I.	BEGIN AREA	END AREA	%CH/ TIME	MAX AREA	MIN AREA	%TOT AREA DIFF	MEAN AREA	ST. DEV. AREA	CV	A-Q INDEX	REACH INDEX	WIDTH INDEX	# EVENTS	X EV SZ
SANDBAR															
2.6L	1	1241	1893	52.54	2101	1101	47.6	1645	417	0.253	25.60	1	2	0	0
16.4L	2	824	955	15.9	1202	676	43.76	932	157	0.168	0.70	2	1	0	0
43.1L	3	2797	2678	-4.25	3060	2452	19.87	2759	164	0.059	5.28	4	2	1	14
44.6L	2	579	696	20.21	766	347	54.7	595	100	0.168	1.09	4	3	0	0
44.65L	1	3528	3890	10.26	4286	2194	48.81	3280	595	0.181	9.57	4	3	0	0
60.1R	1	2333	1824	-21.82	2349	1498	36.23	1931	281	0.146	4.54	4	2	0	0
61.8R	2	4382	4967	13.35	5487	4105	25.19	4616	344	0.075	4.59	5	2	2	665
64.0L	2	2409	3921	62.76	5153	1850	64.1	3179	826	0.26	8.45	5	3	0	0
81.2L	3	1907	2006	5.19	2006	1841	8.23	1910	50	0.026	0.56	6	1	0	0
119.0R	3	3700	4257	15.05	4365	3700	15.23	4180	157	0.038	2.23	7	2	0	0
122.7L	2	2935	3321	13.15	3789	2892	23.67	3277	264	0.081	0.70	7	3	1	44
132.0R	1	2233	2738	22.62	3140	2233	28.89	2744	271	0.099	3.38	8	2	0	0
136.7L	3	3535	4190	18.53	4369	3535	19.09	4035	186	0.046	0.42	8	2	0	0
145.5L	3	956	998	4.39	1051	800	23.88	978	60	0.061	0.02	9	1	2	27
172.2L	2	512	596	16.41	596	504	15.44	549	30	0.055	0.76	10	2	2	2
172.3L	1	1665	1447	-13.09	2263	1419	37.3	1866	241	0.129	0.01	10	2	1	489
173.1L	2	1335	1560	16.85	1741	1251	28.14	1514	156	0.103	0.01	10	2	0	0
211.3L	3	4115	4811	16.91	4829	3045	36.94	4095	459	0.112	0.11	10	2	0	0
MEAN	2	2338	2597	15	2920	1969	32	2449	264	0.11	3.79	6	2	1	78
ST. DV.	1	1247	1465	20	1576	1138	15	1305	205	0.07	6.22	3	1	1	198

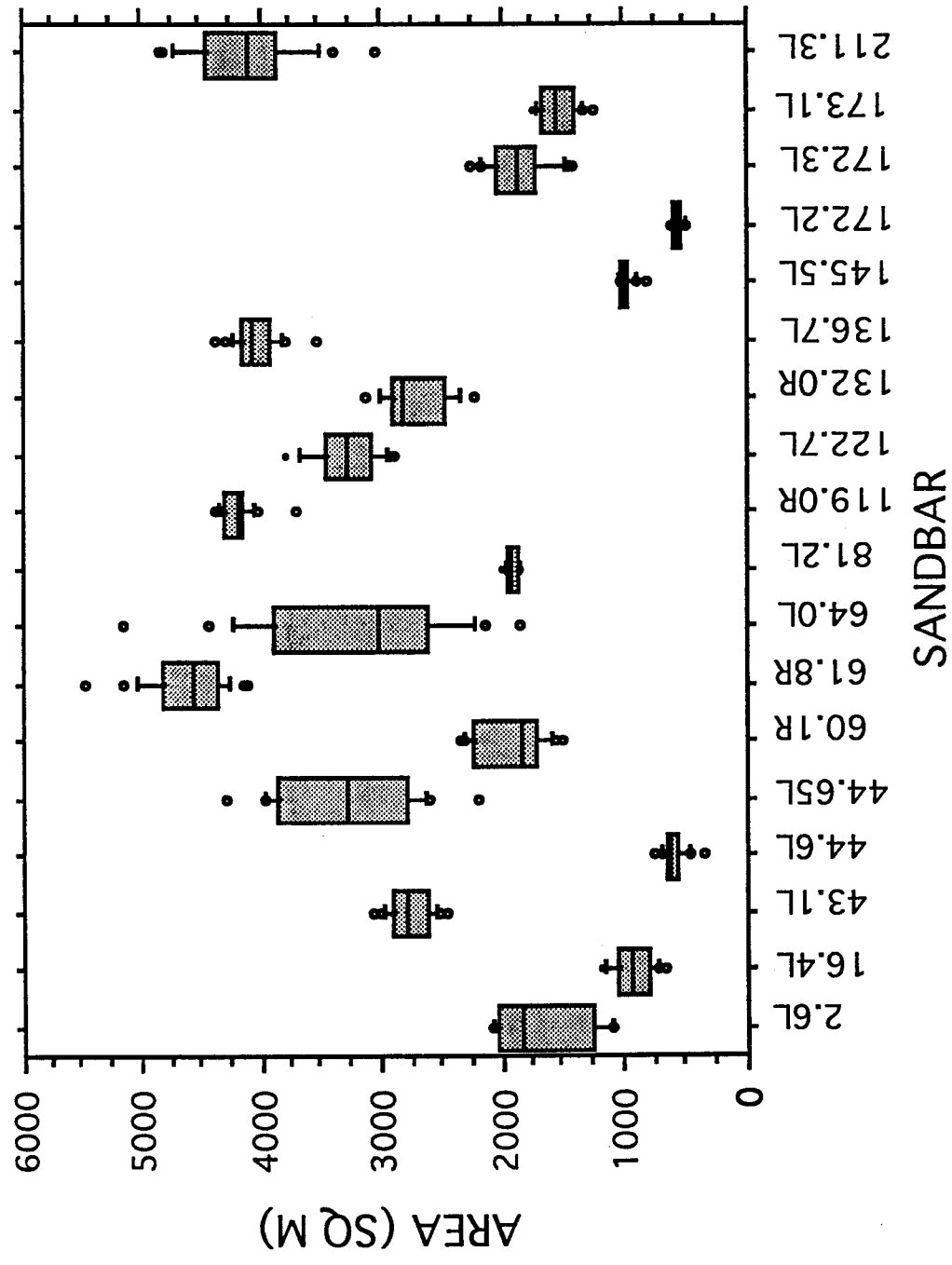


Fig. 37. Box and whisker plots of sandbar area value distribution. The line near the middle of the box is the median, the top of the box is the 75th percentile, the bottom of the box is the 25th percentile, the top whisker is the 90th percentile and the bottom whisker is the 10th percentile. Dots represent individual extreme values. True horizontal axis scale is not implied.

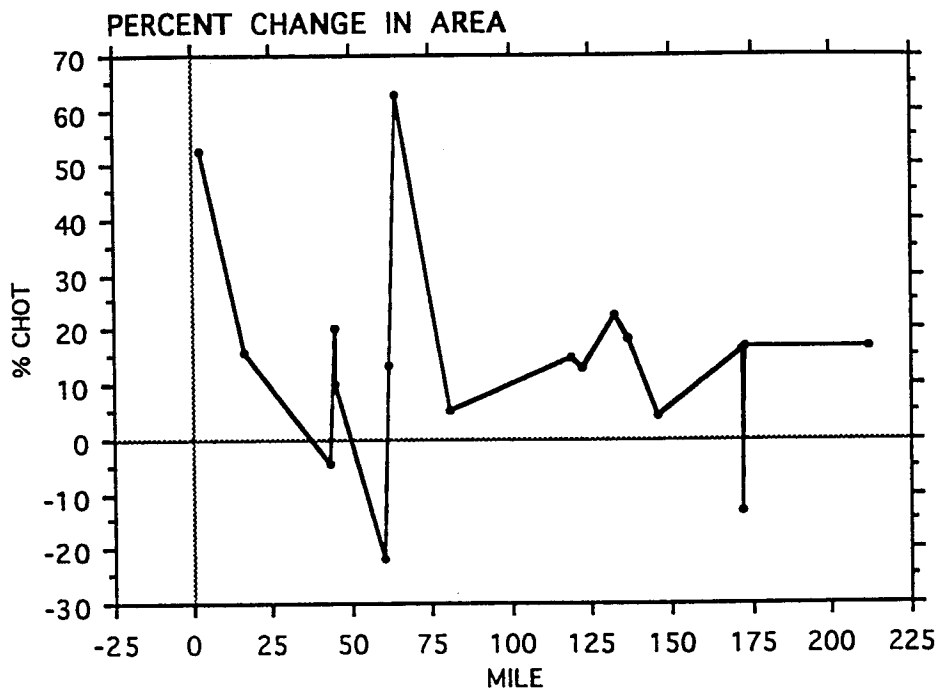


Fig. 38. Relationship between river mile and percent change in sandbar area.

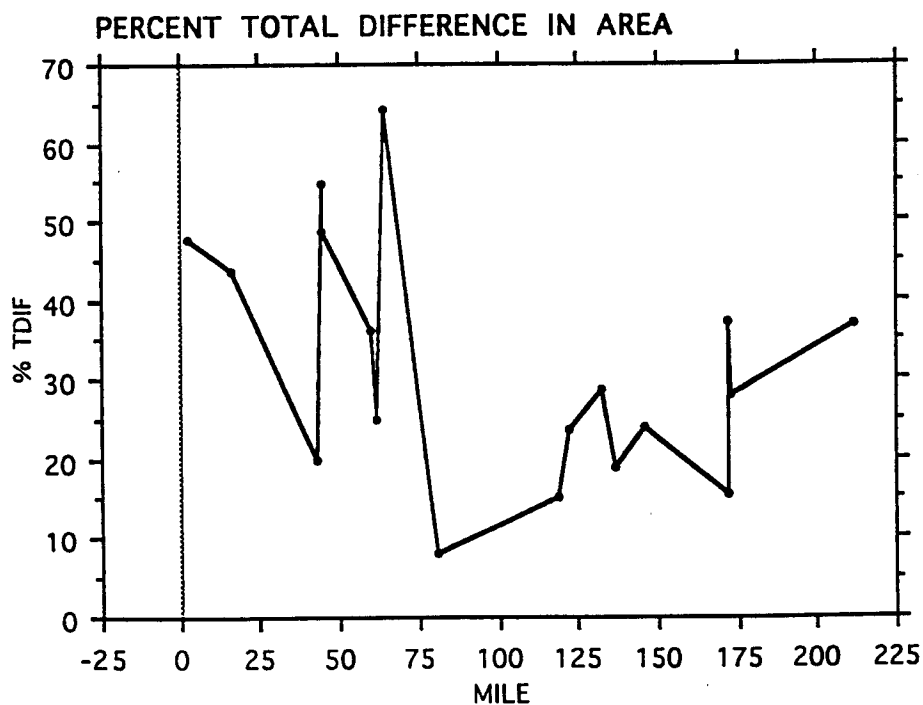


Fig. 39. Relationship between river mile and percent total difference in sandbar area.

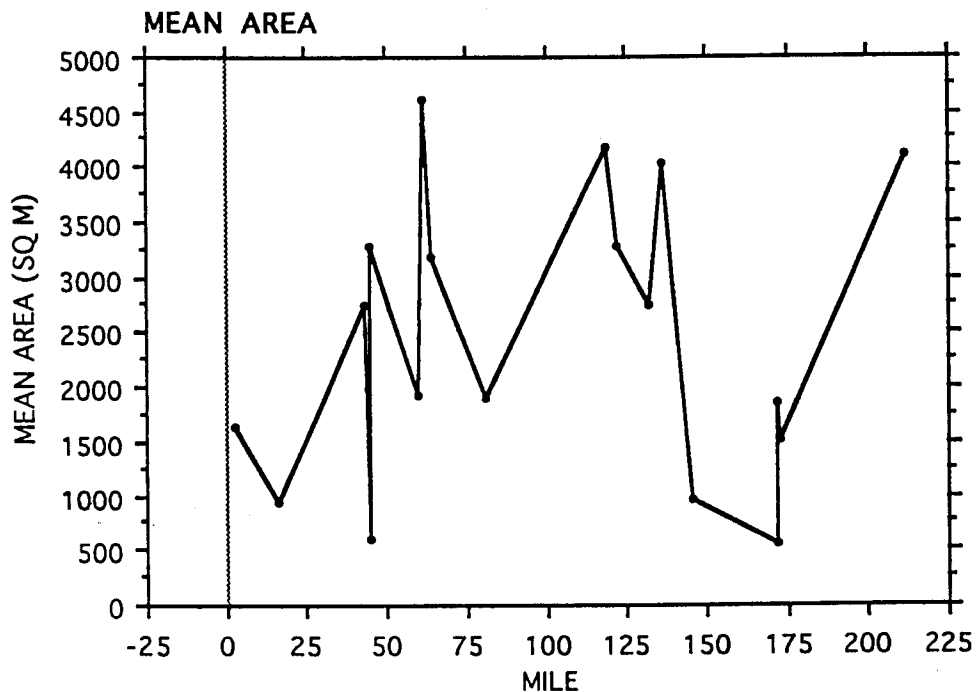


Fig. 40. Relationship between river mile and mean sandbar area.

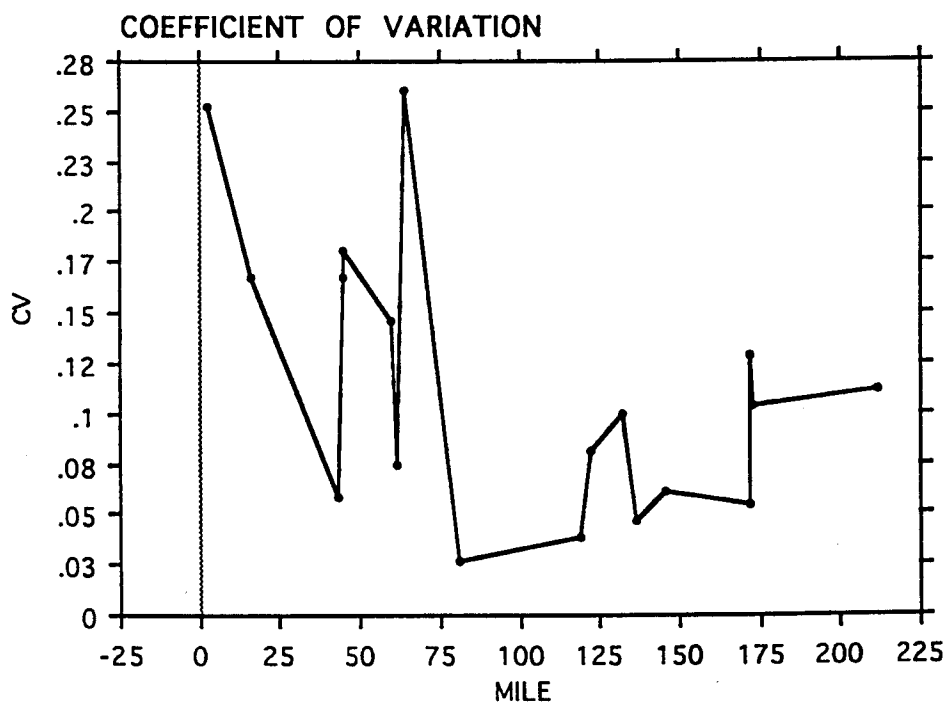


Fig. 41. Relationship between river mile and sandbar coefficient of variation.

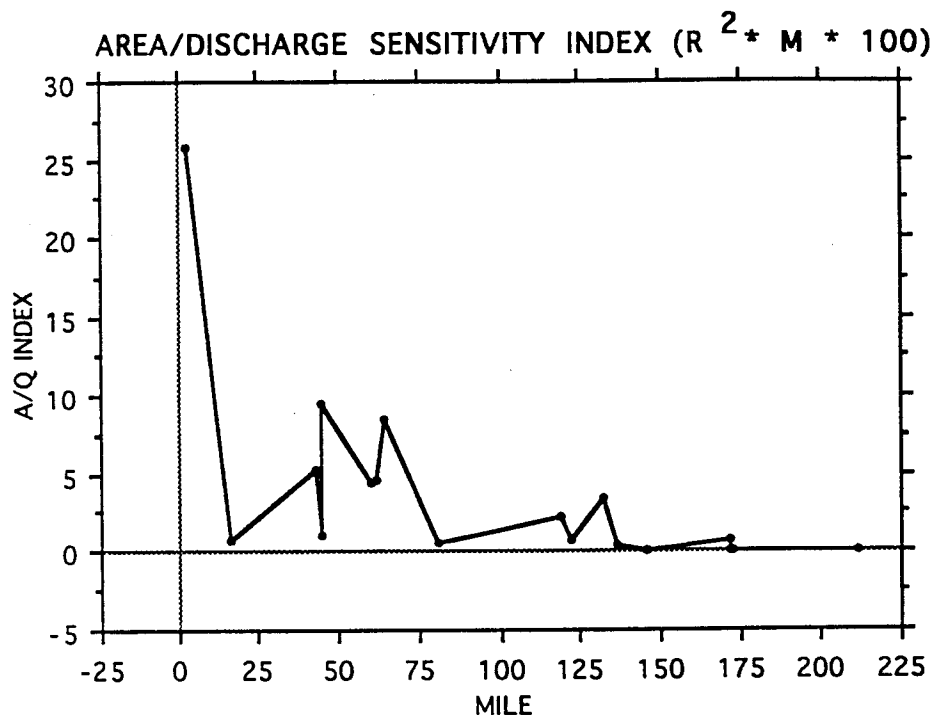


Fig. 42. Relationship between river mile and sandbar area/discharge sensitivity index.

Table 8. A summary of frequency distribution characteristics of the eighteen rectified sandbars incuded in the extension study compared to a synthetically generated, normally distributed, simulated sandbar.

PARAMETER	COUNT	LOWER	LOWER %	MEAN	MEAN %	UPPER	UPPER %	KURTOSIS	SKEWNESS	MODE	NORM	SAME
SANDBAR												
NORMAL	35	10	29	15	43	10	29	0.08	-0.04	UNI	Y	Y
2.6L	10	4	40	0	0	4	40	-1.69	-0.29	BI		N
16.4L	21	8	38	5	24	8	38	-1.05	0.16	UNI		Y
43.1L	22	9	41	5	23	7	32	-0.87	0.01	BI		Y
44.6L	17	4	24	8	47	4	24	0.6	-0.71	UNI	Y	Y
44.65L	19	9	47	2	11	9	47	-1.21	-0.01	BI		Y
60.1R	17	9	53	2	12	6	35	-1.35	0.2	BI		Y
61.8R	21	9	43	6	29	4	19	0.18	0.72	BI		Y
64.0L	20	7	35	7	35	6	30	-0.1	0.61	BI		Y
81.2L	19	7	37	6	32	5	26	-0.61	0.51	BI		Y
119.0R	17	3	18	6	35	5	29	3.24	-0.61	BI		N
122.7L	20	8	40	6	30	6	30	-0.68	0.39	BI		Y
132.0R	14	5	36	4	29	6	43	-0.83	-0.57	BI		NEW
136.7L	20	5	25	6	30	9	45	0.97	-0.71	BI	Y	Y
145.5L	23	4	17	10	43	8	35	2.07	-1.29	UNI	N	N
172.2L	14	5	36	5	36	4	29	-1.17	-0.63	BI?	Y?	Y?
172.3L	17	5	29	5	29	7	41	-0.66	-0.23	BI	N	N
173.1L	20	9	45	3	15	7	35	-1.31	-0.03	BI	Y	Y
211.3L	20	7	35	6	30	6	30	-0.15	-0.34	BI	Y	Y

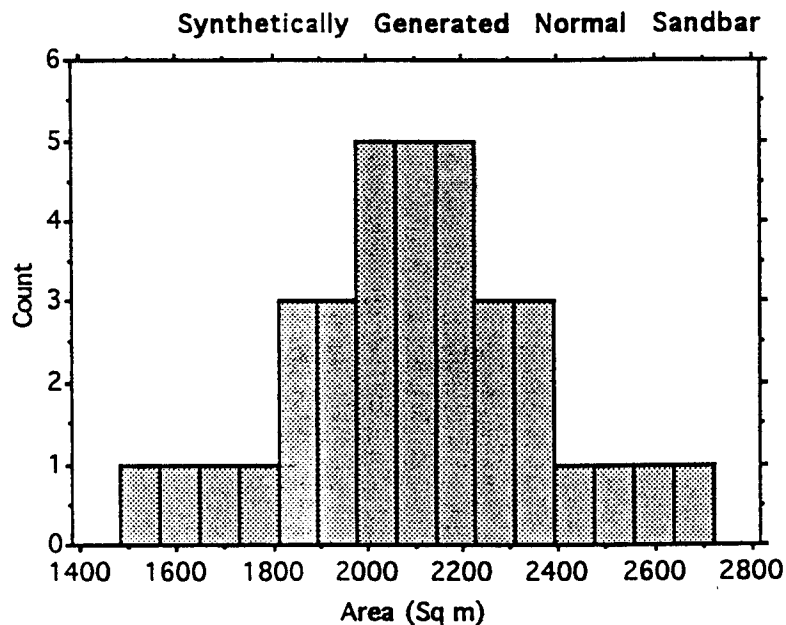


Fig. 43. Frequency distribution of a synthetic sandbar. This normal distribution was generated to produce area values and a sample size similar to that acquired for actual sandbars.

Table 9. Summary statistics for the synthetic normal sandbar distribution.

Mean:	Std. Dev.:	Std. Error:	Variance:	Coef. Var.:	Count:
2104.514	267.611	45.235	71615.904	12.716	35
Minimum:	Maximum:	Range:	Sum:	Sum of Sqr.:	# Missing:
1480	2717	1237	73658	157449254	0
# < 10th %:	10th %:	25th %:	50th %:	75th %:	90th %:
3	1793	1943.25	2100	2289.25	2415
# > 90th %:	Mode:	Geo. Mean:	Har. Mean:	Kurtosis:	Skewness:
3	•	2087.583	2070.149	.083	-.035

Table 10. Seasonal trends in sandbar area. Data in this table were derived by comparing seasonally averaged areas with the overall mean area for each sandbar. A class was assigned as 1 = smaller than average, 2 = average, and 3 = larger than average. An asterisk indicates insufficient data.

SEASON	WI94	SP94	SU94	FA94	WI95	SP95
SANDBAR						
2.6L	1	*	*	*	1	3
16.4L	3	3	*	1	1	*
43.1L	2	3	*	3	1	3
44.6L	3	3	*	3	1	*
44.65L	1	3	*	1	1	3
60.1R	1	3	*	3	2	3
61.8R	1	2	*	1	3	1
64.0L	1	3	*	3	3	1
81.2L	2	3	*	3	1	3
119.0R	2	3	*	3	3	3
122.7L	1	3	*	3	3	1
132.0R	2	3	*	3	1	2
136.7L	2	3	*	3	1	2
145.5L	3	3	*	2	1	3
172.2L	2	3	*	1	2	3
172.3L	3	2	*	1	1	*
173.1L	3	3	*	1	1	2
211.3L	1	3	*	1	2	2
SUM	34	49	*	36	29	35
MEAN	1.89	2.88	*	2.12	1.61	2.33
STD. DEV.	0.83	0.33	*	0.99	0.85	0.82

Table 11. Distribution characteristics within seasonal subsets of the eighteen rectified sandbars included in the extension study. Data represent numbers of individual frequency distributions from seasonally averaged area values showing each of the following diagnostic distribution characteristics.

<i>DISTRIBUTION</i>	<i>INSUFFICIENT DATA</i>	<i>BIMODAL</i>	<i>UNIMODAL/ SKEWED</i>	<i>UNIMODAL/ NO SKEW</i>	<i>TOTAL</i>
SEASON					
WI94	0	5	7	6	18
SP94	1	9	3	5	18
SU94	18				18
FA94	1	13	0	4	18
WI95	0	8	6	4	18
SP95	1	10	1	6	18
SU95	18				18
TOTAL	39	45	17	25	126
PERCENT	31	36	13	20	100

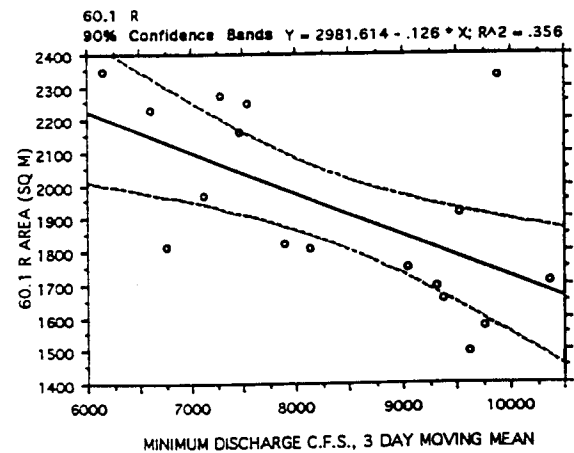
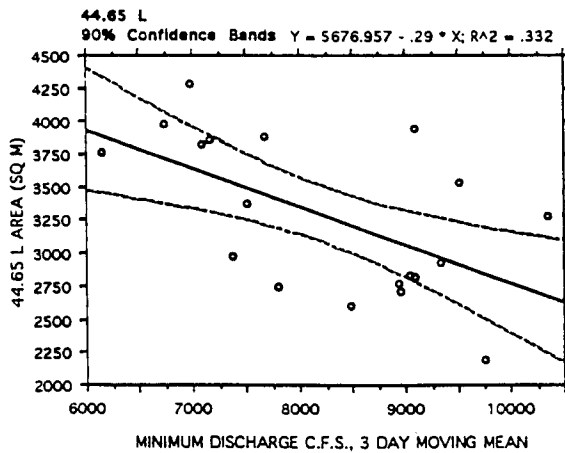
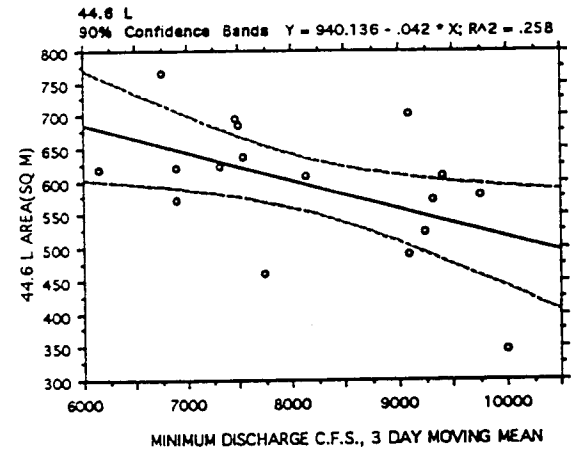
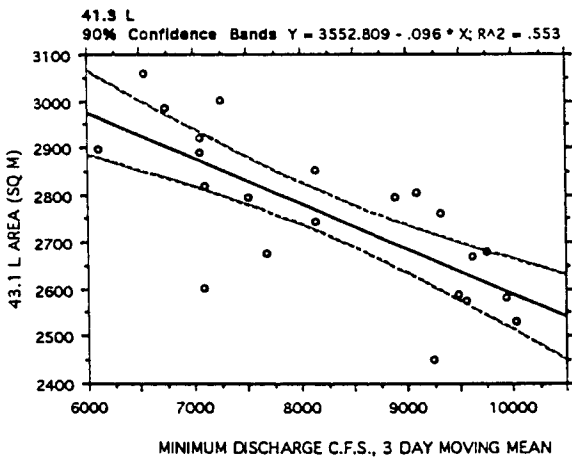
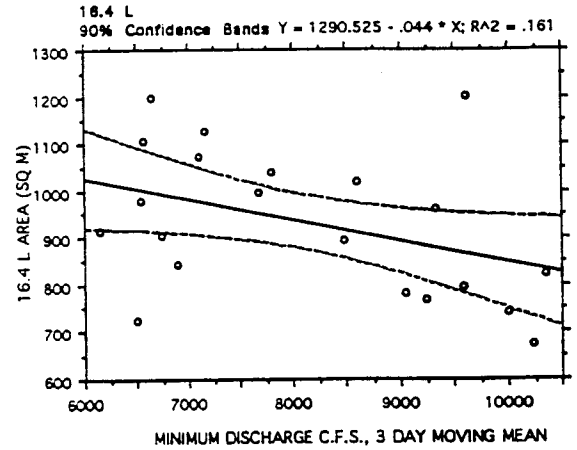
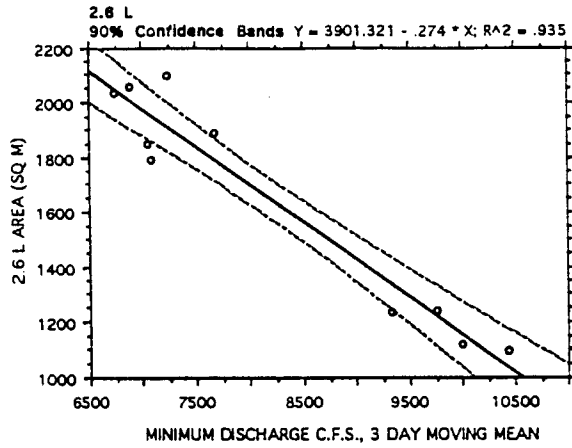


Fig. 44. Composite figure of discharge vs. area regressions for the eighteen rectified sandbars, January 1, 1994 (mjd 672) through June 1, 1995 (mjd 1188).

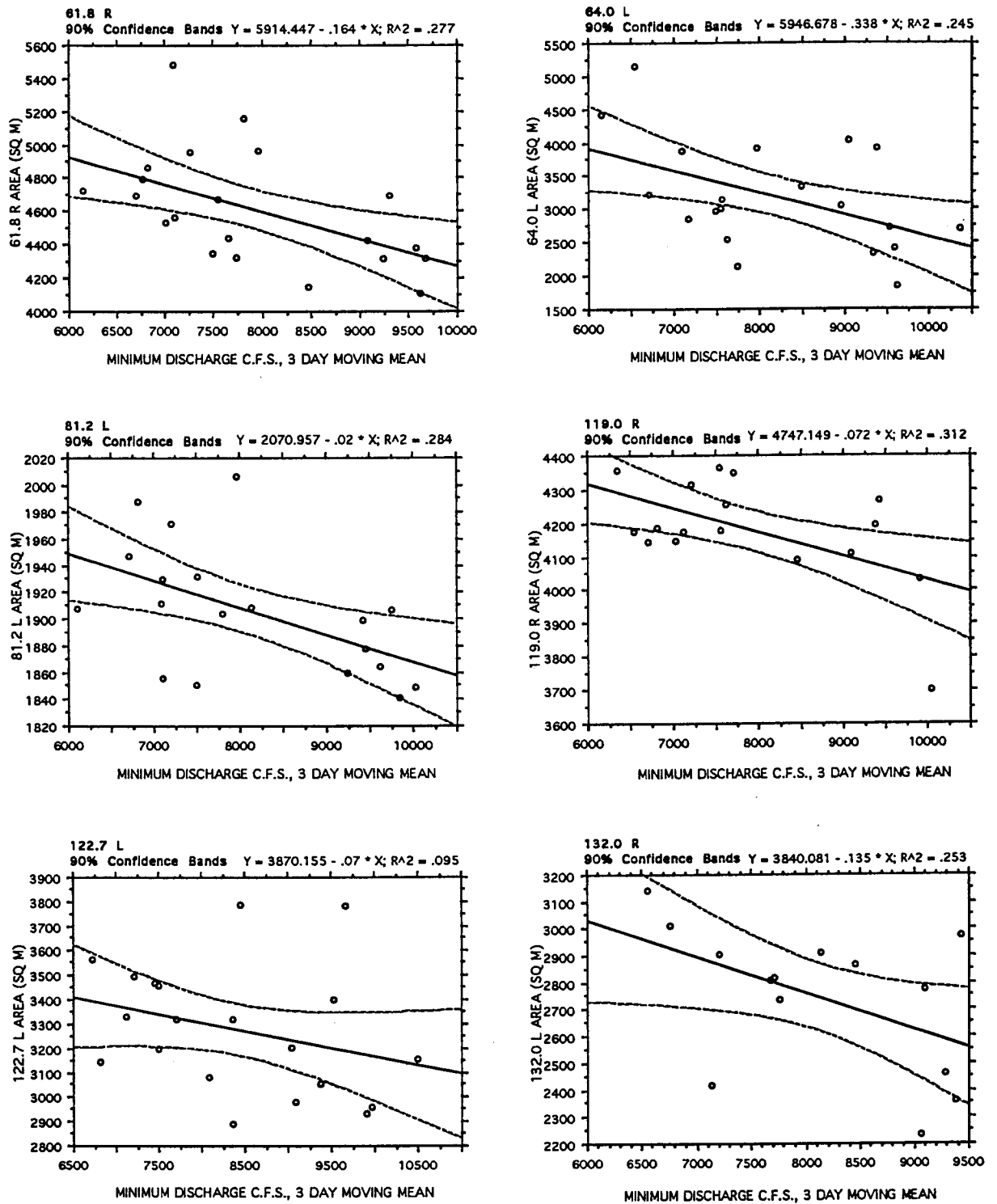


Fig. 44 (Continued). Composite figure of discharge vs. area regressions for the eighteen rectified sandbars, January 1, 1994 (mjd 672) through June 1, 1995 (mjd 1188).

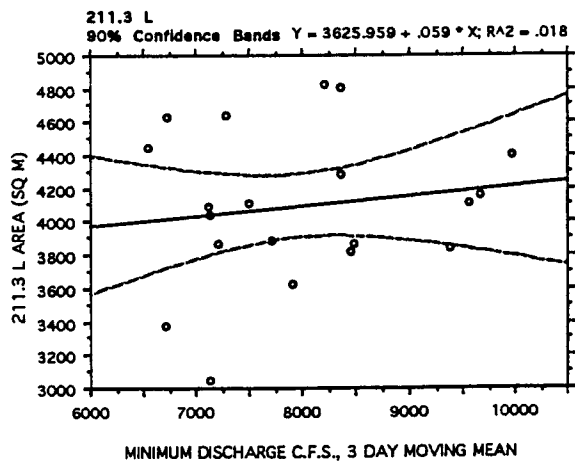
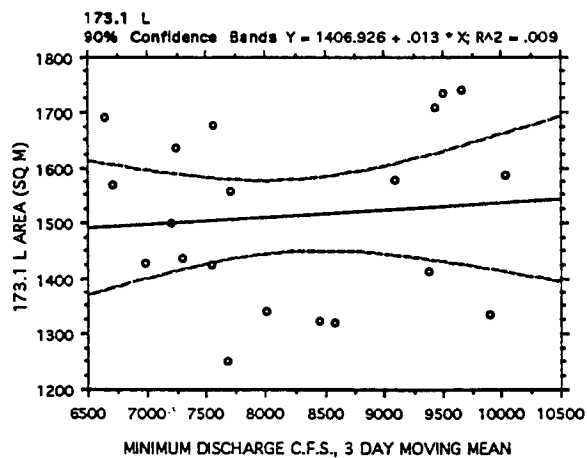
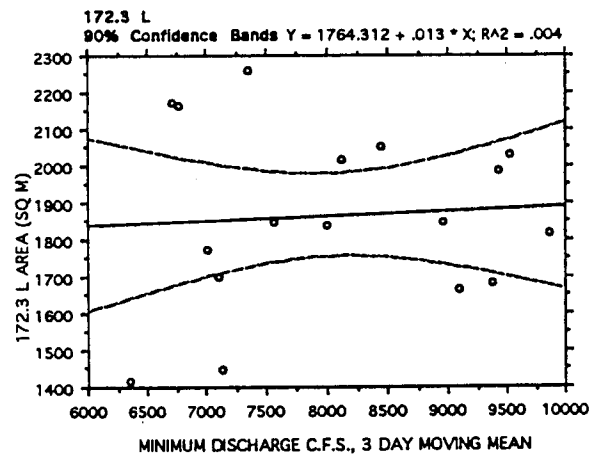
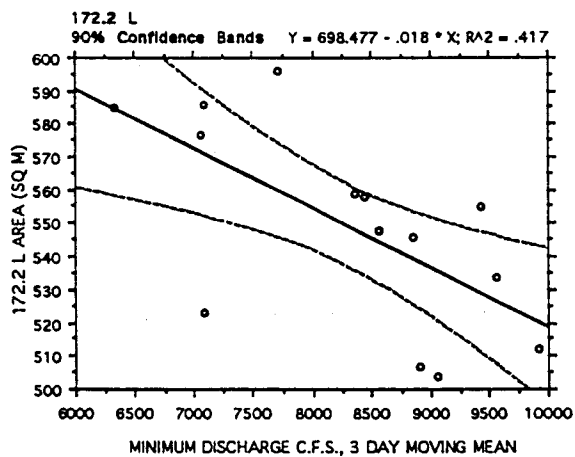
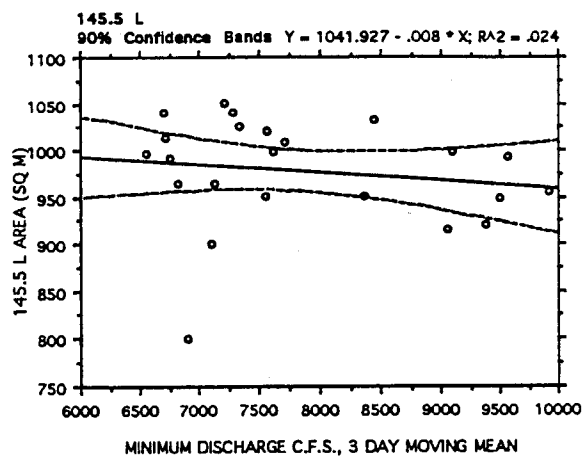
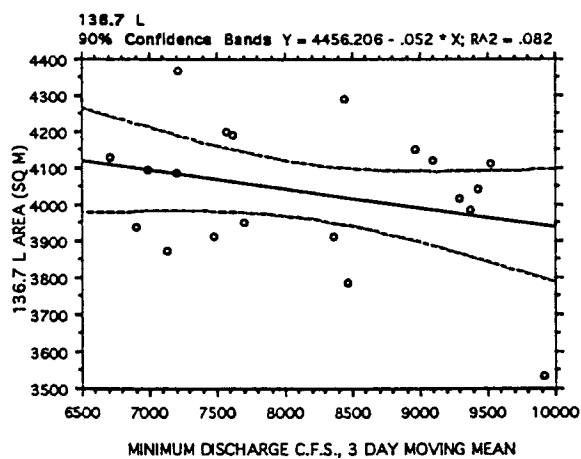


Fig. 44 (Continued). Composite figure of discharge vs. area regressions for the eighteen rectified sandbars, January 1, 1994 (mjd 672) through June 1, 1995 (mjd 1188).

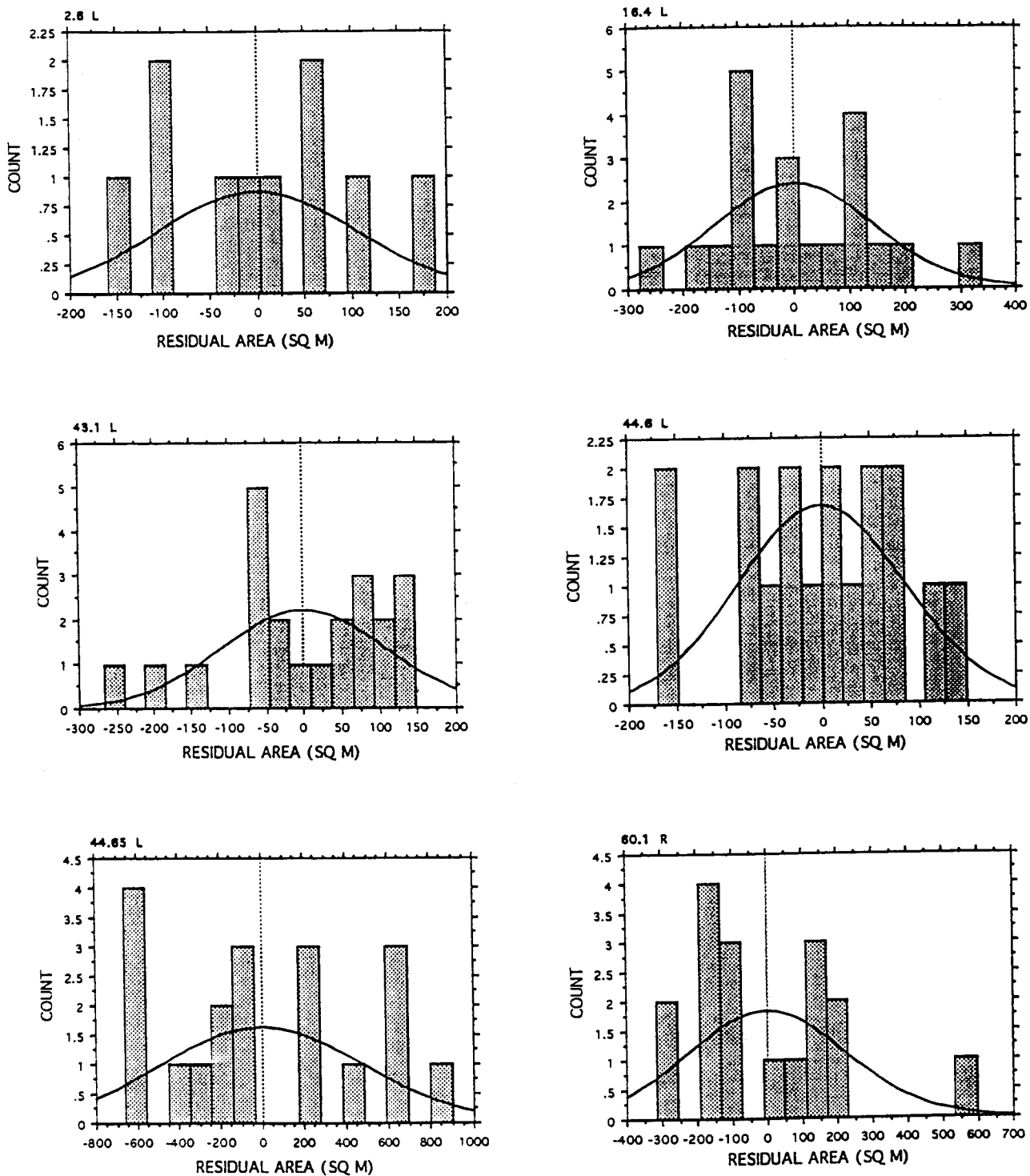


Fig. 45. Composite figure of residual histograms derived from discharge vs. area regressions for eighteen rectified sandbars, January 1, 1994 (mjd 672) through June 1, 1995 (mjd 1188).

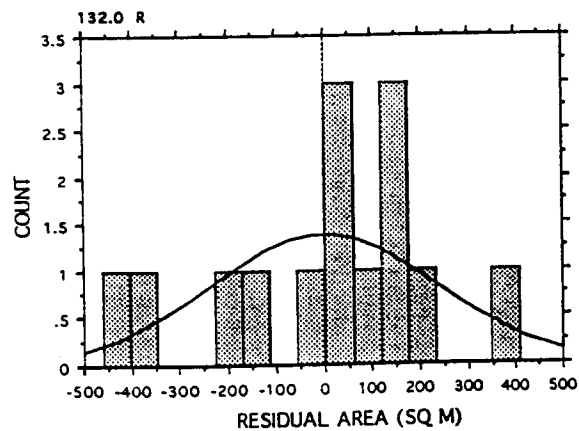
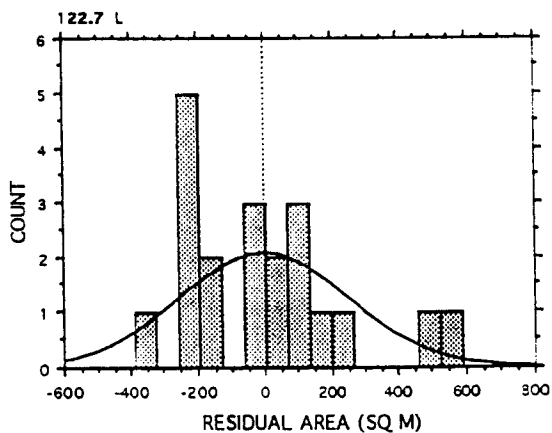
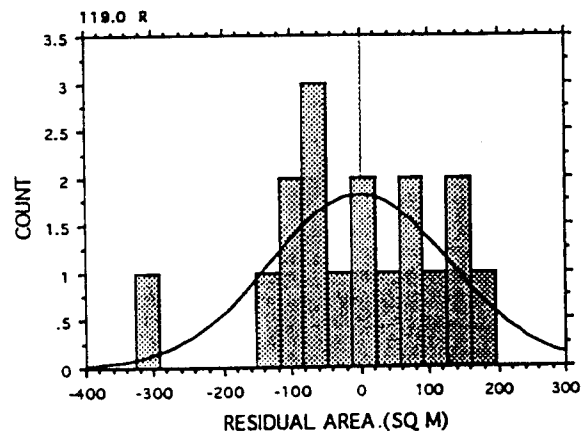
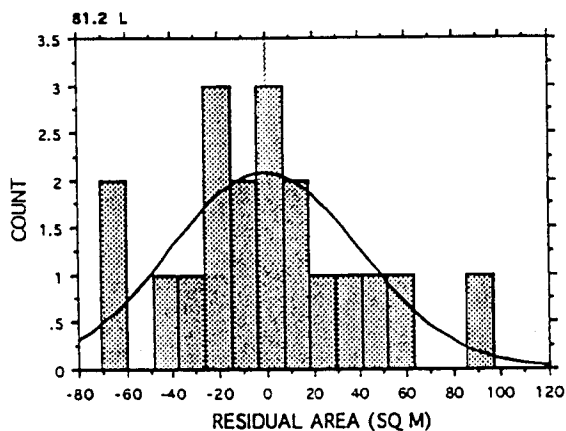
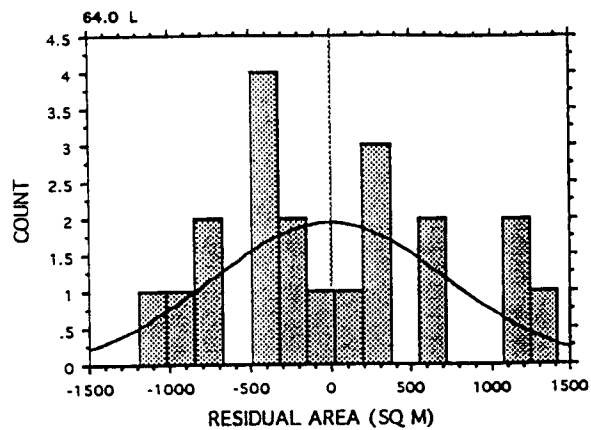
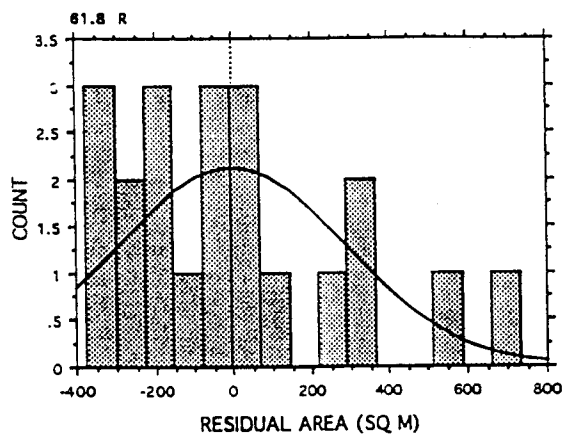


Fig. 45 (Continued). Composite figure of residual histograms derived from discharge vs. area regressions for eighteen rectified sandbars, January 1, 1994 (mjd 672) through June 1, 1995 (mjd 1188).

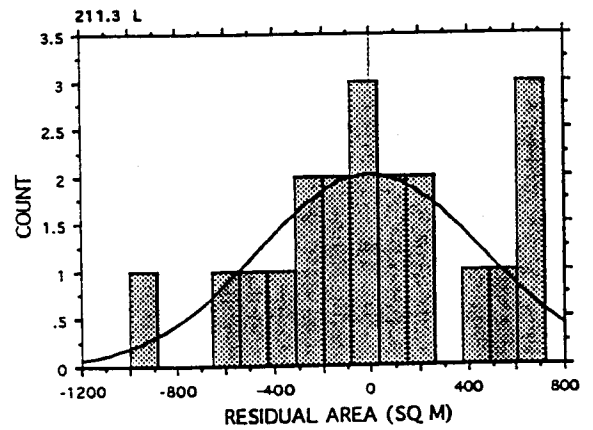
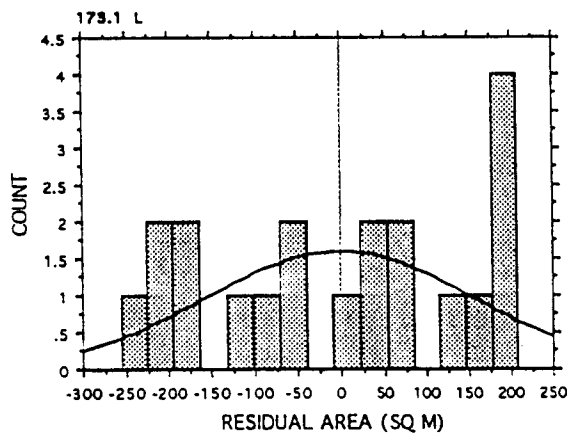
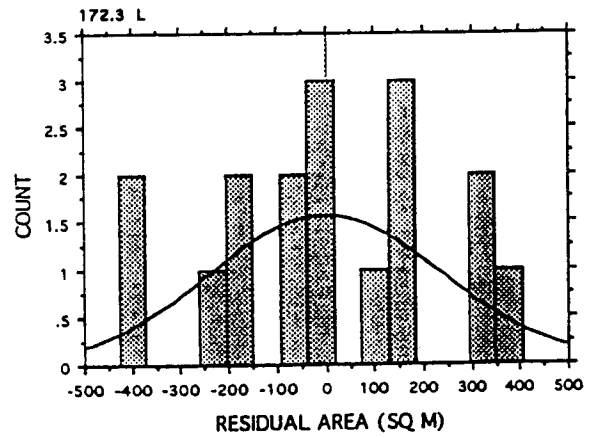
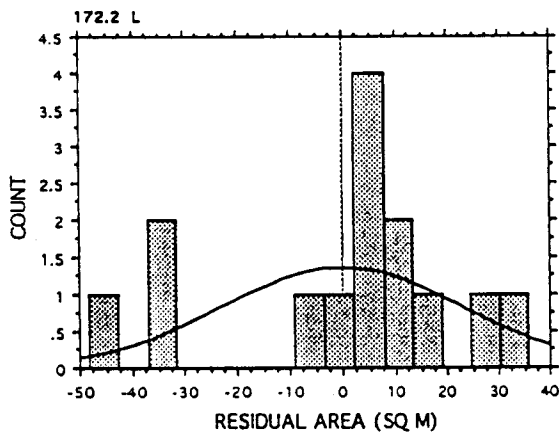
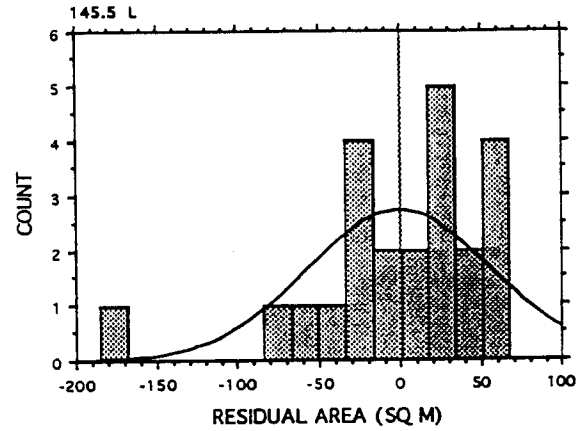
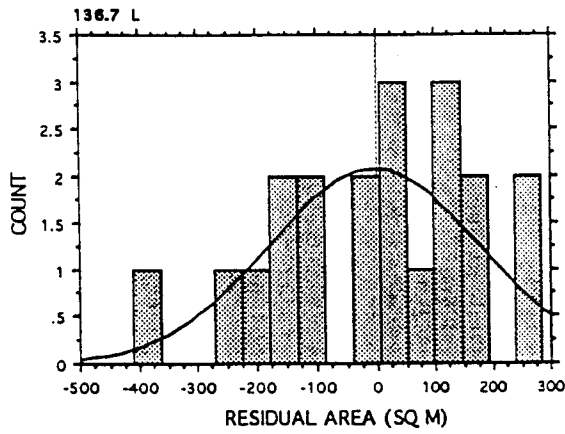


Fig. 45 (Continued). Composite figure of residual histograms derived from discharge vs. area regressions for eighteen rectified sandbars, January 1, 1994 (mjd 672) through June 1, 1995 (mjd 1188).

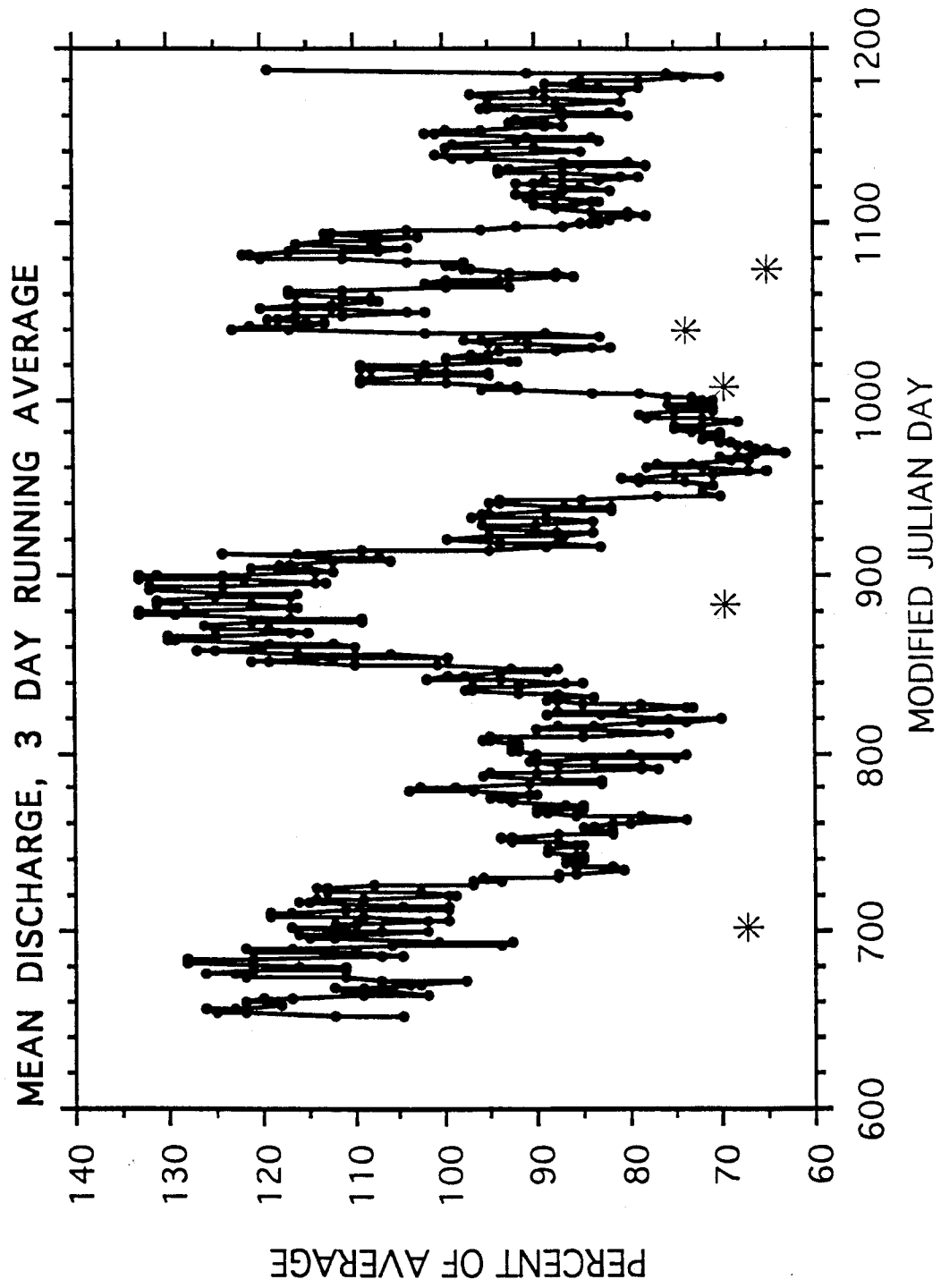


Fig. 46. Time-series plot showing mean discharge for the extension study period. Asterisks indicate periods of rapid reduction in flow.

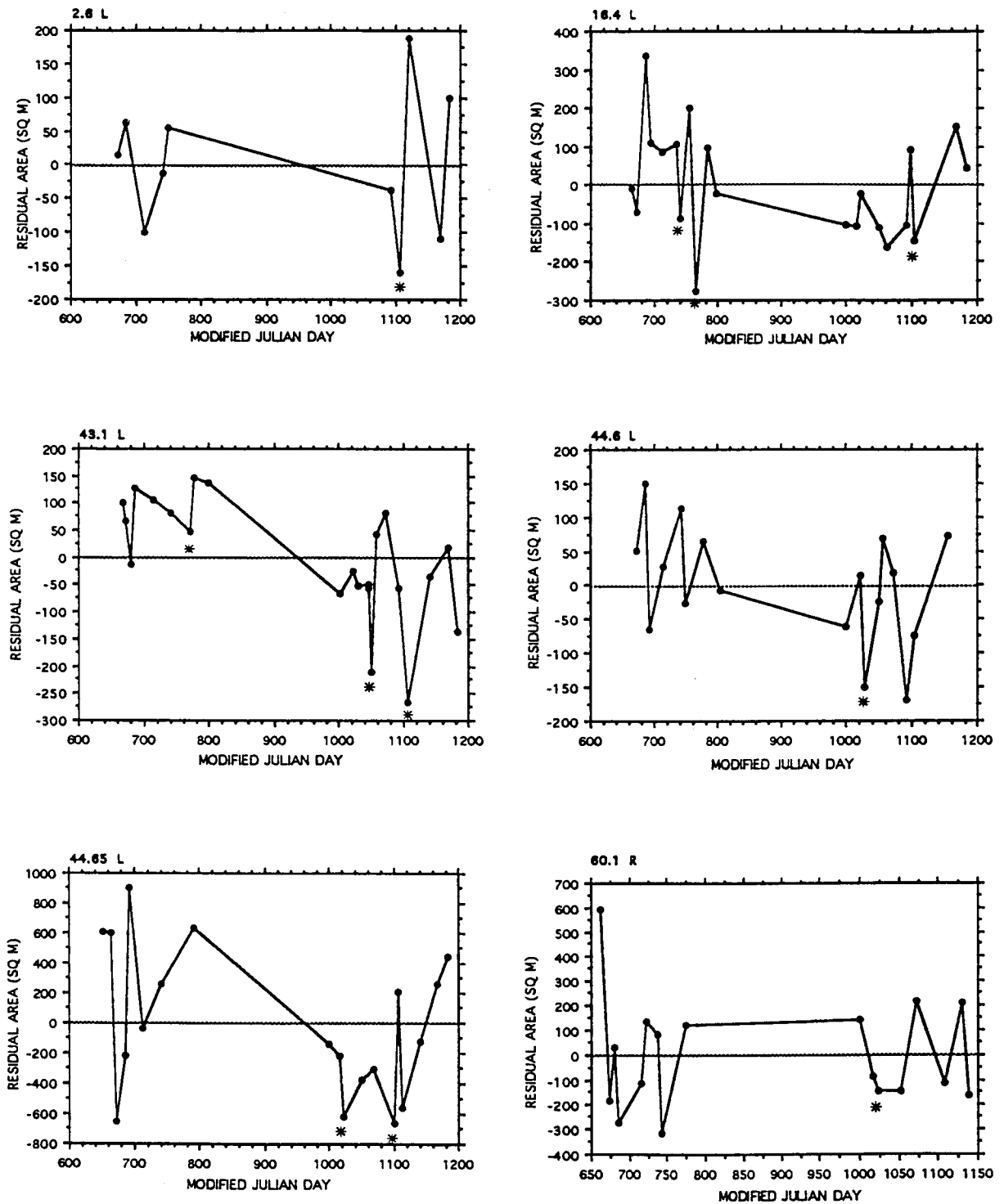


Fig. 47. Composite figure of residual time-series plots derived from discharge vs. area regressions for eighteen rectified sandbars, January 1, 1994 (mjd 672) through June 1, 1995 (mjd 1188). Asterisks represent erosional periods correlated with one of five major flow reductions.

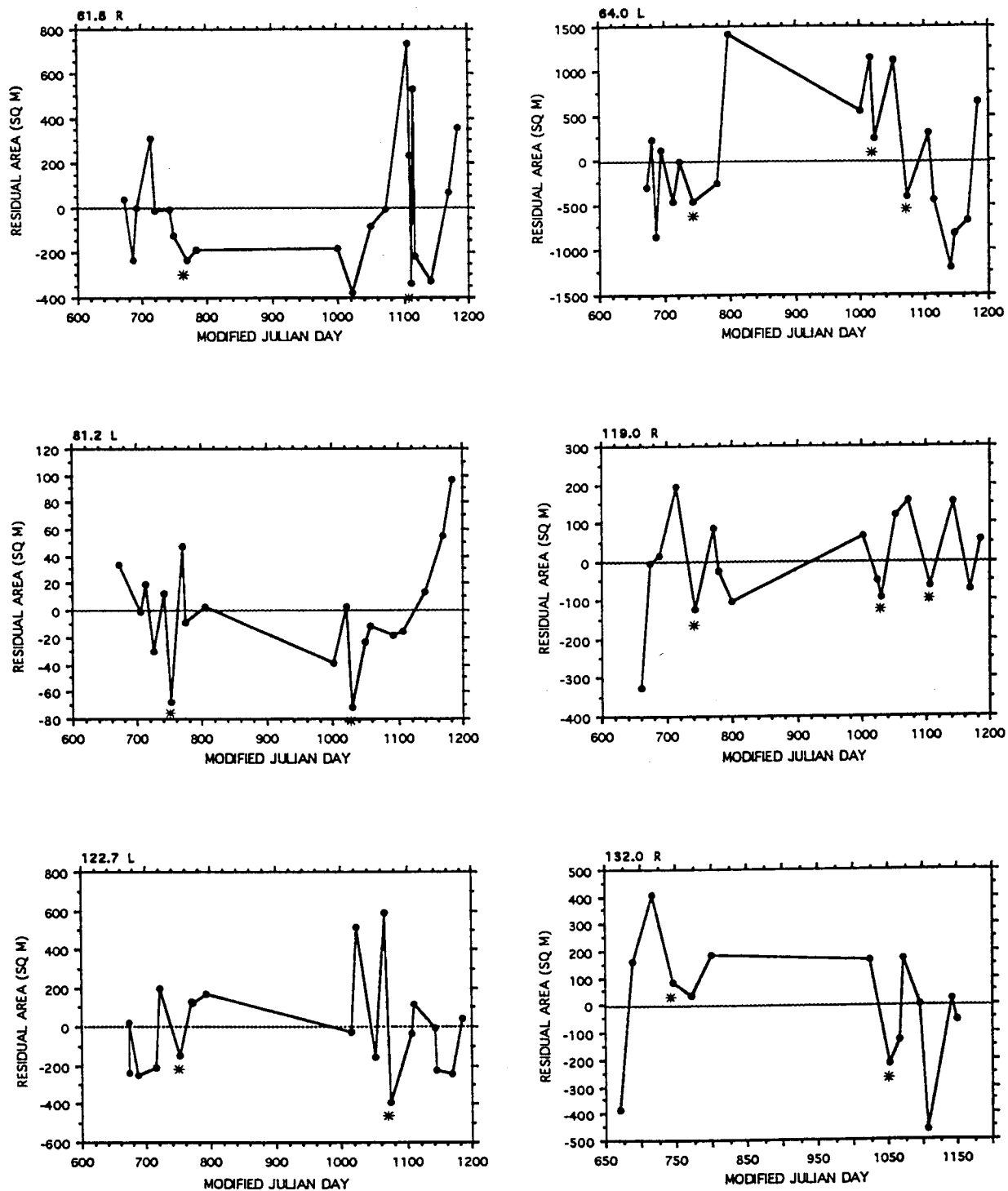


Fig. 47 (Continued). Composite figure of residual time-series plots derived from discharge vs. area regressions for eighteen rectified sandbars January 1, 1994 (mjd 672) through June 1, 1995 (mjd 1188). Asterisks represent erosional periods correlated with one of five major flow reductions.

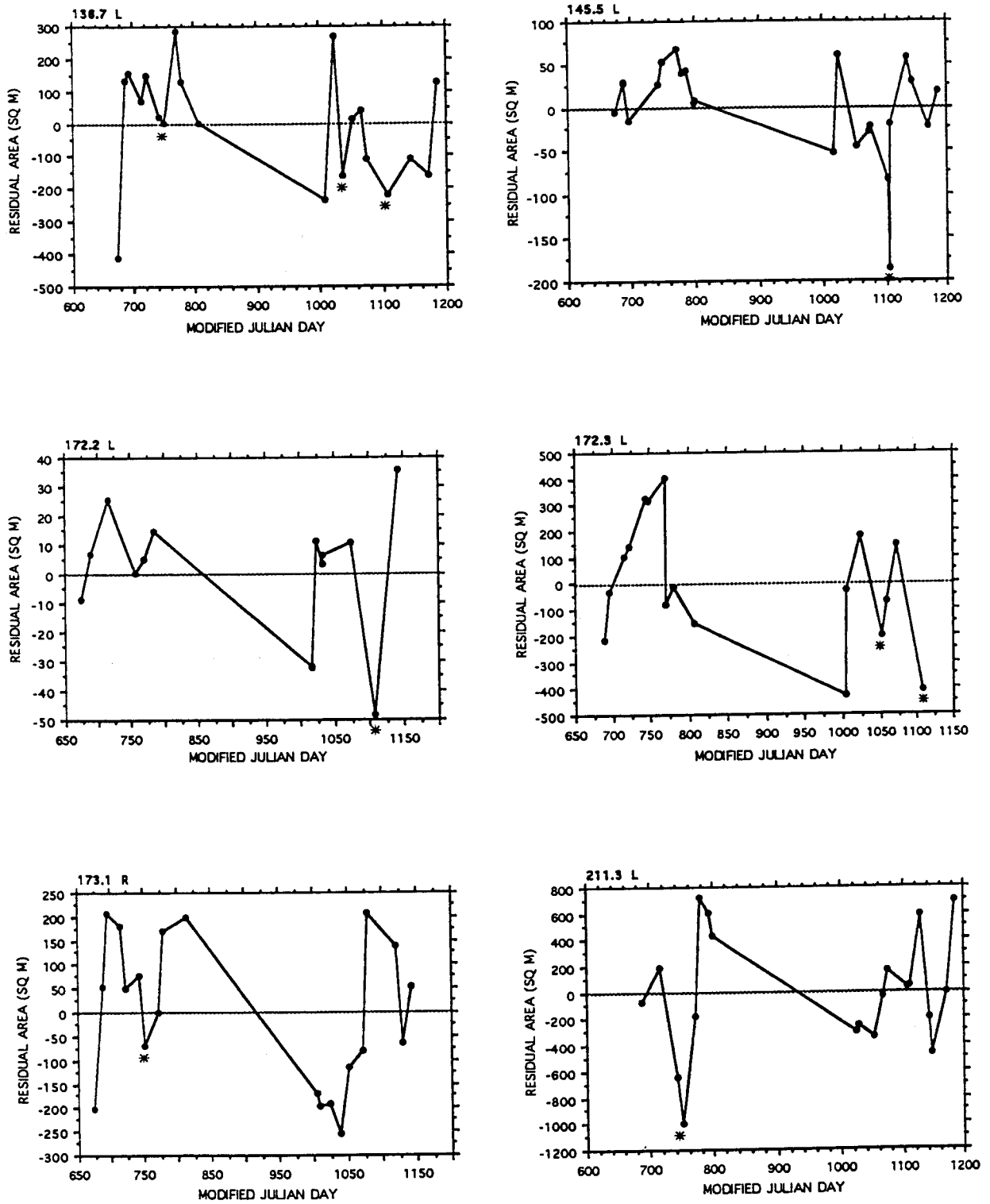


Fig. 47 (Continued). Composite figure of residual time-series plots derived from discharge vs. area regressions for eighteen rectified sandbars January 1, 1994 (mjd 672) through June 1, 1995 (mjd 1188). Asterisks represent erosional periods correlated with one of five major flow reductions.

Table 12. Extreme limits of sandbar erosion as modeled by residuals from area/discharge regression analysis. These values represent maximum and minimum areas corrected for discharge variations. The mean area is included for a reference.

<i>Sandbar</i>	<i>Mean Area (m²)</i>	<i>Extreme Minimum Area Residual (m²)</i>	<i>Extreme Maximum Area Residual (m²)</i>
2.6 L	1645	-159	188
16.4 L	932	-278	336
43.1 L	2759	-267	147
44.6 L	595	-170	149
44.65 L	3280	-659	903
60.1 R	1931	-315	595
61.8 R	4616	-375	736
64.0 L	3179	-1190	1419
81.2 L	1910	-71	97
119.0 R	4180	-327	196
122.7 L	3277	-389	594
132.0 R	2744	-460	408
136.7 L	4035	-410	284
145.5 L	978	-185	68
172.2 L	549	-48	36
172.3 L	1866	-426	406
173.1 L	1514	-256	208
211.3 L	4095	-1001	719

Table 13. Coefficient of variation for eighteen sandbars. The length of record used for this analysis begins in 1992 and uses data from both the initial and extension studies.

<i>Sandbar</i>	<i>CV</i>
2.6L	31.30
16.4L	19.40
43.1L	6.90
44.6L	20.70
44.65L	24.00
60.1R	30.60
61.8R	17.60
64.0L	26.90
81.2L	4.70
119.0R	8.50
122.7L	14.10
132.0R	11.10
136.7L	10.00
145.5L	9.10
172.2L	14.60
172.3L	16.10
173.1R	12.10
211.3L	11.6
min	4.70
mean	15.00
max	31.30

Table 14. Summary of simulation study results.

Mile	Monthly Plus Events			Annual			Biannual 1			Biannual 2								
	CI (%)	mean	STD	n	95% CI	range	mean	STD	n	95% CI	mean	STD	n	95% CI				
81.2L	4.7	1861.3	93.5	42	28.3	1833-1890	1878.2	83.7	4	82.0	1862.5	69.6	6	55.7	1832.6	92.6	5	81.2
172.3L	16.1	1745.4	281.4	72	64.9	1680-1810	1787.6	281.9	5	247.1	1749.7	362.8	7	268.7	1789.1	228.7	7	169.4
2.6L	31.3	1778.1	556.7	32	192.9	1585-1971	2062.0	586.6	4	574.8	1558.5	560.7	4	841.7	2030.3	743.8	3	549.5

Annual represents one measurement each year on or about March 15th.

Biannual 1 simulates measurements taken in March and September each year.

Biannual 2 simulates measurements taken in December and July each year.

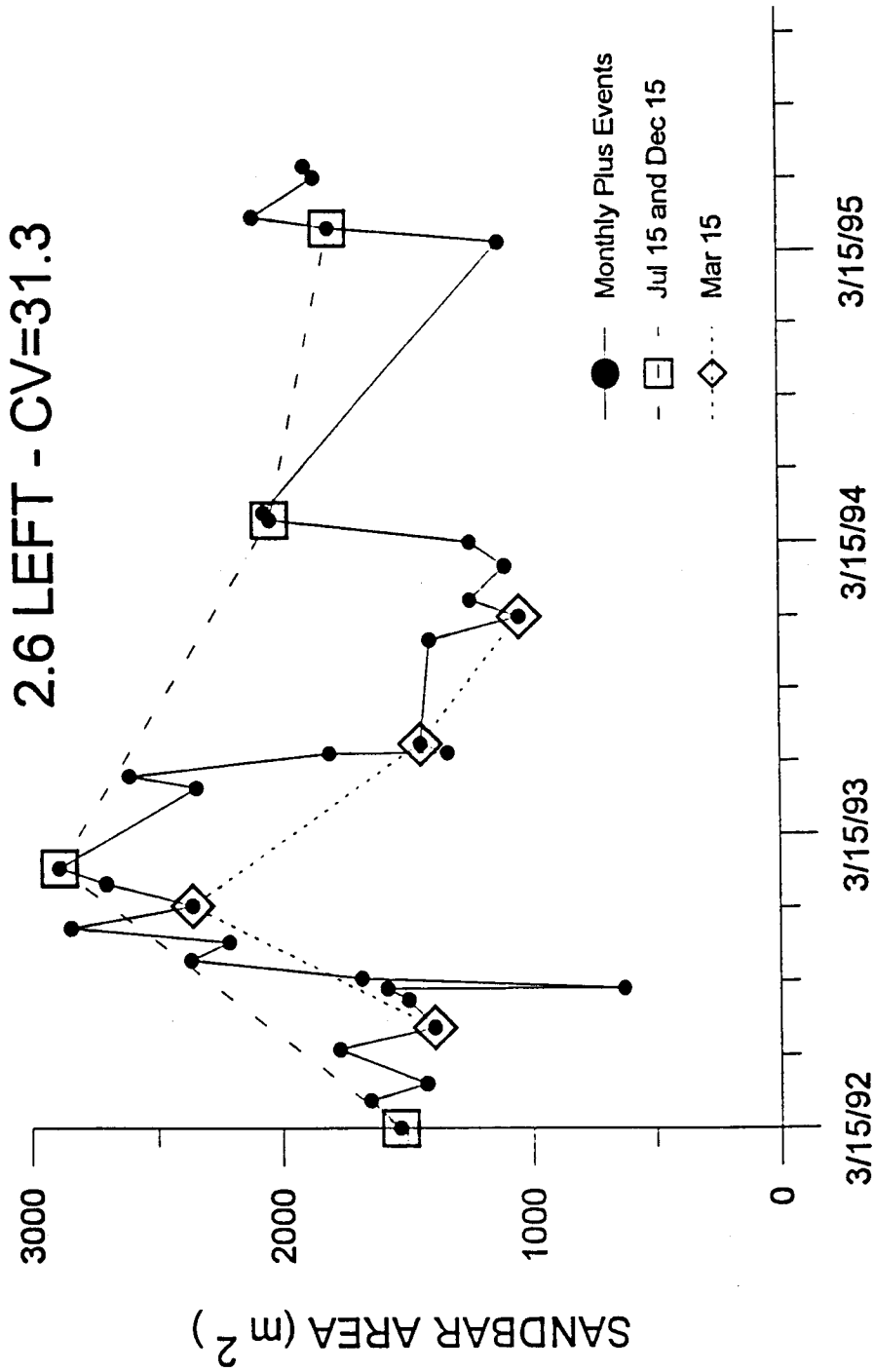


Fig. 48. Time-series plot showing modeled areas for 2.6L.

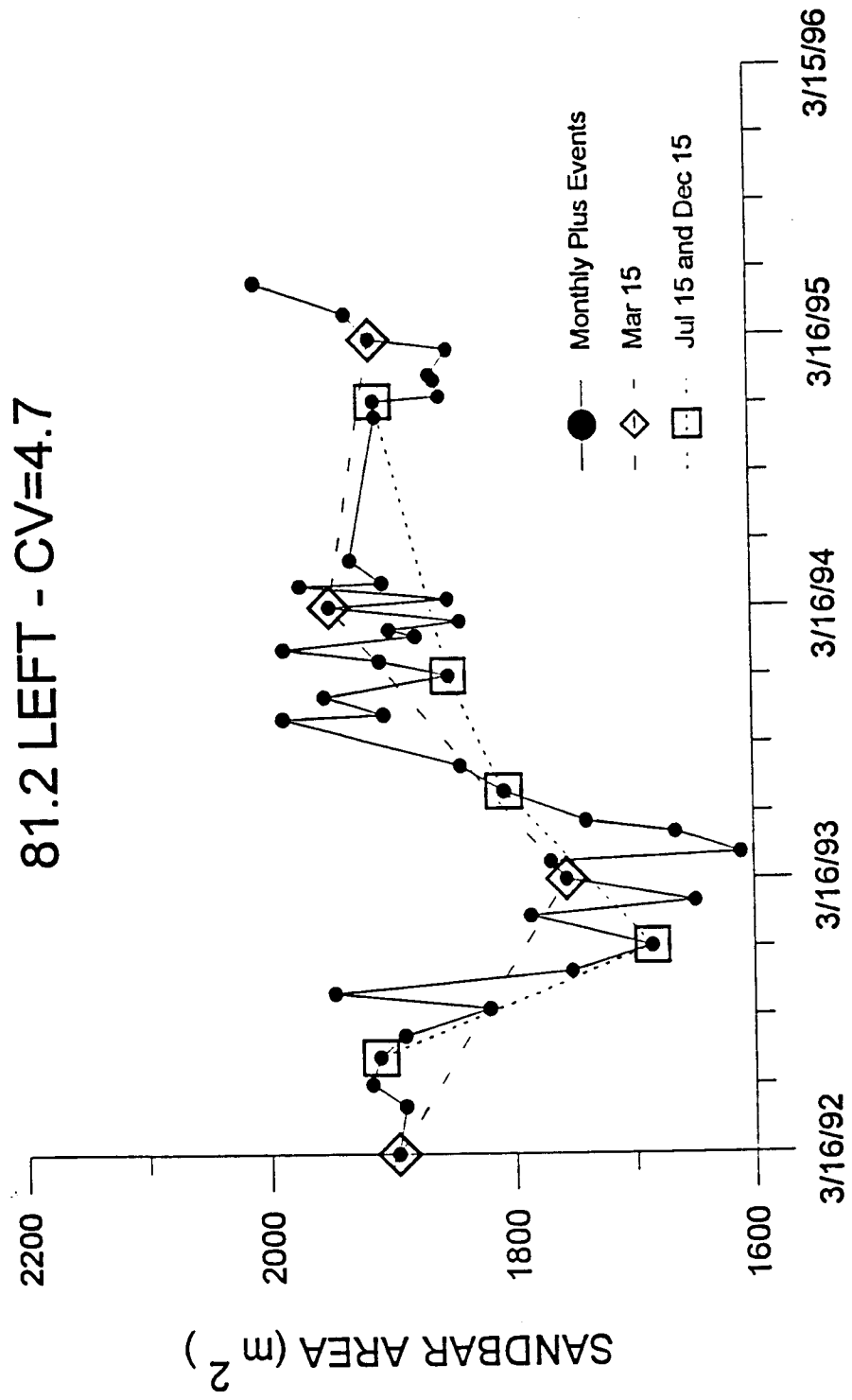


Fig. 49. Time-series plot showing modeled areas for 81.2L.

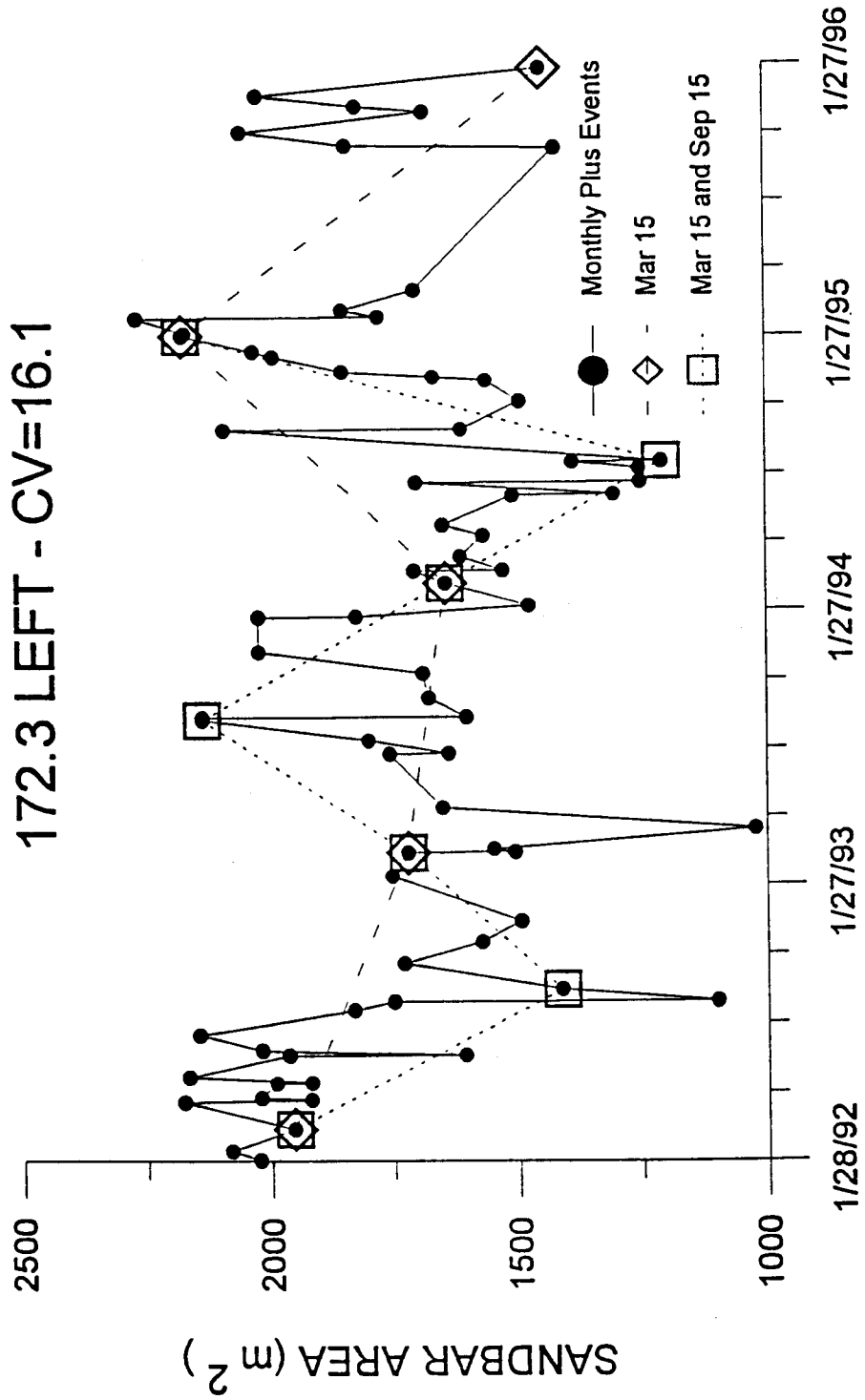


Fig. 50. Time-series plot showing modeled areas for 172.3L.

Discussion & Conclusions

Accuracy of the Methodology

Based on the results of various error analyses presented above, polygon areas can be calculated from rectified high-oblique photographic images to an accuracy level of 1 to 2% in most typical situations. Accurate data can be obtained with camera angles as low as 5 degrees from the horizon if the polygon area of interest is bounded by well surveyed ground control points. Site specific difficulties can significantly reduce the accuracy of the method, however, careful pre-planning and a few test images can minimize such problems.

Magnitude of Erosional Events

While sandbar areas continue to fluctuate over monthly time scales, the number and size of short term (daily) erosional events was much less during the extension study. Only three such events were large enough to discuss. 61.8R displayed rapid erosional events twice in March 1995. An area of 609 m² eroded on the 15th and an area of 720 m² eroded on the 20th. These values represent 12% and 14% of the pre-erosion area respectively. The sandbar had rebuilt and gained additional area in the 4 days between the two erosional events. These events both occurred in mid-week. Another significant erosional event occurred at 172.3L on Friday April 8, 1994 where 489 m² of area (about 22%) was lost.

Determining area changes of short term erosional events is relatively easy using the techniques employed in this study. The effect of stage difference is more easily removed from day to day than from week to week or month to month.

As will be discussed later, large and persistent seasonal fluctuations in discharge occur. Comparison of erosion over longer time spans requires an adjustment to the raw area measurements.

An attempt was made to estimate the magnitude of these discharge related area changes using values obtained during the regression analysis. An index of area sensitivity to discharge was computed by multiplying the R^2 value by the absolute value of the slope of the regression line and scaling the result by 100. Results from this analysis indicate that discharge related (thus non-erosional) area changes, in general, are more significant in the upstream reaches, especially those sandbars upstream of the L.C.R. confluence. In the lower reaches, the statistical relationship becomes insignificant. While this generality is apparent, it is interesting to note several departures from this trend. 16.4L sits in a very geomorphically restricted reach and is close to the dam, yet its area discharge correlation is very low ($R^2 = .16$). In the lower reaches, 172.2L remains relatively highly correlated ($R^2 = .42$) and statistically significant.

Regression residual values may be used as estimators of area loss corrected for discharge effects. These corrected erosion values for the extension study period as a whole are presented in Table 13. This table compares mean sandbar area with maximum and minimum area residuals taken from the regressions of area vs. discharge. The residual values represent our best estimate of erosional area change.

Frequency Distributions of Sandbar Areas

Daily, Weekly and Monthly Time Scales

Within-season histogram analysis shows generally non-normal tail heavy or bimodal area distributions. These results are similar to those found in the initial study.

Frequencies at Seasonal Time Scales

Seasonal fluctuation in areas follow the same trends as in the initial study. Winter sandbar areas are smaller than average, while fall and spring areas are larger than average. Missing data for summer of 1995 does not allow comparison to the smaller than average values found in the summers of the initial study. As stated in the initial report, these six month fluctuations in area are most strongly correlated to average discharge levels and the associated change in stage.

While it may be tempting to relate the bimodal area distributions strictly to sudden changes between high and low seasonal discharge regimes, this does not appear to be the case. Two types of histogram analyses were run to determine if removal of discharge related area changes also removed or reduced the non-normality of the area distributions. First, histograms of sandbar areas by season were constructed. Results from this analysis show that bimodal or tail heavy distributions of sandbar area persist at the within-season level as mentioned above (Table 11). Second, histograms of sandbar area residuals derived from the area-discharge regressions were constructed. The residual histograms show no significant difference in normality from the raw area data. Distributions are typically bimodal (or multi-modal) peaks and tail heavy (Figure 45).

Annual Time Scales

Annual-scale histogram analysis of sandbar area distribution follow much the same trends as in the initial study (Figures 36 and 45). Most sandbars are non-normal with respect to area. Typically, sandbar areas are platykurtic with more representation in the tails of the distribution than would be expected with normal distributions. Also, most sandbar areas are bimodal with a pronounced gap in the center of the distribution where most values should concentrate in a single peak for normal distributions. In general, sandbars which were non-normal in the initial study continue to display this characteristic in the extension study.

Four sandbars changed in character in some way (see last column of Table 8). 16.4L turned unimodal but remained platykurtic, 119.0R remained leptokurtic but turned unimodal, 145.5L turned unimodal and slightly leptokurtic, and 172.3L turned bimodal and platykurtic. These results suggest that sandbar areas overall are not in a stable condition which should allow for normal or leptokurtic, unimodal distributions where extremes in areas are the exception rather than the rule. What is shown by this distribution analysis is that sandbars are transient features that oscillate in size more than would be expected from "stable" features. However, sandbars can change in this characteristic so that periods of relative stability occur between periods of relative instability.

We feel the bimodal area characteristic continues to be evident at several different temporal scales. We continue to integrate this bimodal characteristic into the general erosional-depositional cycle model as discussed in the initial report (Cluer and Dexter, 1994).

Temporal Trends of Erosion

Punctuated Events

A wide range of aggradation and degradation rates were measured during the course of this investigation. Aggradation occurred at rates such that sandbar areas often increased $1,500 \text{ m}^2$ in one month. The greatest aggradation rates on an individual site basis followed erosional events. It was not uncommon for large areas degraded during an event to be aggraded to original size within two weeks. Because aggradation rates are highly variable during the same time period and discharge pattern, the rates appear to depend upon site specific variables such as channel width and sediment supply as much as subsequent hydrologic pattern. Thus, in general, aggradation was greatest immediately following erosional events or upon reversal of degradation periods.

The aggradation rates decreased as areas increased, reaching minimum rates as area approached maximum values.

The major difference between aggradation and degradation rates is the time that it took for each to occur. Many periods of erosion were actually very short periods of time, typically less than 24 h; thus the usage 'events' in this report (see Figures 13 and 14 for examples). Degradation was typically a punctuated event while aggradation was prolonged. This characteristic has been incorporated in an overall sandbar cycle model presented in the initial report (Cluer and Dexter, 1994)

Rapid erosional events were discovered in 1990 during the course of the pilot study leading to this investigation. Werrell and others (1993), Carpenter and others (1995), and Budhu and Gobin (1994) have shown that seepage of bank stored water can result in rapid slope failure when river stage drops faster than the sandbar water level. The process is maximized by high downramping rates and steep slope angles. An important parameter of the interim flow prescription was drastically reduced ramping rates. The results presented in the initial report show that the reduced ramping rates of the interim flows did not reduce the frequency or magnitude of bank failures (Cluer and Dexter, 1994). Rapid erosional events continued into this extension study but at a much reduced frequency. Also, this study has documented rapid erosional events occurring on the most gradual sandbar slopes more frequently than on the greatest slopes. Both observations indicate that seepage is not the dominant process in erosion of sandbars downstream of Glen Canyon Dam.

Documentation that erosional events occur at every site in our sample (this includes the initial and the extension studies) is significant because it illustrates that erosional events are universal from a geomorphic view point. It is hypothesized that erosional events also occurred in the past but were not detected by past investigations because they were designed to measure at time intervals longer than the erosion/deposition cycle.

Results presented here show that through erosional events and rapid redeposition, individual sandbars cycle through large volumes of sand between periods of time traditionally chosen for measurement intervals. Each time a volume of sand is cycled from the sandbar into the channel, another opportunity for large-scale downstream sediment transport is presented.

Temporal Connection to Discharge Patterns

Time series plots constructed from residuals of area/discharge regression analyses may be used to investigate longer term area changes where discharge changes have been removed from the area calculations. Figure 47 shows these area changes and Figure 46 shows discharge fluctuations for the same time period. Asterisks have been included to show rapid reductions in discharge. Five periods of rapid reduction in discharge are found around February 28, 1994 (modified Julian date 730), September 1, 1994 (modified Julian date 915), December 15, 1994 (modified Julian date 1020), January 24, 1995 (modified Julian date 1060), and February 23, 1995 (modified Julian date 1090). The area residual time series plots contain asterisks that mark large reductions in area that correspond closely in time to one of these discharge reduction periods. Thirty two major reductions in area correspond to one of these five discharge reductions.

Sub-Annual Cycles

As noted above, a pronounced seasonal variation in sandbar areas is related to discharge and does not necessarily reflect erosional loss or depositional gain in the resulting area. In addition to the six month lag, several sandbars in the initial study show positive direction autocorrelation peaks at three months (122.3R, 122.7L, 136.6L, 172.3L), four months (44.6L, 64.0L, 119.0R, 212.9L), five months (122.3R, 145.5L), seven months (60.1R, 64.0L, 172.2L), eight months (119.0R), and nine months (44.6L, 136.6L, 172.3L) (Cluer and Dexter, 1994).

Missing data severely hampered a similar analysis in the extension study. Correlograms were run for two separate time periods of 3 to 4 months each in order to miss the gap in data. The time scale was too short to obtain any significant results in terms of repeating cycles in area measurements

Annual Time Scales

Results from averaging the measurements for 18 rectified sandbar images (Table 7) indicate that, overall, the average change was a 6% (s.d. 39) gain in area compared to a 5% loss for the initial study. This result may be biased because the data set ended in the spring when areas are typically larger.

The extremes are represented by 2.6L gaining 69.3% of its initial area and 60.1L losing 21.8% of its initial area. The initial study yielded extremes of 60.1L gaining 91% of its initial area and 44.6L losing 53% of its initial area.

In terms of the complete range of change in areas observed, the extension study period was less than the initial, with a mean percent total area difference of 33%, compared to 44% for the initial study.

It is significant to note that only three sandbars (119.0R, 132.0R and 136.7L) began the study period with a maximum area. Only one sandbar ended in a maximum (81.2L). All other sandbars achieve maximum areas greater than the beginning value and achieve minimum areas less than the ending areas sometime during the study period. No sandbars ended the extension study period at a minimum area configuration.

Comparing the minimum and maximum areas achieved by individual sandbars, the largest relative change was found at 64.0L with a difference of 64% and the smallest relative change was found at 81.2L with a difference of 8%. The coefficient of variation (CV) is one of the best comparative indicators of sandbar activity.

It is derived by dividing the standard deviation by the mean area which normalizes the amount of change removing the effect of deposit size. Sandbar 60.1L displayed the largest CV (0.41) for the initial study. For the extension, 2.6L and 64.0L both display high CV's (0.25 and 0.26 respectively). 81.2L displays the lowest CV (0.058 in initial and 0.026 in extension) in both studies. Overall the coefficient of variation is lower (0.16 to 0.11) from the initial to the extension studies.

Spatial & Geomorphic Trends

Distance Downriver

An attempt to relate sandbar characteristics and dynamics to simple downriver distance was largely unsuccessful as in the initial study. The only parameters which show a strong relation is the area/discharge sensitivity index developed from the area-discharge regressions. Given the non-normal distribution of sandbar area, we used non-parametric methods. The Spearman correlation coefficient (Spearman's Rho) was $-.749$ for the area/discharge sensitivity index which suggests that sandbar area fluctuation becomes less strongly coupled to discharge downstream.

Comparison to Reach Type

A slightly more productive approach to systematizing the overall results spatially is to relate sandbar characteristics and dynamics to geomorphology. We have done a crude analysis of this relationship by classifying general inner canyon widths at each study sandbar into one of three ordinal classes (1 = narrow, 2 = medium, 3 = wide). Again, given the non-normal distribution of sandbar properties and given the ordinal nature of the geomorphic data, we used non-parametric methods. Comparing width to mean sandbar area yields a Spearman's Rho of $.360$. Comparing width to coefficients of variability yields a Rho of $.519$. Comparing width to area/discharge sensitivity yields a Rho of $.495$.

It appears that the morphometry of the inner canyon exerts some control on these variables. Measurements of channel geometry will need to be developed more quantitatively in order to pursue this promising approach further.

Simulation Studies

Effects of Different Sampling Intervals

Previous reports based on daily monitoring information mentioned differences that might be measured in monitoring sandbars simply by using different sampling intervals. By now it is well documented that the sizes of sandbars fluctuate with discharge and sediment supply. The scale of size fluctuation is as large as 30-50% of the deposit area. It is also well documented that erosion and deposition are cyclic, repeating as often as three times per year and as infrequently as once in two to three years depending upon local site characteristics. These effects and the monitoring implications were described in detail in a recent paper by Cluer (1995). Additional information presented in this and previous reports show that the majority of sandbars display highly non-normal area frequency distributions with respect to time.

The effects of different sampling frequencies used in sandbar monitoring was explored by simulating various annual and biannual measurements using the detailed sandbar area time-series plots. For this analysis, the entire length of record was used from 1992 and includes the data set from the initial report as well as this report. Measurements were obtained from the daily photographic monitoring program and consist of at least one measurement per month plus measurements bracketing erosional events. The acronym MPE (for monthly plus events) will be used to distinguish this frequency of sampling from other frequencies such as annual or biannual. Representative subsamples covering the range of dynamic activity displayed by the sample of sandbars were selected based on ranked coefficients of variation (CV) obtained from the quotient of one standard deviation and the mean in area (Table 13).

Approximately equal numbers of sandbars occurred in three CV groups; $0 < CV < 10$, $10 < CV < 20$, and $20 < CV$. Three sandbars were selected for simulation based on the mean, minimum and maximum CV. The sites were 172.3L, 81.2L, and 2.6L, respectively. These sandbars are well known by other researchers and have long histories of physical or biological monitoring.

Results from simulating different sampling frequencies are summarized in Table 14 and presented graphically in Figures 48-50. Comparing these results for site 81.2L, the least dynamic site in the sample, shows the mean size ranges from 1833 m² for biannual measurements to 1878 m² for annual measurements. These values agree well with the mean size of 1861 m² (differing by +/- 1.5% area) determined from n=42 MPE measurements for the same period. However, the 95% confidence intervals for the simulated sampling intervals range from two to three times the confidence interval for the more frequent MPE measurements. Therefore, annual measurements have accuracy of approximately +/- 5% of the mean at sandbar 81.2L.

Comparison of different sampling intervals simulated at one of the most dynamic sandbars in the sample, 2.6L, better illustrate the adverse effects on annual and semi-annual measurements made on shorter cycles of erosion and deposition. The mean size as measured from n=32 MPE measurements was 1778 m². This compares to mean areas ranging from 2062 m² for annual sampling to 1559 m² for biannual sampling, each with n=4. The confidence intervals for annual and biannual sampling range three to four times that of the more frequent MPE sample which is approximately +/-193 m². In terms of sandbar area, the MPE confidence interval is about 22% of the mean area 1778 m², while the confidence interval for biannual measurements is approximately 95% of the mean area. Due to the highly dynamic nature of sandbar 2.6L, simulated annual measurements taken on March 15 tend to coincide with relative minimum areas while biannual measurements taken on July 15 and December 15 coincide with relative maximum areas. Both sampling scenarios disagree with the MPE measurements by up to 50%.

A large number of MPE measurements have been made from sandbar 172.3L (n=72). This sandbar's dynamic activity has been the subject of numerous investigations and several publications (i.e. Budhu and Gobin, 1994; Cluer 1992; Cluer and others 1994; Cluer 1995). This intensity of study and publication activity may have given other investigators the impression that it is anomalous in its dynamic activity. Coefficients of variation in area (Table 13) show that 172.3L lies at approximately the mean CV value for the sample presented in this report, indicating that this sandbar and its dynamic activity are normal for the sample selected. The mean area from n=72 MPE measurements is 1745 m² with a 95% CI of approximately 65 m², or +/- 7%. Simulated annual (n=5) and biannual (n=7) measurements have similar mean area values but much larger confidence intervals ranging between approximately 170 and 270 m², or 19% to 31% of the mean area.

The mean area values that lie within the 95% confidence range for the MPE measurements are useful for comparing the significance of the simulated measurements. The simulated biannual-2 measurements for 81.2L resulted in a mean area of 1833 m² which is at the lower limit of the confidence range for MPE measurements. The means of the other simulations for 81.2L are within the 95% CI for the MPE measurements. For sandbar 172.3L all of the simulated means are within the MPE 95% CI. For sandbar 2.6L, which has the greatest CV in the sample, all of the simulated mean areas are outside the MPE 95% CI. In this case, the means of the simulated measurements tend to represent outliers as illustrated in Figure 48. The simulated annual measurements coincide with relative minimum MPE values. Conversely, the simulated biannual measurements coincide with the relative maximum MPE values. Both scenarios consistently and significantly misrepresent the mean area.

A logical progression of the simulation study results in sandbar management by tracking those measurements that represent outliers. If several subsequent outliers occur, this condition would signal significant changes in sandbar size rather than just normal variation. A fairly large sample of regularly spaced temporal measurements would be required in order to maintain a small confidence interval.

Thus, a trade off is available to management between a large sample over a short time period (such as the MPE approach) and a large sample over a long time period (the traditional annual monitoring approach).

Summary

The methodology developed over the course of this project has proven to be a reliable, low cost, low impact way to assess certain environmental variables over short time steps. Many dynamic environmental processes may require sampling at such short time intervals to capture the essence of the processes involved (Cluer, 1995).

Combining the results of the initial report (Cluer and Dexter, 1994) with this extension report, sandbars in the Grand Canyon appear to be dynamic in an irregular fashion. Areas appear not to be stable and area changes can occur in a semi-cyclic or irregular temporal scale. It appears from limited evidence, that local geomorphic and hydrologic conditions affect the stability of each individual deposit.

Of the hydrological effects imparted at the dam, rapid changes in the reduction of discharge seem to be correlated to most short term (day to week) erosional events.

Sandbars that display fluctuating area changes, where erosion is replaced by deposition in a cyclic fashion, should not necessarily be construed as simply sand exchange between eddy and sandbar. While the bulk of the mobile sand may or may not exchange in this fashion, every time sand becomes mobile an opportunity for some of it to move downchannel is presented.

Acknowledgments

We wish to thank the National Park Service for funding support. We also thank Dave Wegner and others on the Glen Canyon Environmental Studies staff for direct and in kind support of this project. We especially want to thank Chris Brod (GCES) for surveying assistance. Listing of specific brand names of equipment or software are in no way official endorsements of those products.

Literature Cited

- Andrews, E. D. 1991. Sediment transport in the Colorado River Basin. Pages 54-74 in Colorado River Ecology and Dam Management: Proceedings of a Symposium, May 24-25, 1990, Santa Fe, New Mexico. National Academy Press, Washington, D. C.
- Beus, S.S., and C.C. Avery, 1992. The influence of variable discharge regimes on Colorado River sandbars below Glen Canyon Dam. Final report. Glen Canyon Environmental Studies, Flagstaff, Arizona.
- Beus, S. S. 1992. Colorado River Investigations, Northern Arizona University, Flagstaff, Arizona.
- Budhu, M., and Gobin, R., 1994. Instability of sandbars in Grand Canyon. Journal of Hydraulic Engineering, v.120, n.8, p.919-933.
- Budhu, M.R. 1992. Mechanisms of erosion and a model to predict seepage-driven erosion due to transient flow. Chapter 2, pages 1-75 in Beus, S. and C. Avery, editors. The influence of variable discharge regimes on Colorado River sandbars below Glen Canyon Dam. Final report. Glen Canyon Environmental Studies, Flagstaff, Arizona.
- Carpenter, M.C., Carruth, R.L., Fink, J.B., Boling, J.K., and Cluer, B.L., 1995. Hydrogeology and deformation of sandbars in response to fluctuations in flows of the Colorado River in the Grand Canyon, Arizona. U.S. Geological Survey, Water-Resources Investigations Report 95-4010, 16 p.
- Carpenter, M.C., R.L. Carruth, and B.L. Cluer, 1991. Beach erosion and deformation caused by outward flowing bank storage associated with fluctuating flows along the Colorado River in the Grand Canyon. EOS (Trans. Am. Geophys. Union), v.72, p.222.
- Cluer, B.L. 1992. Daily responses of Colorado River sand bars to releases from Glen Canyon Dam, 1990-1991: instantaneous erosion and dependent deposition. Chapter 5, pages 1-47 in Beus, S. and C. Avery, editors. The influence of variable discharge regimes on Colorado River sandbars below Glen Canyon Dam. Final report. Glen Canyon Environmental Studies, Flagstaff, Arizona.
- Cluer, B.L., 1995. Cyclic fluvial processes and bias in environmental monitoring, Colorado River in Grand Canyon. Journal of Geology, v.103, p.411-421.

- Cluer, B.L., M.C. Carpenter, L.J. Martin, M.A. Wondzell, L.R. Dexter, and M.F. Manone, 1993. Rapid erosion and slow redeposition of sand bars along the regulated Colorado River in the Grand Canyon. *EOS (Trans. Am. Geophys. Union)*, v.74, p.321.
- Cluer, B.L. and L.R. Dexter, 1994. Daily dynamics of Grand Canyon sandbars; monitoring with terrestrial photogrammetry. Final report. Glen Canyon Environmental Studies, Flagstaff, Arizona.
- Committee to Review the Glen Canyon Environmental Studies. 1987. River and Dam Management: A Review of the Bureau of Reclamation's Glen Canyon Environmental Studies. National Academy of Science, Washington, D. C. 152 pp.
- Dawdy, D. R. 1991. Hydrology of Glen Canyon and Grand Canyon. Pages 40-53 in *Colorado River Ecology and Dam Management: Proceedings of a Symposium*, May 24-25, 1990, Santa Fe, New Mexico. National Academy Press, Washington, D. C.
- Dolan, R., A. D. Howard, and A. Gallenson. 1974. Man's impact on the Colorado River in Grand Canyon. *American Scientist* 62:393-401.
- ERDAS Inc. 1992. P.C. ERDAS V.7.5 software, users guide and technical manuals. ERDAS, Inc., Atlanta, Georgia.
- Howard, A.D. 1975. Establishment of benchmark study sites along the Colorado River in Grand Canyon National Park for monitoring of beach erosion caused by natural forces and human impact. University of Virginia Grand Canyon Study, Technical Report 1, 182p.
- Howard, A. D., and R. Dolan. 1979. Changes in the fluvial sandbars of the Colorado River in the Grand Canyon caused by Glen Canyon Dam. Pages 845-851 in *Proceedings of the First Conference on Scientific Research in the National Parks*, v. 2, New Orleans, Louisiana, November 9-12, 1976, National Park Service Transactions and Proceedings Series no. 5.
- Howard, A.D., and R. Dolan. 1981. Geomorphology of the Colorado River in the Grand Canyon. *Journal of Geology*, 89. pp. 269-298.
- Ingram, H., D. A. Tarlock, and C. R. Oggins. 1991. The law and politics of the operation of Glen Canyon Dam. Pages 10-27 in *Colorado River Ecology and Dam Management: Proceedings of a Symposium*, May 24-25, 1990, Santa Fe, New Mexico. National Academy Press, Washington, D. C.
- Kieffer, S.W. 1985. The 1983 hydraulic jump in Crystal Rapid: implications for river-running and geomorphic evolution in the Grand Canyon. *Journal of Geology*, 93(4). pp. 385-406.

- Johnson, R. R. 1991. Historic changes in vegetation along the Colorado River in Grand Canyon. Pages 178-206 in *Colorado River Ecology and Dam Management: Proceedings of a Symposium, May 24-25, 1990, Santa Fe, New Mexico*. National Academy Press, Washington, D. C.
- Patten, D.T. 1993. Long-term monitoring in Glen and Grand Canyon: response to operations of Glen Canyon Dam. Pages A1-A25 in *Operation of Glen Canyon Dam, Draft Environmental Impact Statement, Appendices*. U.S. Bureau of Reclamation.
- Schmidt, J.C. 1990. Recirculating flow and sedimentation in the Colorado River in Grand Canyon, Arizona. *Journal of Geology*, 98. pp. 704-724.
- Schmidt, J.C., and J.B. Graf. 1990. Aggradation and degradation of alluvial sand deposits, 1965 to 1986, Colorado River, Grand Canyon National Park, Arizona. U.S. Geological Survey Professional Paper 1493, 74p.
- Smillie, G.M., W.L. Jackson, and D. Tucker. 1993. Colorado River sand budget: Lees Ferry to Little Colorado River, National Park Service Technical Report NPS/NRWRD/NRTR-92/12, 11p.
- Tukey, J. W. 1977. *Exploratory Data Analysis*. Addison-Wesley Publishing Co., Reading, Massachusetts. 688p.
- Webb, R.H. in press. A century of environmental change in Grand Canyon: repeat photography of the 1889-90 Stanton expedition on the Colorado River. University of Arizona Press.
- Werrell, W., Inglis, R., Jr., and Martin, L., 1993. Geomorphic stability of sandbar 43.1L on the Colorado River in the Grand Canyon in response to ground water seepage during fluctuating flow releases from Glen Canyon Dam. National Park Service, Natural Resources Technical Report 92/10, 54 p.
- Valdez, R. A., and R. D. Williams. 1993. Ichthyofauna of the Colorado and Green Rivers in Canyonlands National Park. Pages 2-22 in *Proceedings of the First Biennial Conference on Research in Colorado Plateau National Parks, Flagstaff, Arizona, 22-25 July 1991*. Transactions and Proceedings Series NPS/NRNAU/NRTP-93/10. U.S.N.P.S., U.S.D.I., Denver, Co.

APPENDIX A: BASIC DATA SET

Phase II Sandbar	Date	Low Flow	Areas (sq. M)	Fail Area	Slope Area Index*
2.6L	940102		1241		S.I.=1
Mean=	940114		1101		
1644.70	940212		1239		
STD=	940312		2037		
416.95	940320		2063		
VAR=	gap				
173849.34	950225		1120		
RMS=	950312		1797		
3.83	950326		2101		
	gap				
	950513		1855		
	950527	8000	1893		
16.4L	931225	9870	824		S.I.=2
Mean=	940101		796		
931.90	940115		1202		
STD=	940123	9568	1018		
156.66	940212		963		
VAR=	940306		1107		
24541.59	940312	9580	904		
RMS=	940326	9241	1197		
5.38	940409		725		
	940423	9200	1073		
	940507		979		
	gap				
	941126		915		
	941212	9400	783		
	941217		893		
	950115		770		
	950126	high	676		
	950225		743		
	950304		1038		
	950311		842		
	gap				
	950512		1127		
	950527	8000	995		
43.1L	931229		2797		S.I.=3
Mean=	940102		2681		
2758.82	940109		2582		
STD=	940116		2806		
164.13	940213		2762		
VAR=	940312		2985		
26937.68	940410		2921		
RMS=	940417		3002		
3.81	940509		3060		
	gap				
	941127		2898		
	941218		2745		
	941225		2818		

	950110	*		2590	
	950111	**		2576	14
	950115			2452	
	950122			2669	
	950206			2852	
	950226			2531	
	950312			2603	
	950416			2795	
	950513			2891	
	920527		8000	2678	
44.6L	940102			579	S.I.=2
Mean=	940116			704	
595.35	940122			490	
STD=	940213			573	
100.08	940313			766	
VAR=	940320			621	
10016.24	940416			686	
RMS=	940514			624	
3.27	gap				
	941126			618	
	941218			610	
	941224			462	
	950115			525	
	950121			609	
	950205			638	
	950225			347	
	950311			573	
	950429			696	
44.65L	931212		9490	3528	S.I.=1
Mean=	931225		9870	3279	
3280.01	940102			2194	
STD=	940116			2821	
594.54	940122		9568	3944	
VAR=	940212			2931	
353483.72	940312		9878	3978	
RMS=	gap				
3.56	940430		9222	4286	
	gap				
	941126			3758	
	941212		9490	2836	
	941217			2598	
	950114			2709	
	950202			2778	
	950305			2753	
	950312			3826	
	950319			2979	
	950416			3374	
	950512			3857	
	950527		8000	3890	

60.1R	931222		2333		S.I.=1
Mean=	940102		1574		
1930.82	940110		1710		
STD=	940115		1498		
281.39	940213		1695		
VAR=	940221		1916		
79180.03	940307		2231		
RMS=	940313		1815		
6.50	940413		2164		
	gap				
	941125		2349		
	941212		1754		
	941218		1811		
	950116		1657		
	950205		2250		
	950313		1969		
	950403		2274		
	950413		1824		
61.8R	940101		4382		S.I.=2
Mean=	940115		4105		
4615.71	940122		4425		
STD=	940213		4699		
344.05	940219		4317		
VAR=	940313		4797		
118371.11	940319		4692		
RMS=	940409		4532		
2.77	940423		4565		
	gap				
	941126		4723		
	941217		4148		
	950115		4318		
	950205		4672		
	950312		5487		
	950315 *		4958		
	950316 **		4349	609	
	950321 *		5163		
	950322 **		4443	720	
	950415		4322		
	950514		4866		
	950528	8000	4967		
64.0L	940101		2409		S.I.=2
Mean=	940110	9520	2689		
3178.66	940115		1850		
STD=	940124	8050	3048		
825.54	940212		2340		
VAR=	940221	8760	2714		
681516.59	940314	6800	3221		
RMS=	940418	6710	3139		
3.91	940507		5153		
	gap				
	941126		4422		
	941212	9320	4037		

	941217		3336	
	950116		3906	
	950205		2999	
	950312		3869	
	950320		2974	
	950415		2144	
	950422		2546	
	950512		2856	
	950528	8000	3921	
81.2L	940102		1907	S.I.=3
Mean=	940205		1878	
1910.00	940214		1899	
STD=	940225		1841	
50.23	940314		1948	
VAR=	940324		1851	
2523.26	940411		1972	
RMS=	940415		1904	
3.88	940516		1930	
	gap			
	941127		1908	
	941218		1909	
	941225		1856	
	950115		1860	
	950122		1864	
	950226		1849	
	950312		1912	
	950416		1932	
	950514		1988	
	950528	8000	2006	
119.0R	931220		3700	S.I.=3
Mean=	940103		4033	
4179.94	940117		4112	
STD=	940214		4267	
156.96	940314		4143	
VAR=	940411		4316	
24637.81	940418		4181	
RMS=	940509		4174	
8.78	gap			
	941128		4358	
	941219		4092	
	941226		4150	
	950116		4197	
	950205		4365	
	950313		4175	
	950417		4351	
	950514		4188	
	950529	8000	4257	
122.7L	940103		2935	S.I.=2
Mean=	940104	9030	3154	
3276.90	940117		2979	

STD=		940215		2958	
264.35		940221	8760	3400	
VAR=		gap			
69882.51		940324	6930	3197	
RMS=		940411 *		3495	
1.27		940412 **	6570	3467	28
		940503	5900	3565	
		941212	8330	3206	
		941219		3789	
		950116		3055	
		950131		3783	
		950207		2892	
		950313		3334	
		950316		3460	
		950417		3321	
		950420		3079	
		950514		3148	
		950530	8000	3321	
132.0R		920323		2583	S.I.= 1
Mean=		920427		2759	
2888.42		gap			
STD=		920705		2212	
660.21		920831		1842	
VAR=		gap			
435878.63		921004		3166	
RMS=		921123		2813	
3.58		930125		3010	
		930228		3535	
		930322		4437	
		930426		3656	
		930511		4481	
		gap			
		930709		4411	
		930726		1973	
		930821		1790	
		930926		2832	
		931019		3097	
		931107		3328	
		931122		2684	
		931230		2233	
		940117		2773	
		940214		2974	
		940316		3012	
		940411		2903	
		940509		3140	
		gap			
		941219		2867	
		950116		2360	
		950130		2459	
		950206		2911	
		950302		2808	
		950306			in progress
		950307			in progress
		950308			in progress

	950309				in progress	
	950313			2417		
	950417			2819		
	950424			2738		
	132C			2295		
136.7	136-7c			4118	S.I.= 2	
Mean=	940103			3535		
4039.14	940117			4121		
STD=	940124			4151		
182.32	940214			4042		
VAR=	940221			4115		
33241.23	940314			4132		
RMS=	940321			4097		
6.62	940411			4369		
	940418			4198		
	940517			4088		
	gap					
	941204			3785		
	941219			4290		
	950101			3911		
	950116			3986		
	950130			4017		
	950207			3914		
	950313			3873		
	950417			3951		
	950515			3939		
	950529			4190		
145.5L	940103			956	S.I.=3	
Mean=	940117 *			998		
977.77	940118 **	8450		993	5	
STD=	940125	8050		950		
59.63	940314			1014		
VAR=	940319	6590		1041		
3555.55	940411			1051		
RMS=	940418	6710		1021		
7.11	940425	6660		1025		
	940506	7010		992		
	940509			997		
	gap					
	941212	8330		916		
	941219			1033		
	950116			920		
	950205			952		
	950207			951		
	950309 *			901		
	950311 **			800	49	
	950313			965		
	950410			1041		
	950417			1009		
	950514			965		
	950529	8000		998		

172.2L		940103		512	S.I.=2
Mean=		940118		534	
549.29		940214		555	
STD=		940328		585	
30.31		940410		577	
VAR=		940524		586	
918.68		gap			
RMS=		941211 *		507	
5.95		941212 **		504	3
		941219		558	
		941228 *		548	
		941229 **		546	2
		gap			
		950207		559	
		950312		523	
		950417		596	
172.3L		940117		1665	S.I.=1
Mean=		940124		1848	
1866.29		940214		1989	
STD=		940221		2029	
241.06		940314		2173	
VAR=		940317		2166	
58108.10		940408 *		2263	
RMS=		940409 **		1774	489
1.86		940418		1848	
		940515		1701	
		gap			
		941128		1419	
		941201		1838	
		941219		2051	
		950116		1682	
		950123		1817	
		950206		2017	
		950313		1447	
173.1L		940103		1335	S.I.=2
Mean=		940117		1579	
1514.20		940125		1737	
STD=		940214		1711	
156.25		940222		1589	
VAR=		940314		1572	
24412.69		940321		1428	
RMS=		940411		1502	
1.86		940418		1677	
		940523		1694	
		gap			
		941201		1341	
		941205		1323	
		941219		1326	
		950102		1251	
		950116		1415	
		950205		1425	
		950313		1741	

	950326			1639		
	950403			1439		
	950417			1560		
211.3L	940118			4115	S.I.=3	
Mean=	940215			4401		
4095.37	940314			3381		
STD=	940322			3045		
459.32	940411			3870		
VAR=	940419			4829		
210975.31	940503			4629		
RMS=	940509			4449		
7.99	gap					
	941219			3823		
	941223			3870		
	950116			3838		
	950131			4163		
	950207			4282		
	950313			4087		
	950316			4113		
	950403			4641		
	950417			3889		
	950421			3629		
	950516			4042		
	950530		8000	4811		

APPENDIX B: HYDROLOGICAL STATISTICS OF THE BASIC DATA SET

Descriptive Statistics

	Q MIN	Q MEAN	Q MAX	RANGE	UPRAMP	DOWNRAMP
Mean	8635.052	11486.331	14198.826	5563.774	463.722	-464.813
Std. Dev.	2197.561	2499.256	2818.106	1553.693	129.477	151.874
Std. Error	91.249	103.776	117.015	64.514	5.376	6.312
Count	580	580	580	580	580	579
Minimum	5090.000	6968.000	8010.000	50.000	4.000	-1064.000
Maximum	16330.000	18523.000	23000.000	10220.000	852.000	-4.000
# Missing	38	38	38	38	38	39
Variance	4829273.745	6246278.550	7941719.795	2413960.966	16764.291	23065.585
Coef. Var.	.254	.218	.198	.279	.279	-.327
Range	11240.000	11555.000	14990.000	10170.000	848.000	1060.000
Sum	5008330.000	6662072.000	8235319.000	3226989.000	268959.000	-269127
Sum Squ...	46043338100	80139359648	121530116161	19351921341	134428841	138425763
Geom. M...	8388.808	11224.962	13915.564	5170.305	430.928	.
Harm. M...	8169.760	10974.135	13627.923	2740.519	227.934	.
Skewness	1.228	.562	.180	-.276	-.275	-.053
Kurtosis	1.617	-.320	-.636	1.035	1.037	.545
Median	8030.000	10992.500	13710.000	5680.000	473.000	-472.000
IQR	2885.000	3540.000	4020.000	1595.000	133.000	189.000
Mode	10290.000	10183.000	13000.000	.	488.000	.
10% Tr. ...	8364.569	11324.677	14171.248	5580.472	465.101	-463.890
MAD	1370.000	1652.500	1900.000	830.000	69.000	97.000

APPENDIX C: SANDBAR STATISTICS OF THE BASIC DATA SET

Descriptive Statistics

	2.6L	16-4L	43.1L	44.6L	44.65L	60.1R
Mean	1644.700	931.905	2758.818	595.353	3279.947	1930.824
Std. Dev.	416.952	156.658	164.127	100.081	594.541	281.389
Std. Error	131.852	34.185	34.992	24.273	136.397	68.247
Count	10	21	22	17	19	17
Minimum	1101.000	676.000	2452.000	347.000	2194.000	1498.000
Maximum	2101.000	1202.000	3060.000	766.000	4286.000	2349.000
# Missing	608	597	596	601	599	601
Variance	173849.344	24541.590	26937.680	10016.243	353478.830	79180.029
Coef. Var.	.254	.168	.059	.168	.181	.146
Range	1000.000	526.000	608.000	419.000	2092.000	851.000
Sum	16447.000	19570.000	60694.000	10121.000	62319.000	32824.000
Sum Squar...	28615025	18728208	168009402	6185827	210765659	64644232
Geom. Mean	1593.605	919.337	2754.147	586.383	3227.864	1911.671
Harm. Mean	1540.958	906.839	2749.469	576.083	3175.204	1892.814
Skewness	-.293	.156	.012	-.712	.013	.202
Kurtosis	-1.690	-1.050	-.868	.595	-1.211	-1.348
Median	1826.000	915.000	2778.500	610.000	3279.000	1824.000
IQR	798.000	254.000	288.000	89.000	1060.500	529.500
Mode	.	.	.	573.000	.	.
10% Tr. ...	1655.625	927.647	2758.278	600.533	3284.647	1931.800
MAD	256.000	123.000	116.000	37.000	526.000	167.000

Descriptive Statistics

	61.8R	64.0L	81.2L	119.0R	122.7L	132.0L
Mean	4615.714	3178.650	1906.000	4179.941	3276.900	2743.857
Std. Dev.	344.051	825.524	48.225	156.964	264.370	271.345
Std. Error	75.078	184.593	11.064	38.069	59.115	72.520
Count	21	20	19	17	20	14
Minimum	4105.000	1850.000	1841.000	3700.000	2892.000	2233.000
Maximum	5487.000	5153.000	2006.000	4365.000	3789.000	3140.000
# Missing	597	598	599	601	598	604
Variance	118371.114	681489.924	2325.667	24637.809	69891.568	73628.286
Coef. Var.	.075	.260	.025	.038	.081	.099
Range	1382.000	3303.000	165.000	665.000	897.000	907.000
Sum	96930.000	63573.000	36214.000	71059.000	65538.000	38414.000
Sum Squa...	449768608	215024625	69065746	297416645	216089412	106359696
Geom. Mean	4603.851	3080.730	1905.427	4177.050	3266.923	2730.843
Harm. Mean	4592.324	2986.555	1904.858	4174.034	3257.109	2717.291
Skewness	.723	.610	.509	-1.569	.392	-.571
Kurtosis	.184	-.098	-.614	3.244	-.680	-.828
Median	4565.000	3023.500	1907.000	4181.000	3263.500	2813.500
IQR	472.000	1270.000	70.500	144.000	396.500	452.000
Mode	3321.000	.
10% Tr. ...	4589.824	3125.250	1903.941	4199.600	3258.688	2753.417
MAD	232.000	546.000	41.000	76.000	200.000	129.000

Descriptive Statistics

	136.7L	145.5L	172.2L	172.3L	173.1L	211.3L
Mean	4035.200	977.783	549.286	1866.294	1514.200	4095.350
Std. Dev.	186.137	57.216	30.310	241.056	156.246	459.404
Std. Error	41.622	11.930	8.101	58.465	34.938	102.726
Count	20	23	14	17	20	20
Minimum	3535.000	800.000	504.000	1419.000	1251.000	3045.000
Maximum	4369.000	1051.000	596.000	2263.000	1741.000	4829.000
# Missing	598	595	604	601	598	598
Variance	34647.116	3273.632	918.681	58108.096	24412.695	211052.345
Coef. Var.	.046	.059	.055	.129	.103	.112
Range	834.000	251.000	92.000	844.000	490.000	1784.000
Sum	80704.000	22489.000	7690.000	31727.000	30284.000	81907.000
Sum Squar...	326315076	22061373	4235950	60141643	46319874	339447827
Geom. Mean	4031.020	976.089	548.506	1851.134	1506.478	4069.948
Harm. Mean	4026.729	974.292	547.724	1835.469	1498.724	4043.511
Skewness	-.709	-1.293	-.063	-.225	-.031	-.300
Kurtosis	.974	2.068	-1.167	-.663	-1.305	-.153
Median	4065.000	993.000	551.500	1848.000	1531.000	4100.000
QQR	215.000	68.000	54.000	338.250	280.000	571.000
Mode	.	.	.	1848.000	.	3870.000
10% Tr. ...	4045.312	984.000	549.167	1869.667	1514.500	4115.062
MAD	119.500	37.000	27.000	169.000	131.000	269.500

APPENDIX D: SANDBAR SUMMARY STATISTICS

Descriptive Statistics

	BEGIN	END	% CHOT	MAX	MIN	% TDIF
Mean	2337.941	2597.111	14.720	2919.611	1969.056	32.059
Std. Dev.	1247.447	1465.253	19.628	1576.222	1137.952	15.187
Std. Error	302.550	345.364	4.626	371.519	268.218	3.580
Count	17	18	18	18	18	18
Minimum	512.000	596.000	-21.820	596.000	347.000	8.230
Maximum	4382.000	4967.000	62.760	5487.000	4105.000	64.100
# Missing	1	0	0	0	0	0
Variance	1556123.434	2146967.634	385.244	2484474.369	1294934.173	230.636
Coef. Var.	.534	.564	1.333	.540	.578	.474
Range	3870.000	4371.000	84.580	4891.000	3758.000	55.870
Sum	39745.000	46748.000	264.960	52553.000	35443.000	577.070
Sum Squares	117819447	157908200	1.045E4	195670387	91803117	2.242E4
Geom. Mean	1949.497	2151.844	.	2436.237	1611.243	28.472
Harm. Mean	1529.941	1713.388	.	1921.621	1237.855	24.714
Skewness	.045	.204	.693	.105	.348	.457
Kurtosis	-1.192	-1.348	1.158	-1.291	-.953	-.640
Median	2333.000	2342.000	15.475	2704.500	1845.500	28.515
IQR	2289.500	2474.000	13.340	2624.000	1791.000	23.890
Mode
10% Tr. M...	2323.400	2574.062	14.001	2904.375	1936.938	31.546
MAD	1195.000	1365.500	4.975	1542.000	895.000	9.105

Descriptive Statistics

	MEAN	ST. DEV.	CV	R2	M (SLOPE)	A/Q INDEX
Mean	2449.167	264.333	.114	-.253	-.092	3.788
Std. Dev.	1304.764	204.912	.070	.234	.111	6.219
Std. Error	307.536	48.298	.016	.055	.026	1.466
Count	18	18	18	18	18	18
Minimum	549.000	30.000	.026	-.940	-.338	.010
Maximum	4616.000	826.000	.260	.018	.059	25.760
# Missing	0	0	0	0	0	0
Variance	1702408.971	41989.059	.005	.055	.012	38.678
Coef. Var.	.533	.775	.609	-.926	-1.205	1.642
Range	4067.000	796.000	.234	.958	.397	25.750
Sum	44085.000	4758.000	2.060	-4.559	-1.664	68.180
Sum Squares	136912465.000	1971512.000	.318	2.089	.365	915.769
Geom. Mean	2053.309	194.955	.095	.	.	.832
Harm. Mean	1630.030	132.174	.077	.	.	.067
Skewness	.099	1.293	.765	-1.311	-.939	2.646
Kurtosis	-1.233	1.297	-.348	2.154	-.097	6.827
Median	2337.500	213.500	.101	-.255	-.061	.925
IQR	1766.000	188.000	.109	.250	.117	4.170
Mode	.	157.000	.168	.	.013	.
10% Tr. Mean	2432.500	243.875	.111	-.227	-.087	2.651
MAD	941.000	90.500	.046	.130	.059	.915

Descriptive Statistics

	WIDTH	DEPTH	W/D	RCH	WI	#EVTS	XEV SZ
Mean	63.000	4.554	16.736	6.125	2.062	.500	68.944
Std. Dev.	14.436	1.795	8.191	2.986	.680	.786	187.656
Std. Error	3.609	.498	2.272	.747	.170	.185	44.231
Count	16	13	13	16	16	18	18
Minimum	42.000	2.500	6.000	1.000	1.000	0.000	0.000
Maximum	96.000	7.000	30.000	10.000	3.000	2.000	665.000
# Missing	2	5	5	2	2	0	0
Variance	208.400	3.221	67.086	8.917	.463	.618	35214.761
Coef. Var.	.229	.394	.489	.488	.330	1.572	2.722
Range	54.000	4.500	24.000	9.000	2.000	2.000	665.000
Sum	1008.000	59.200	217.570	98.000	33.000	9.000	1241.000
Sum Squares	66630.000	308.240	4446.313	734.000	75.000	15.000	684211.000
Geom. Mean	61.444	4.235	14.596	5.255	1.944	.	.
Harm. Mean	59.886	3.949	12.460	4.141	1.811	.	.
Skewness	.335	.297	-.033	.031	-.067	1.122	2.577
Kurtosis	-.031	-1.691	-1.432	-1.179	-.702	-.367	4.919
Median	63.000	3.500	18.000	5.500	2.000	0.000	0.000
IQR	19.500	3.500	14.255	5.500	.500	1.000	14.000
Mode	70.000	3.000	23.330	4.000	2.000	0.000	0.000
10% Tr. Mean	62.143	4.518	16.506	6.214	2.071	.438	36.000
MAD	7.000	1.000	5.330	1.500	0.000	0.000	0.000